IDA PAPER P-2175

IDA GAMMA-RAY LASER ANNUAL SUMMARY REPORT (1988)

Investigation of the Feasibility of Developing a Laser Using Nuclear Transitions

Bohdan Balko
David A. Sparrow
Irvin W. Kay
Collen Holcomb
Karen K. Garcia

December 1988

Prepared for
Strategic Defense Initiative Organization
Innovative Science and Technology Office

Dwight Duston, *Director*

Approved for public release; distribution unlimited.

INSTITUTE FOR DEFENSE ANALYSES
1801 N. Beauregard Street, Alexandria, Virginia 22311-1772

IDA Log No. HQ 88-34045

DEFINITIONS

IDA publishes the following documents to report the results of its work.

Reports

Reports are the most authoritative and most carefully considered products IDA publishes. They normally embody results of major projects which (a) have a direct bearing on decisions affecting major programs, (b) address issues of significant concern to the Executive Branch, the Congress and/or the public, or (c) address issues that have significant economic implications. IDA Reports are reviewed by outside panels of experts to ensure their high quality and relevance to the problems studied, and they are released by the President of IDA.

Group Reports

Group Reports record the findings and results of IDA established working groups and *panels composed of senior individuals addressing major issues which otherwise would be* the subject of an IDA Report. IDA Group Reports are reviewed by the senior individuals responsible for the project and others as selected by IDA to ensure their high quality and relevance to the problems studied, and are released by the President of IDA.

Papers

Papers, also authoritative and carefully considered products of IDA, address studies that are narrower in scope than those covered in Reports. IDA Papers are reviewed to ensure that they meet the high standards expected of refereed papers in professional journals or formal Agency reports.

Documents

IDA Documents are used for the convenience of the sponsors or the analysts (a) to record substantive work done in quick reaction studies, (b) to record the proceedings of conferences and meetings, (c) to make available preliminary and tentative results of analyses, (d) to record data developed in the course of an investigation, or (e) to forward information that is essentially unanalyzed and unevaluated. The review of IDA Documents is suited to their content and intended use.

The work reported in this document was conducted under contract MDA 903 84 C 0031 for the Department of Defense. The publication of this IDA document does not indicate endorsement by the Department of Defense, nor should the contents be construed as reflecting the official position of that Agency.

REPORT DOCUMENTATION PAGE

Form Approved
OMB No. 0704-0188

1. AGENCY USE ONLY *(Leave blank)*	2. REPORT DATE	3. REPORT TYPE AND DATES COVERED
	December 1988	Final--October 1987 to December 1988

4. TITLE AND SUBTITLE
IDA Gamma-Ray Laser Annual Summary Report (1988): Investigation of the Feasibility of Developing a Laser Using Nuclear Transitions

5. FUNDING NUMBERS
C - MDA 903 84 C 0031

T - T-R2-316

6. AUTHOR(S)
Bohdan Balko, David A. Sparrow, Irvin W. Kay, Colleen Holcomb, Karen K. Garcia

7. PERFORMING ORGANIZATION NAME(S) AND ADDRESS(ES)
Institute for Defense Analyses
1801 N. Beauregard St.
Alexandria, VA 22311-1772

8. PERFORMING ORGANIZATION REPORT NUMBER
IDA Paper P-2175

9. SPONSORING/MONITORING AGENCY NAME(S) AND ADDRESS(ES)
Strategic Defense Initiative Organization
The Pentagon
Washington, DC 20301-7100

10. SPONSORING/MONITORING AGENCY REPORT NUMBER

11. SUPPLEMENTARY NOTES

12a. DISTRIBUTION/AVAILABILITY STATEMENT
Approved for public release; distribution unlimited.

12b. DISTRIBUTION CODE

13. ABSTRACT *(Maximum 200 words)*

This report summarizes the IDA research effort in FY 1988 in investigating the feasibility of developing a γ-ray laser.

14. SUBJECT TERMS
Nuclear Laser, Gamma-ray Laser, Graser, Superradiance, Superfluorescence, Mossbauer Effect, Borrman Effect, Nuclear isomers, energy deposition, temperature rise during pumping , upconversion, closely spaced levels, experimental technique for upconversion, search for closely spaced levels

15. NUMBER OF PAGES
121

16. PRICE CODE

17. SECURITY CLASSIFICATION OF REPORT	18. SECURITY CLASSIFICATION OF THIS PAGE	19. SECURITY CLASSIFICATION OF ABSTRACT	20. LIMITATION OF ABSTRACT
UNCLASSIFIED	UNCLASSIFIED	UNCLASSIFIED	SAR

IDA PAPER P-2175

IDA GAMMA-RAY LASER ANNUAL SUMMARY REPORT (1988)

Investigation of the Feasibility of Developing a Laser Using Nuclear Transitions

Bohdan Balko
David A. Sparrow
Irvin W. Kay
Colleen Holcomb
Karen K. Garcia

December 1988

INSTITUTE FOR DEFENSE ANALYSES
Contract MDA 903 84 C 0031
Task T-R2-316

PREFACE

In January 1985 the Director of the Science and Technology Directorate of the Strategic Defense Initiative Organization (SDIO) asked members of the IDA research staff to investigate the feasibility of developing a γ-ray laser. The staff determined what work had been done, who was currently working in the field, and what work should be encouraged or supported. A workshop was convened for researchers directly involved both in gamma-ray laser work and in ancillary fields such as nuclear structure, radiation propagation in crystals, Mössbauer Effect, and optical lasers. Next, an in-house study was undertaken to clarify critical issues concerning the various pumping schemes proposed at the workshop as well as systems questions about the γ-ray laser as a working device.

The proceedings of the workshop were published in the form of a report to the Innovative Science and Technology Office (IST) of the SDIO. The work completed in 1985 was presented in an IDA Paper (Ref. 1).

In 1986, the in-house work focused on extending the data base, the nature of superradiance in the γ-ray laser context, and a detailed investigation of the upconversion pumping scheme. A discussion of nuclear systematics, investigations of electron-nuclear-driven pumping, and lifetime measurements rounded out that study. The results of the FY 1986 effort were also presented in an earlier IDA paper (Ref. 2).

In 1987, the IDA research staff looked at the state of the art and assessed the situation in γ-ray laser work with focus on two areas of research interest critical to concepts for developing a γ-ray laser. Heating effects associated with upconversion techniques were discussed. The sources of inhomogeneous broadening which destroy the Mössbauer Effect were investigated and techniques available for restoring the resonance by external or internal fields were considered.

This report covers the work done in FY 1988. In 1988 the in-house work concentrated on (1) establishing a theoretical model of nuclear superfluorescence which took into account specific characteristics of nuclear radiation emission and transport that are important for superfluorescence on the nuclear scale, (2) examining in more detail and for more realistic parameters the heating effects inherent in upconversion concepts, and

(3) examining the speed of response of nuclei to applied external fields, as exhibited by their spectra.

The development of a γ-ray laser is viewed as a high-risk/high-payoff undertaking. IDA's involvement focuses on minimizing the risk and on striving to redirect the effort when proposed schemes are shown not to be feasible.

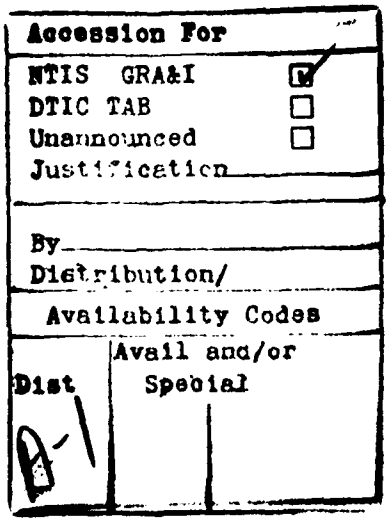

CONTENTS

FIGURES

EXECUTIVE SUMMARY

This report describes the 1988 research effort by members of the IDA staff in the field of γ-ray lasers. The work is part of a continuing task in support of the Innovative Science and Technology Office (IST) of the Strategic Defense Initiative Organization (SDIO). The development of a γ-ray laser is a high-risk science and technology undertaking. IDA involvement has focused in large measure on minimizing the risk and attempting to redirect the program as quickly as possible when proposed schemes prove infeasible. The report is presented in six independent chapters.

Chapter I discusses the nuclear superfluorescence (SF) problem. Seven areas of concern critical to the observation of nuclear SF but not relevant or as important to SF at longer wavelengths are discussed. A model of nuclear SF based on the Maxwell Bloch formalism as adapted to SF by Haake and Riebold is developed. A closed form solution to the linear part of the problem is obtained and a direct solution for the nonlinear part for the average intensity is discussed. The importance of this result is that it avoids the use of Monte Carlo techniques and explicitly exhibits the dependence of the pulse intensity on the strength of competing processes, (e.g., internal conversion), the beam attenuation due to scattering or absorption processes, (e.g., the photoelectric effect), and the finite pumping time of the lasing level. The effects of beam attenuation and competing transitions on SF emission are investigated and the different roles attenuation plays in SF and stimulated emission are discussed.

Chapter II discusses SF at wavelengths shorter than the internuclear distances. A condition for SF under these conditions for a crystalline solid is obtained from the Bonifacio-Lugiato theory.

Chapter III discusses our recent investigation of heating triggered by the photoelectric effect during upconversion in a γ-ray laser. This is a continuation of last year's effort, as presented in the 1987 report. We find that pumping transitions with energy between 10 eV (the ionization threshold) and 10 keV are infeasible because of this heating. This is true even if light low photoelectric cross section materials are used as a heat shield. We remain skeptical about possibilities for pumping transitions with energy

greater than 10 keV. Below 10 eV no nuclear states are known. A proposal to search for such states is presented in a subsequent contribution.

Chapter IV discusses simple and inexpensive ways of searching for nuclear states located close to isomeric levels. We have shown (1987 report and Chapter III of this report) that photoelectric heating eliminates the possibility of pumping transitions in the 10 eV to 10 keV region. No nuclear states are known to lie within 10 eV of isomers. We propose to search for such states using blackbody radiation. Our calculations indicates that such a state, if connected to an isomer by a reasonably strong M1 matrix element, could be identified if it were about 0.1 eV to 10 eV above the isomer. Below 0.1 eV even a strong single-particle M1 transition would probably have too small a cross section to allow easy detection. In the near future, with the advent of tunable coherent sources, the energy regime within 0.1 eV of an isomer could also be searched for states.

Chapter V describes a numerical technique for solving the heat diffusion problem for a multimedia system when distributed sources are present. The technique is used to study the dynamics of heat removal from an active regime by a heat sink when the system is subjected to an upconversion laser pulse.

Chapter VI calculates the response of the nuclear system to externally varying fields as exhibited in the nuclear spectrum. This calculation addresses the length of time a system has to be subjected to line-narrowing pulses in order to narrow inhomogeneously broadened lines to acceptable widths for lasing.

I. NUCLEAR SUPERFLUORESCENCE

A. INTRODUCTION

Superfluorescence (and superradiance)[1] is the cooperative spontaneous emission by identical atoms (or other radiators) of coherent radiation characterized by directed intense pulses of duration much shorter than the spontaneous emission lifetime of individual radiators (Ref. 3).

Generally speaking, the emission of a superfluorescent (SF) pulse requires the preparation of an inverted population of the identical radiators. Experimentally, the emitted pulses are characterized by a SF time τ_R and a delay time τ_D, following the inversion of the population. From simple theory, Ref. 4, a relationship can be obtained between τ_R and τ_D, the density of cooperating radiators ρ, the natural radiative lifetime τ_o, the wavelength of the emitted light, λ, the number N of radiators, and the cavity length l. In terms of those parameters[2],

$$\tau_R = \frac{8\pi\,\tau_o}{\rho\lambda^2 l} \ ,$$

$$\tau_D = \frac{1}{2}\tau_R\, ln\,(N) = \frac{4\pi\,\tau_o}{\rho\lambda^2 l}\, ln\,(N) \ ,$$

and the theory predicts a pulse intensity $I_s(t)$ given by the "inverted pendulum expression"

$$I_s(t) = \frac{1}{2} N/\tau_R \ \mathrm{sech}^2\left[\frac{1}{\tau_R}(t - \tau_D)\right]$$

---

1 We follow the convention of Bonifacio and Lugiato (Ref. 4) who distinguish between radiation emitted by coherently prepared systems and with initially a macroscopic dipole moment, which they call superradiant, and incoherently prepared systems which do not have a macroscopic dipole moment initially but interact through normal fluorescent decay to evolve a macroscopic dipole which then radiates coherently in a cooperative mode, which they call superfluorescent. In both cases, the intensity is proportional to N^2.

2 The value of the characteristic SF time τ_R used here is that used by Bonifacio and Lugiato (Ref. 4) and results from assuming an isotropic distribution of the dipole moment. It differs by a factor 1/3 from the value derived by Polder et al. (Ref. 44) who take into account the anisotropy of the two level transition. We will use this value $\tau_{SR} = 1/3\ \tau_R$ in further discussions.

(Ref. 4), where t is measured from the time of the (instantaneous) inversion.

Clearly, to describe more realistic experimental conditions, more general theories have to be involved.

It is expected that if a "gamma-ray laser" is developed it most probably will emit in a superradiant (SR) or superfluorescent (SF) mode instead of a stimulated emission (SE) mode (Ref. 5)[3]. There are some characteristic features of superfluorescent decay which may provide ways of overcoming specific nuclear problems (Ref. 6) which at present prevent CW or pulsed laser (SE) action. The purpose of this paper is to investigate the possibility of nuclear superfluorescence and describe the interrelationship of the pertinent nuclear and solid-state parameters that govern the experimental realization of this phenomena. We also contrast the nuclear problem with the atomic and molecular SF problem.

Superradiance has been observed in atomic and molecular systems and the phenomena have been explained theoretically (Ref. 7). An excellent discussion of the experimental results is presented by Q.H.F. Vrehen and H.M. Gibbs (Ref. 7) and of the present state of theoretical understanding by M. Gross and S. Haroche (Ref. 8) and M.F.H. Schuurmans, Q.H.F. Vrehen and D. Polder (Ref. 9). Just as the observation of resonance in nuclear systems requires special conditions that are more stringent than in atomic systems, the realization of superradiance on the nuclear level must overcome restrictions that are often not important in atomic and molecular systems. Some special consideration has to be given to the short wavelength of the nuclear radiation, the crystalline structure and its effect on SR and SF, attenuation of the beam due to inelastic scattering, destruction of resonance due to recoil of the nucleus, inhomogeneous broadening, and relaxation effects. A strong Mössbauer Effect (recoilless emission) and a strong Borrmann Effect (enhanced photon transmission in certain directions in a crystal) are generally considered indispensible for nuclear superfluorescence but not for atomic or molecular superfluorescence.

---

3 The following example illustrates the reason. An active cylindrical volume, with a radius = 10^{-5} cm, and length = 10^{-2} cm, composed of Fe^{57} (density = 8×10^{22} cm^{-3}) will contain 2.5×10^{11} nuclei. If the nuclei are all excited to an energy level of 10^{4}ev (1Å) with a natural linewidth of 10^{-9}ev, corresponding to a lifetime of 6.6×10^{-7} sec, the superfluorescence time τ_{SF} will be 6.9×10^{-11} sec. Since each photon has the energy 10^{4}ev, the total energy emitted will be 2.5×10^{14}ev if the recoilless fraction is 1/10. This is 4×10^{-5} J; therefore, the power in the emitted superfluorescence pulse will be 5.8×10^{5} W. However, if the emitted pulse width were that of the natural lifetime the power would only be 61W.

The extensive literature on superradiance and superfluorescence offers a detailed physical understanding of the phenomenon (see, for example, review paper, Ref. 8). However, it is not yet clear whether any of the proposed mathematical models of SR and SF can give reliable quantitative predictions of effects in nuclear rather than atomic emission levels.

The model presented by R. Bonifacio and L.A. Lugiato (B-L) in Ref. 4 appears to rely on the fewest *ad hoc* assumptions. It includes (non relativistic) quantum effects, line-broadening, and (non-Markovian) stimulation of the atomic system by the spontaneously emitted photons. The only significant *ad hoc* assumption in the model appears to be its restriction of the electromagnetic field to a pair of independent resonant modes. The authors partially justify this assumption by limiting the geometrical configuration to a needle-shaped cavity which, if thin enough, will support just two identical waves propagating in opposite directions parallel to the cavity axis (endfire modes).

Besides the well-known weak points of the B-L theory, such as the assumptions of two modes and the independence of those modes, the theory does not easily allow for the calculation of effects due to competing transitions (internal conversion, emission with recoil, etc.) and transport effects (photoelectric absorption). Other theories have been developed which are based on the Maxwell-Bloch equations and allow for the inclusion of quantum initiation statistics and modeling of the fluctuation statistics. This is not of particular importance or interest to the γ-ray laser problem at the present state of sophistication and development. What is of interest is that these theories can deal in a straightforward way with the phenomena of competing transitions and photon transport in the medium; two problems of great significance to the γ-ray laser feasibility study.

The detailed characteristics of nuclear inversion pumping, radiation emission, and transport through media have an impact on the generation of nuclear superradiant pulses. These phenomena must be carefully treated in an analysis of the feasibility of nuclear superfluorescence. We are not interested in the details of specific γ-ray laser or superradiator concepts at this stage, but only in general features exhibiting the differences between nuclear and atomic systems and we concentrate on those that may not have been adequately addressed by workers considering atomic systems.

In particular, we feel that the following special issues that differentiate nuclear superfluorescence from the well-studied atomic superradiance and superfluorescence have to be addressed.

1. Short Wavelength of the Emitted Radiation

Atomic transition energies are on the order of 1 eV to 10 eV, and wavelengths on the order of 10^3 Å to 10^4 Å. On the other hand, nuclear transitions of interest are on the order of 10^3 eV to 10^5 eV, with corresponding wavelengths on the order of about 0.1 Å to 10 Å. The original Dicke theory of superradiance deals with systems in which the wavelength of the radiation is greater than the diameter of the volume containing the individual radiators. It has been generalized to deal with a less restrictive case: the wavelength less than the diameter of the volume containing the radiators cooperating in the emission but greater than the interradiator distance. In the case of nuclear radiators, the condition has to be further generalized, because the interatomic distance of the radiators may be larger than the wavelength of the radiation.

The issue of the short wavelength of the emitted radiation as compared to the internuclear spacing (Ref. 10) has been discussed by Trammel. It is generally ignored by other authors dealing with nuclear superradiance (Ref. 11), although it is certainly controversial as exemplified by the series of letters to the editor following an article on the subject by H. Lipkin (Ref. 12). We discuss the problem of shorter wavelengths in Chapter II of this report in the formalism of the Bonifacio-Lugiato theory.

2. Large Recoil Energy Compared to the Natural Linewidth

A nucleus or atom emitting a photon will recoil with energy $E_R = E_o^2/2Mc^2$ where E_o is the resonance energy, M the mass of the emitter and c the speed of light. A typical atom with resonance energy on the order of an eV and an atomic mass of 50 will recoil with an energy of about 10^{-11} eV, which is much smaller than the typical atomic linewidth of 10^{-9} eV. On the other hand, the same atom in a typical nuclear transition of 10^4 eV will recoil with an energy of about 10^{-3} eV, which is orders of magnitude higher than the typical nuclear linewidth of 10^{-9} eV. The result is that while the emitting atom is in resonance with the other atoms in the cavity, the emitting nucleus will be out of resonance with the other nuclei.

Emission with recoil will be treated in our formalism as a competing process which has the effect of reducing the excited state population. We believe that in the present stage of the development of nuclear superradiance this is an appropriate assumption. Under

certain well understood conditions (Mössbauer Effect) a nucleus will emit without recoil, strongly resonate with other nuclei and thus alleviate this problem.

3. High Multipolarity

The transitions of interest in nuclear superfluorescence are generally of high multipolarity (M1, E2, M2, or higher) unlike in atomic transitions where electric dipole is the prevalent mode of emission. All the theories of superradiance known to the authors up to now have dealt with electric dipole transitions. Complications with high multipoles could arise in cases where competing transitions occur (Ref. 13). Such considerations will have to be introduced in future more complete analyses. Problems of high multipolarity superfluorescent transitions will not be discussed in this paper.

4. Competing Transitions

The effect of several transitions competing for the depopulation of a level has recently been introduced into theoretical calculations for atomic superfluorescence systems. In nuclear systems internal conversion is not only common but strongly competes with the radiation transition in depopulation of low-energy nuclear states.[4] Internal conversion plays an especially important role in low-energy nuclear transitions and has to be considered carefully in discussing nuclear superfluorescence. Other competing electromagnetic transitions are also common in nuclear systems and can be treated similarly.

5. Electronic Attenuation

For the cases of interest, the linear attenuation coefficient μ is much higher for the energy range involved in the nuclear transition (10^3 eV to 10^5 eV) than in the energy range involved in the atomic transitions (1 eV to 10 eV). Multiple passes in an optical cavity of a few centimeters can be achieved while nuclear radiation is limited to a path length of less than about 0.1 mm. The exact relationship of μ and the population inversion in the generation of nuclear superradiance is very important and has to be carefully investigated.

---

[4] The internal conversion coefficient $\alpha = \frac{\text{rate of electron emission}}{\text{rate of photon emission}}$ can typically range from on the order of 10 to 10^3 in the range of energies of interest (Ref. 14).

6. Finite Pumping Times

The pumping problem for nuclear SF is severe and pumping times on the order of the lifetime of the lasing level are usually required. Instantaneous pumping to inversion is not expected, thus calculations using this assumption are not realistic and have to be abandoned. Realistic pumping times are important and have to be included in the analysis of nuclear superradiance.

7. Geometrical Considerations

Although for the convenience of analysis the acicular geometry (long cylinder) is very desirable, it may not be realistic in terms of the attainable experimental conditions. The acicular geometry permits the restriction of analysis to a single mode emission, and when the Fresnel number F ($F=d^2/l\lambda$, where d is the cavity diameter, l the length and λ the radiation wavelength) is one, guarantees the optimum diffraction limited condition (Ref. 15). To achieve a condition for the active region determined by F = 1 may be difficult experimentally. Consideration of the feasibility of superfluorescence in a more realistic, three-dimensional geometry is desired. Some theoretical work on three dimensional geometries has been presented in recent publications (Refs. 16, 17). Further discussions regarding general three-dimensional geometries will be left for subsequent publications.

In this paper we will discuss the effect on nuclear superfluorescence of (1) competing transitions (e.g., internal conversion, emission with recoil, branching ratios),[5] (2) transport effects (electronic attenuation), and (3) finite pumping times using incoherent sources. The question of the feasibility of superradiance in a system of radiators with separations longer than the wavelength of the emitted radiation is discussed in Chapter II. The questions related to superfluorescence in a three-dimensional active medium will be discussed in a future publication.

B. THEORY

Superfluorescence with competing transitions and including transport effects such as beam attenuation due to incoherent inelastic processes can be modeled using Maxwell-Bloch equations (Ref. 8) modified to include vacuum fluctuations. Our discussion follows

---

[5] In this paper we treat all of these mechanisms in the same way, assuming their impact to be due to their effect on the reduction of the inversion only.

the Haake and Reibold theory presented without derivation in Ref. 18. Appendix A outlines and discusses a possible derivation of the original equations. The analysis in this section which deals with a modified version of those equations for 3 rather than 5 energy levels is new.

Corresponding to the excitation level diagram in Fig. 1, the (Ref. 18) system of differential equations satisfied by the excited population number operators N_i, the atomic polarization operators $R_{ij}^{\pm}$, and photon field operators $E_{ij}^{\pm}$ is

$$\frac{\partial}{\partial t} N_4 = -\gamma N_4 + \xi_4 \qquad 1(a)$$

$$\frac{\partial}{\partial t} N_3 = -\left(E_{31}^{+}R_{31}^{+} + E_{32}^{+}R_{32}^{+} + E_{31}^{-}R_{31}^{-} + E_{32}^{-}R_{32}^{-}\right) - \Gamma_3 N_3 + \gamma N_4 - \xi_4 \qquad 1(b)$$

$$\frac{\partial}{\partial t} N_2 = +\left(E_{32}^{+}R_{32}^{+} + E_{32}^{-}R_{32}^{-}\right) - \Gamma_2 N_2 + \Gamma_3' N_3 + \xi_2 \qquad 1(c)$$

$$\frac{\partial}{\partial t} N_1 = +\left(E_{31}^{+}R_{31}^{+} + E_{31}^{-}R_{31}^{-}\right) + \Gamma_2 N_2 - \Gamma_1 N_1 + \Gamma_3 N_3 + \xi_1 \qquad 1(d)$$

$$\frac{\partial}{\partial t} R_{32}^{\pm} = \left(N_3 - N_2\right) E_{32}^{\mp} - E_{31}^{\mp}R_{21}^{\pm} - \frac{1}{2}\left[\Gamma_3 + \Gamma_2\right] R_{32}^{\pm} + \xi_{32}^{\pm} \qquad 2(a,b)$$

$$\frac{\partial}{\partial t} R_{31}^{\pm} = \left(N_3 - N_1\right) E_{31}^{\mp} - E_{32}^{\mp}R_{21}^{\pm} - \frac{1}{2}\left[\Gamma_3 + \Gamma_1\right] R_{31}^{\pm} + \xi_{31}^{\pm} \qquad 2(c,d)$$

$$\frac{\partial}{\partial t} R_{21}^{\pm} = E_{31}^{\mp}R_{32}^{\pm} + E_{32}^{\mp}R_{31}^{\pm} - \frac{1}{2}\left(\Gamma_1 + \Gamma_2\right) R_{21}^{\pm} + \xi_{21}^{\pm} \qquad 2(e,f)$$

$$\frac{\partial}{\partial x} E_{3i}^{\pm} = g_i R_{3i}^{\mp} - \frac{1}{2}\mu E_{3i}^{\pm} \quad (i = 1, 2) \qquad 3(a,b)$$

In eqs. (1-3) the $\pm$ superscripts for the fields and polarization operators refer to the positive and negative frequency components of these quantities. $\xi_{ij}^{\pm}$ are stochastic noise operators[6] with zero means and second moments that satisfy

---

6 The stochastic noise operators are defined by their statistics. Polder, Shuurmans, and Vrehen (Ref. 9) derived the classical noise equivalent sources from a quantum mechanical model. They identified three distinct components of the EM field, namely, (1) vacuum fluctuations, E_{vac}, (2) E_{dd} or dipole contributions from different atoms and (3) the self force or radiative reaction, E_{rr} which is the dipole contribution from the local atom. Initially, the only non zero component is E_{vac}. This sets up correlations in the polarizations of atoms which produces a non zero E_{dd}. The E_{vac} wave vectors corresponding to the appropriate geometry of the active region (cavity) set up the polarization appropriate for cooperative emission with those wave vectors. This results in the observed SF emission. The E_{rr} field gives rise to the natural width of the emission line only. Haake and Reiboild (Ref. 18) use this theory to model noise sources which trigger SF. Their noise source is due to the incoherent pumping mechanism with time constant γ or the natural spontaneous decay from the excited state with time constant Γ_3. In the present development we use the noise source, as described in equations 4, from the incoherent pumping mechanism for the SF triggering.

$$< \xi^{+}_{ij} \xi^{+}_{ij} > = < \xi^{-}_{ij} \xi^{-}_{ij} > = < \xi^{-}_{ij} \xi^{+}_{ij} > = 0 \ ,$$

$$< \xi^{+}_{ij} (x,t) \, \xi^{-}_{ij} (x',t') > = \left(\frac{1}{N}\right) e^{-\gamma t} \gamma \delta(x - x') \, \delta(t - t') \ . \qquad (4)$$

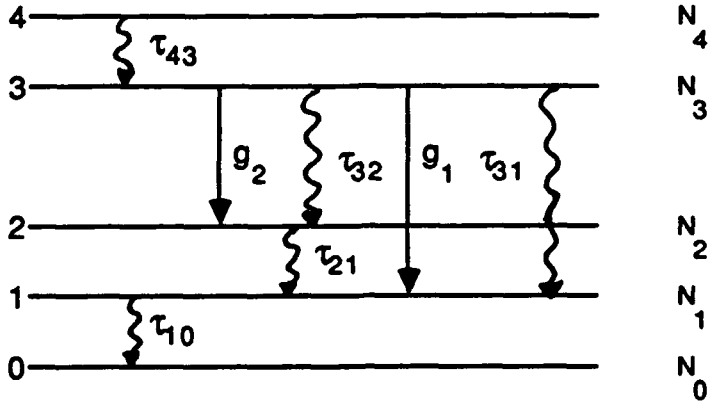

Figure 1. Energy level diagram for the five-state system modeled by eqs. (1-3). The two competing SF transition are between upper state 3 and lower states 1 and 2 and are indicated by g_1 and g_2, respectively. Level 4 populates level 3, providing the inversion. The decay rates γ, Γ_3, Γ_2, and Γ_1 are given by τ_{43}^{-1}, $\left(\tau_{31}^{-1} + \tau_{32}^{-1}\right)$, τ_{21}^{-1} and τ_{10}^{-1}, respectively.*

* Other depopulation transitions are generally allowed. We indicate only those of interest at present.

The initial values of the operators, referred to the vacuum state for the electromagnetic field, are prescribed by their vacuum state expectation values:

$$E^{+}_{31} (x, 0) \, | 0 > = E^{+}_{32} (x, 0) \, | 0 > = N_3 (x, 0) \, | 0 > = 0 \ ,$$

$$N_4 (x, 0) \, | 0 > = 1 \ . \qquad (5)$$

In addition, boundary conditions implying that no external signals impinge on the system are imposed:

$$E^{\pm} (0, t) = 0 \ .$$

The objective is to calculate the mean radiation intensity I(t) (at the right end of the collection of atoms or nuclei), where

$$I(t) = < E^{-} (l,t) \, E^{+} (l,t) > \ . \qquad (6)$$

Eqs. (1-3) are written in terms of the retarded time so that $t = t' - \frac{x'}{c}$, $x = x'$ and $\frac{\partial}{\partial x} = \frac{\partial}{\partial x'} + \frac{1}{c}\frac{\partial}{\partial t'}$, $\frac{\partial}{\partial t} = \frac{\partial}{\partial t'}$ where t' and x' are the normalized time and space coordinate. The real time and space coordinates are normalized to the superfluorescence time and cavity length, respectively, so that $t' = \frac{t''}{\tau_{SF}}$, $x' = \frac{x''}{l}$ where t" and x" are the real time and space coordinates. The superfluorescence time is given by

$$\tau_{SF} = \frac{8\pi\tau_o}{3\lambda^2\rho l} \quad ,$$

l is the cavity length, λ is the wavelength of the emitted photon, τ is the natural radiative lifetime, and ρ is the inversion density of cooperating nuclei. Of the parameters indicated in Fig. 1, τ_{ij} give the radiative spontaneous emission lifetime of the state i due to the transition $i \rightarrow j$, with corresponding emission rates Γ_{ij} and Γ_3, Γ_2, and Γ_1 give the total single resonator spontaneous incoherent emission rates from states 3, 2, and 1, respectively. The coupling constants for transitions $3 \rightarrow 2$ and $3 \rightarrow 1$ are given by g_2 and g_1, respectively.

Calculations of superradiant phenomena, described by the general eqs. (1-3) and the level structure of Fig. 1, using Monte Carlo techniques, will be described in a subsequent publication. Presently we are interested in studying (1) the effect of competing transitions such as the incoherent decay process described by the decay rate Γ_3, which removes excited state nuclei from the system, (2) the effect of transport phenomena as included in the model through the linear attenuation coefficient μ in eqs. (3a, 3b), and (3) the effect on superfluorescence of the pumping rate γ.

Equations (1-3) can be solved for some special cases to get insight into the effect of these parameters on the phenomena of superradiance. With this intent we simplify the problem by considering levels 4, 3, and 1 only and drop the noise source ξ_4. The relevant set of equations can be separated into two groups. The first group describes the formation of superradiance and consists of

$$\frac{\partial R_{31}^{\pm}}{\partial t} = f(x,t)\, E_{31}^{\mp} - \frac{\Gamma_3}{2} R_{31}^{\pm} + \xi_{31}^{\pm} \qquad 7(a)$$

$$\frac{\partial E_{31}^{\pm}}{\partial x} = g_1 R_{31}^{\mp} - \frac{1}{2}\mu E_{31}^{\pm} \qquad 7(b)$$

The second group of equations describes the population dynamics of the three states and is used to calculate the inversion function $f(x,t) = N_3 - N_1$,

$$\frac{\partial N_4}{\partial t} = -\gamma N_4 \qquad 8(a)$$

$$\frac{\partial N_3}{\partial t} = -\left(E_{31}^{+}R_{31}^{+} + E_{31}^{-}R_{31}^{-}\right) - \Gamma_3 N_3 + \gamma N_4 \qquad 8(b)$$

$$\frac{\partial N_1}{\partial t} = +\left(E_{31}^{+}R_{31}^{+} + E_{31}^{-}R_{31}^{-}\right) + \Gamma_3 N_3 \quad . \qquad 8(c)$$

Initially, only level 4 is populated so that

$$N_4(0) = N_o$$

$$N_3(0) = N_1(0) = 0 \quad ,$$

and since

$$N_4 + N_3 + N_1 = N_o \text{ for all time,} \qquad (9)$$

we get

$$f(x,t) = 2N_3(t) + N_4(t) - N_o \quad . \qquad (10)$$

Equations (7a, 7b), after dropping the subscripts, can be combined to give

$$\frac{\partial^2 E^{\pm}}{\partial t \partial x} = \left[g f - \frac{\Gamma\mu}{4}\right] E^{\pm} - \frac{\Gamma}{2}\frac{\partial E^{\pm}}{\partial t} - \frac{1}{2}\mu\frac{\partial E^{\pm}}{\partial x} + g\,\xi^{\pm} \quad . \qquad (11)$$

Assuming that f(x,t) is a function of time alone and taking the Laplace transform of (11) with respect to x leads to

$$\left(\frac{1}{2}\mu + s\right)\frac{\partial \bar{E}}{\partial t} + \left[\frac{\Gamma}{2}\left(\frac{1}{2}\mu + s\right) - g f\right]\bar{E} = \frac{\partial E}{\partial t}(0, t) + \frac{\Gamma}{2}E(0, t) + g\,\bar{\xi} \quad , \qquad (12)$$

where

$$\bar{E}(s) = \int_0^{\infty} e^{-sx} E(x)\, dx$$

and

$$\bar{\xi}(s) = \int_0^{\infty} e^{-sx} \xi(x)\, dx \quad .$$

Taking the appropriate initial condition that

$$E(x,0) = 0 \ ,$$

which implies

$$\bar{E}(s,0) = 0 \ ,$$

the solution of eq. (12) is

$$\bar{E}(s,t) = g \int_0^t \bar{\xi}(s,t') \, e^{-\frac{\Gamma}{2}(t-t')} \left(\frac{e^{k(t,t')/(s+\frac{1}{2}\mu)}}{s+\frac{1}{2}\mu} \right) dt' \quad , \tag{13}$$

where

$$k(t,t') = g \int_{t'}^{t} f(t'') \, dt'' \quad . \tag{14}$$

Since $\frac{e^{k/s}}{s}$ is the Laplace transform of the Bessel function $I_o\left(2\sqrt{kx}\right)$, $\frac{e^{k/s}}{s+\frac{1}{2}\mu}$ is the Laplace transform of $e^{-\frac{1}{2}\mu x} I_o\left(2\sqrt{kx}\right)$. Therefore,

$$E^{\pm}(x,t) = g \int_0^t \int_0^x I_o\left(2\sqrt{k(t,t')\,(x-x')}\right) e^{-\frac{1}{2}\mu(x-x') - \frac{\Gamma}{2}(t-t')} \bar{\xi}^{+}(x',t') \, dx' \, dt \quad . \tag{15}$$

The experimentally measured intensity of the superfluorescent emission is given as the average of the product of E^+ and E^- at the right boundary, $l = 1$. From eqs. (15) and (4) this is given by

$$I(t) = \langle E^-(1,t) \, E^+(1,t) \rangle$$

$$= \frac{g^2\gamma}{N} \int_0^t \int_0^1 \int_0^t \int_0^1 I_o\left(2\sqrt{k(t,t')\,(1-x')}\right)$$

$$e^{-\frac{1}{2}\mu(1-x') - \frac{\Gamma}{2}(t-t')} \, {}_oI\left(2\sqrt{k(t,t'')\,(1-x'')}\right)$$

$$e^{-\frac{1}{2}\mu(1-x'') - \frac{\Gamma}{2}(t-t'') - \gamma t'} \, \delta(x'-x'') \, \delta(t'-t'') \, dx' \, dt' \, dx'' \, dt''$$

$$= \frac{g^2\gamma}{N} e^{-\mu - \Gamma t} \int_0^t \int_0^1 I_o^2\left(2\sqrt{k(t,t')\,(1 - x')}\right) e^{\mu x' + (\Gamma - \gamma)t}\, dx'\, dt'$$

$$= \frac{g^2\gamma}{N} e^{-\Gamma t} \int_0^t \int_0^1 I_o^2\left(2\sqrt{k(t,t')\,x'}\right) e^{-\mu x' + (\Gamma - \gamma)\,t'}\, dx'\, dt' \quad . \qquad (16)$$

In general, including the nonlinear terms $E^+R^+ + E^-R^-$, the expression for k(t,t') according to eqs. (10) and (14) is given by

$$k(t,t') = 2\int_{t'}^{t} N_3(t'')\, dt'' + N_o \frac{\left(e^{-\gamma t'} - e^{-\gamma t}\right)}{\gamma} - N_o(t - t') \quad . \qquad (17)$$

because of

$$N_4 = N_o\, e^{-\gamma t} \quad . \qquad (18)$$

In the linear region of validity of equations (7) and (8), ignoring the $E^+R^+ + E^-R^-$ terms, the population density eq. (8) lead to

$$N_3 = \gamma \int_0^t e^{-\Gamma(t - t')}\, N_4(t')\, dt'$$

$$= \frac{\gamma N_o e^{-\Gamma t}}{\Gamma - \gamma}\left(e^{(\Gamma - \gamma)t} - 1\right)$$

$$= \frac{\gamma N_o}{\Gamma - \gamma}\left(e^{-\gamma t} - e^{-\Gamma t}\right) \qquad (19)$$

From eqs. (17) and (19) we get

$$k(t,t') = \int_{t'}^{t} \left[2N_3(t'') + N_4(t'') - N_o\right] dt''$$

$$= \frac{2\gamma N_o}{\Gamma - \gamma}\left[\frac{e^{-\gamma t'} - e^{-\gamma t}}{\gamma} - \frac{e^{-\Gamma t'} - e^{-\Gamma t}}{\Gamma}\right] + N_o\left(\frac{e^{-\gamma t'} - e^{-\gamma t}}{\gamma}\right) - N_o(t - t') \quad . \qquad (20)$$

We next consider the modification of eq. (19) for the nonlinear regime. Defining

$$S = -\frac{\partial}{\partial x} \langle E^- E^+ \rangle \quad , \tag{21}$$

it follows from eq. (7b) that

$$S = -g\,(R^+ E^+ + R^- E^-) + \mu E^- E^+ \quad , \tag{22}$$

where the fact that the $R^{\pm}$ and the $E^{\pm}$ commute has been used. From eqs. (8b), (19), and (22) it follows that

$$N_3 = \frac{\gamma N_o}{\Gamma - \gamma}(e^{-\gamma t} - e^{-\Gamma t}) + \frac{1}{g}\int_o^t e^{-\Gamma (t-t')}\,(S - \mu E^- E^+)\,dt' \quad . \tag{23}$$

Now, defining an average N_3 by

$$\hat{N}_3 = \int_o^1 \langle N_3 \rangle\, dx \quad ,$$

eq. (23) can be replaced by

$$\hat{N}_3 = \frac{\gamma \langle N_o \rangle}{\Gamma - \gamma}\,(e^{-\gamma t} - e^{-\Gamma t}) - \frac{1}{g}\int_o^t e^{-\Gamma (t-t')}\, I\,(t')\,dt' - \frac{\mu}{g}\, I_2 \tag{24}$$

where

$$I_2 = \int_o^t e^{-\Gamma (t-t')} \int_o^1 \langle E^- E^+ \rangle\, dx dt' \quad .$$

For $\mu = o$ the last term in eq. (24) disappears and the solution to the problem can be written as an iterative procedure in terms of I(t), the intensity at right side of cavity. For finite values of μ the third term describes a loss due to absorption in the medium.

The third term in eq. (24) will be small for small values of μ. For larger values, an approximation in which the integral of $\langle E^- E^+ \rangle$ is taken to be proportional to the radiation intensity I can be used. Then (24) can be replaced b

$$\hat{N}_3 \sim \frac{\lambda \langle N_o \rangle}{\Gamma - \lambda}\,(e^{-\lambda t} - e^{-\Gamma t}) - \frac{\beta}{g}\int_o^{\tau} e^{-\Gamma (t-t')}\, I\,(t')\,dt' \quad , \tag{25}$$

where

$$\beta = 1 + \mu \bar{l}$$

and $\bar{l}$ is an appropriate length lying between 0 and 1. It has to be determined from test runs on convergence ($\bar{l}$ = 0.1 and 0.025 were found convenient for our runs).

Using eq. (25) instead of eq. (19) in the calculation of $k(t, t')$ and iterating with (16) gives us the solution to the nonlinear problem. Appendix B discusses the numerical approach used in implementing the solution.

C. DISCUSSION OF RESULTS

With reference to eq. (16), we can analyze the effects of

(1) Transitions competing with the SF transition. In this paper we have concentrated on the first two effects. The modification of the SF pulse due to finite pumping time will be treated in a subsequent publication. Competing transitions such as emission with recoil characterized by the recoilless fraction *f* and electron ejection from the nucleus as characterized by the internal conversion coefficient α, as well as other processes characterized by the branching ratio β, although quite different physically, are treated similarly here. It is assumed that their sole effect is to reduce the inverted population,

(2) Electronic absorption, as characterized by the linear extinction coefficient μ, and

(3) The finite pumping time to obtain the required inversion.

There are two first-order effects expected from a finite linear extinction μ. One effect is clearly expected from eq. (16), because of the exponential factor $e^{-2\mu x'}$ which attenuates the beam as it traverses the medium. This would be exhibited in the experimental results as a decrease in the intensity of the emitted superfluorescent pulse. The other effect is a result of the suppressed development of the electric field as expressed by eq. 7. For increasing values of μ, one expects that a longer time would be required for the generation of a large enough E to initiate the SF pulse. This would be observed experimentally as an increase in the time delay, τ_D.

Equation (16) was used to calculate the pulse shape as a function of the decay rate Γ and the linear attenuation coefficient μ for $\mu = 0$. Figure 2 shows the variation in the lineshape as Γ is varied. Notice the expected decrease in the peak intensity and the shift in the peak position as Γ increases. Figure 3 shows the variation in the pulse shape as a

function of μ. Notice again the decrease in intensity, increase in the delay time, and broadening of the pulse as μ increases.

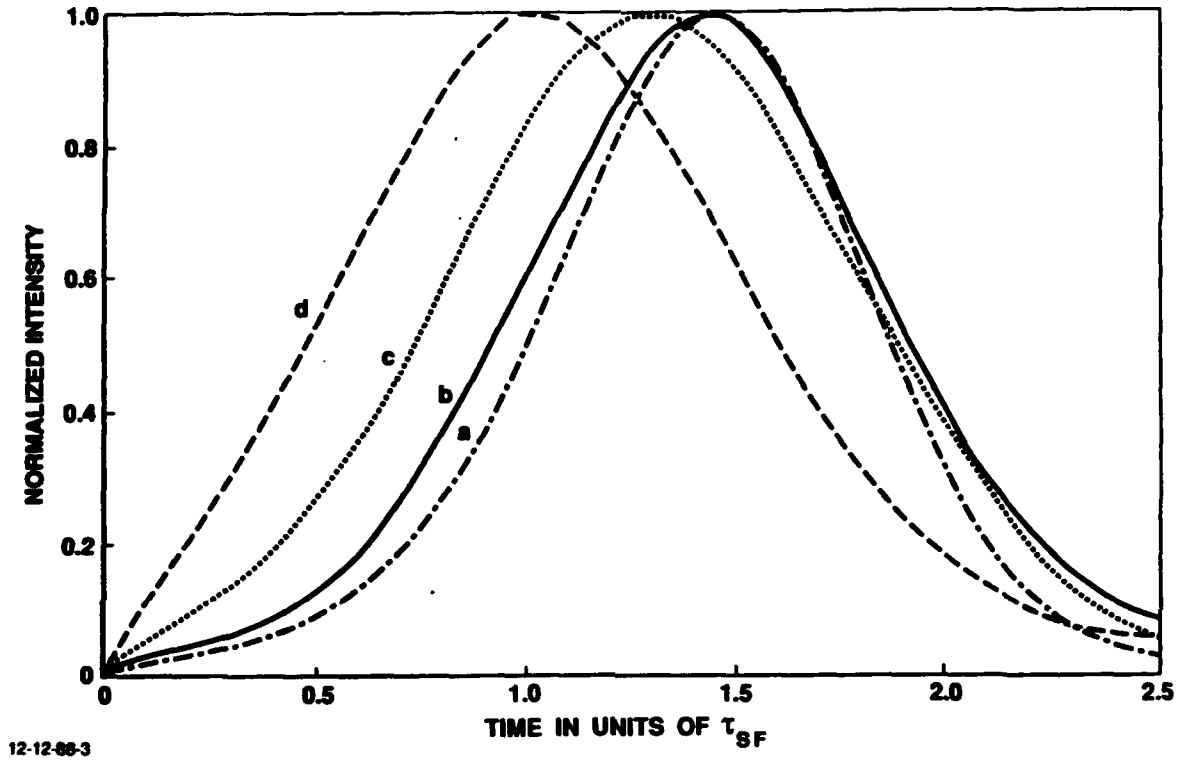

Figure 2. Superfluorescent pulse calculated with $\gamma = 5\,\tau_{SF}^{-1}$ for $\mu = 0$ and different values of Γ. Curves are all normalized to the curve label (a). The Γ values and the relative intensities I_m (parentheses) are:
(a) $\Gamma = 0.01$ (1.0)
(b) $\Gamma = 0.2$ (0.61)
(c) $\Gamma = 0.5$ (0.30)
(d) $\Gamma = 1.0$ (0.19)

It is instructive to compare the effect of μ on lasing and superfluorescence. These are different phenomena that have been unified in a theoretical description (Ref. 19) but can be differentiated experimentally as observed by Okada et al. (Ref. 20). In their experiments, the onset of superfluorescence was preceded by amplified spontaneous emission pulses as the inversion density increased.

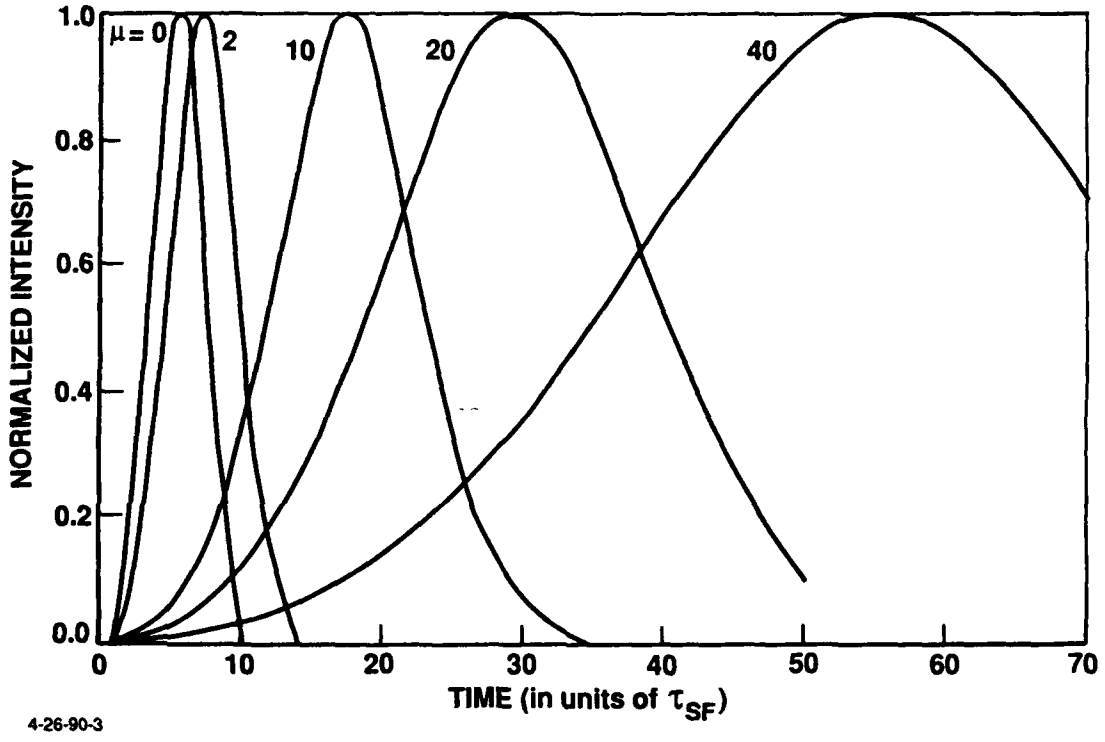

Figure 3. Superfluorescent pulses calculated using the program described in Appendix B for $\gamma = 50\,\tau_{SF}^{-1}$, $\Gamma = 0.001\,\tau_{SF}^{-1}$, $g_1 = 1.0$ and different values of μ as indicated next to the curves in the figure. The curves are all normalized to 1. The relative intensity values are 0.16, 0.11, 0.037, 0.0074 and 0.00073 for increasing values of μ.

Our study shows that the effect of beam attenuation (characterized by the linear attenuation coefficient μ) on the development of lasing is different than its effect on the development of a superfluorescent pulse. The stimulation cross section σ_s, inversion Δn^* [$= f(x, t) = N_3 - N_1$ as in eq. (7a)] and μ are coupled in a linear relation forming the gain coefficient k which characterizes the lasing phenomena. The Schawlow-Townes condition for lasing demands that the gain coefficient $k = \sigma_s \Delta n^* - \mu > 0$ in order for lasing to take place. The gain in a system exhibiting amplified spontaneous emission (ASE) is given by

$$G = \frac{e^{kl} - 1}{kl} .$$

For $k > 0$ gain is observed, but for $k < 0$ only attenuation of the beam traversing the medium is possible. In SF inversion Δn^* and attenuation μ interact through the nonlinear relationship given in eqs. (1-3) and thus their combined effect on SF is more complex.

For SF, inversion ($\Delta n^* > 0$), is required to promote the development of the polarization from the quantum fluctuation, eq. (7), but the effect of μ on the development of E is only to delay the SF pulse and modify its shape but not prevent it if other effects

such as competing processes do not destroy the inversion. This can be seen from the solution of eq. (7b) which can be written as

$$E_{31}^{\pm}(x) = E_{31}^{\pm}(0)\, e^{-\mu x} + \int_0^x e^{\frac{1}{2}\mu(y-x)}\, g_1 R_{31}(y)\, dy \ .$$

For large μ the first term is unimportant and only regions of the integral for $y \approx x$ contribute. However, there is a gradual decrease and not a sharp cutoff or threshold. Further quantitative investigation of this phenomenon with the complete theory is necessary.

The pulse shape as a function of initial inversion and the linear attenuation coefficient μ for amplified spontaneous emission and superfluorescence are compared in Appendix C. These results were obtained assuming instantaneous inversion. In general, the ASE lineshape peaks at the natural lifetime and only the relative intensity decreases as the initial inversion Δn^* or μ decrease. For SF, in addition to these effects, the lines broaden and shift to later times as Δn^* and μ decrease. For high inversion and low attenuation, the SF peak is much narrower than the natural lifetime τ and appears much earlier than the ASE pulses.

The effect of the linear attenuation coefficient (on the SF pulse shape) has been considered as arising from the limitation on the effective cavity length L, and thus on the maximum number of cooperating emitters N (Ref. 21). This effect would be observed as an increase in the delay time τ_D, an increase in the width of the pulse τ_R and a decrease in the intensity of the pulse. The inverted pendulum expression for the SF pulse could then be modified to take this into account by assuming that N, τ_R, and τ_D are functions of μ, and the pulse is given by

$$I(t) = \frac{N(\mu)}{2\tau_R(\mu)}\, \mathrm{sech}^2\left[\frac{1}{\tau_R(\mu)}\left(t - \tau_D(\mu)\right)\right] \ . \qquad (26)$$

The effect of μ in eq. (26) is assumed to be in decreasing the active volume by a factor of $\frac{\theta}{\mu}$, where θ is an *ad hoc* parameter.

It is interesting to compare the results from the reduced effective volume assumption represented by eq. (26) with the results obtained with the modified Maxwell-Bloch equations, including random sources [eqs. (7a, 7b and 8a, 8b, 8c)]. We assume that the modified Maxwell-Bloch equations model SF from an incoherently pumped two-state

system correctly while eq. (26) provides a simpler intuitive but *ad hoc* model. The SF pulses obtained from eqs. (7, 8) for five values of μ are plotted in Fig. 3 with all peaks normalized to 1.0 independently. The widths, intensities, and delay times of these pulses are given in Table 1.

Table 1. Pulse Parameters Derived from Figure 3

μ	τ_D	I	W	A
0	6	0.16	5.0	0.80
2	8.5	0.11	6.5	0.72
10	18	0.037	13.5	0.50
20	29	0.0074	23.0	0.17
40	55	0.00073	46.0	0.034

μ = attenuation coefficient
t_D = delay time
I = intensity
W = width
A = area under peak (I x w)

The delay time is increased because the effective length L of the active region is decreased to $L' \approx \frac{L}{\mu}$ for $\mu >> 1$. In Figure 4 we compare the delay times τ_D calculated from equations 7 and 8 (pulses shown in Fig. 3) with those computed by assuming a reduction in cooperation number from an increase in μ given by $\bar{\tau}_D = \frac{K(\mu + 1)}{N_o} \ln\left(\frac{N_o}{\mu + 1}\right)$.

The horizontal arrows in Fig. 4 indicate the reduction in μ required for $\bar{\tau}_D = \tau_D$ and values of θ give the actual reduction factors. In Figure 5 we plot $\frac{1}{A}$ and $\frac{\mu}{\theta}$ as a function of μ to compare the total emission calculated from the equations 7 and 8 with the expected emission if the total volume of cooperating nuclei were decreased by $\frac{1}{\mu + 1}$. A reduction parameter of $\theta = 3.1\text{-}6.7$ for $\mu = 5$ to 20 represents consideration of an effective average

length corresponding to the notion that not all the photons travel the total length of the cavity.[7] These findings compare qualitatively with the results of MacGillivray and Feld (Ref. 22) who calculated the effect of beam attenuation in order to explain their experimental results on HF gas (see their Fig. 5). Their calculations show an increase in the delay time and a decrease in the beam intensity as the attenuation increases. Specifically for L = 1, $\mu = 2.5\ cm^{-1}$, and $5.0\ cm^{-1}$ their results show about 40 percent and 60 percent increases, respectively, in the delay times from the $\mu = 0$ delay time. Our results (Fig. 5) show larger delay time increases (about twice their amount) but an exact quantitative comparison was not expected because other parameters in the two calculations are different.

---

[7] The reduction parameter of $\theta = 3.1\text{-}6.7$ is obtained from the relationship $e^{-\frac{\mu l}{\theta}} = \frac{1 - e^{-\mu l}}{\mu l}$ when $l = 1$, and $\mu = 5$ and 20.

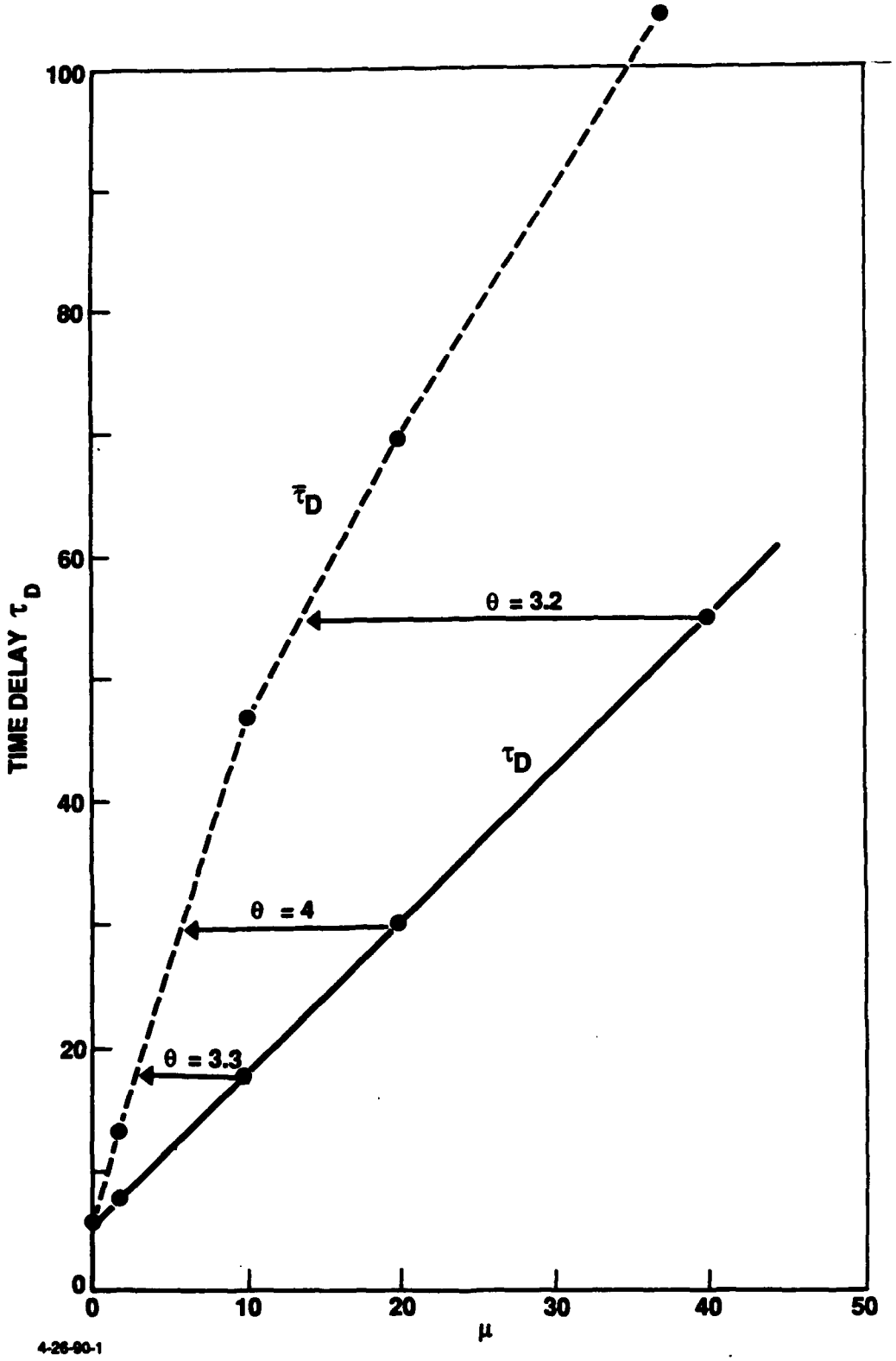

Figure 4. The delay time τ_D (solid line) taken from Fig. 3 for different values of μ and the delay time $\bar{\tau}_D$ (dashed line) calculated assuming μ reduces the cooperative volume plotted as a function of μ. The values of θ represent reduction factors for different μ values so that $\bar{\tau}_D = \tau_D$. The circles show points calculated, the connecting lines are drawn to help the eye follow trends.

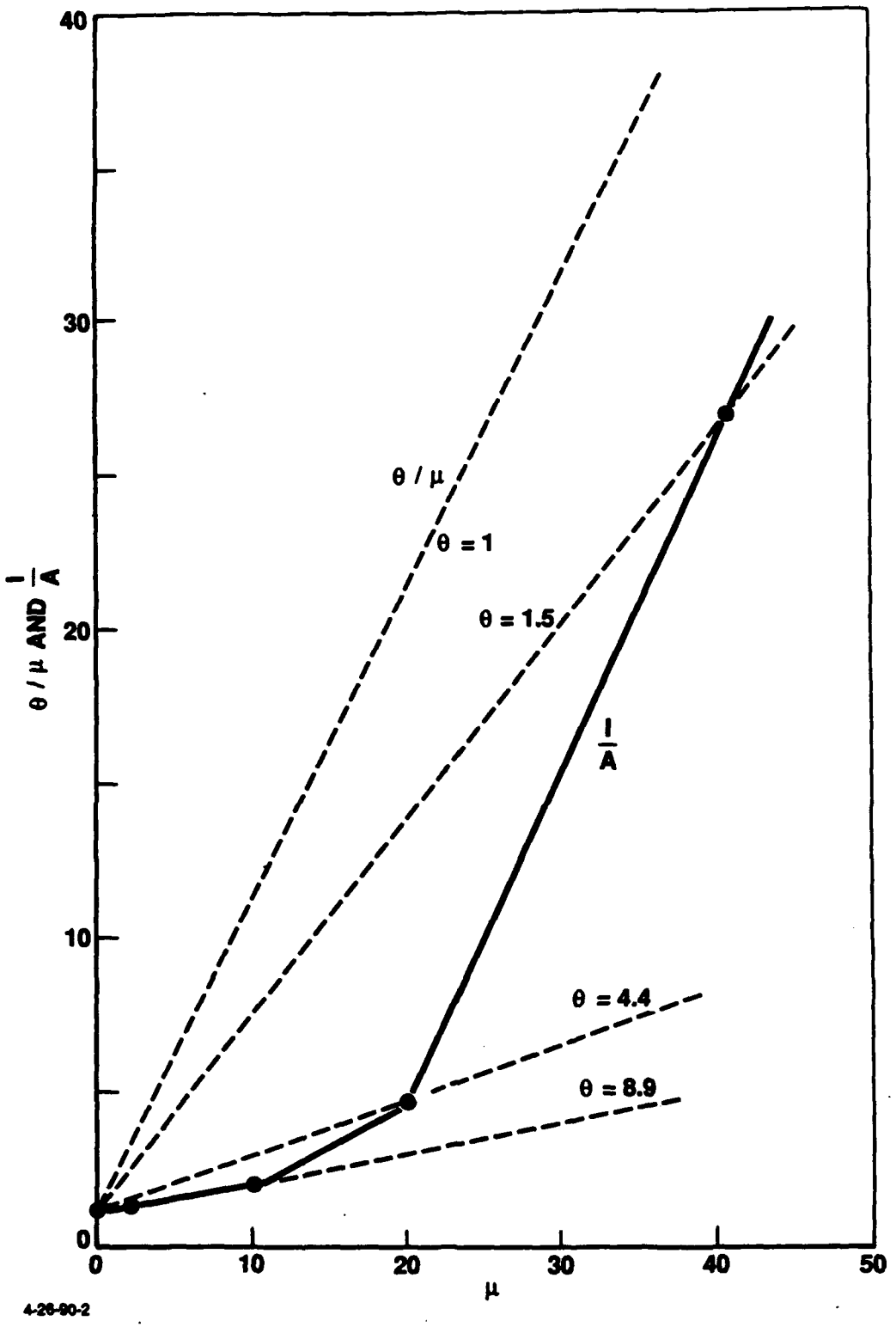

Figure 5. Plot $\frac{1}{A}$ and $\frac{\mu}{\theta}$ as a function of μ for the different pulses shown in Fig. 3. Again the different values of θ represent reductions factors on μ that describe effectiveness of μ in reducing cooperation volume. Circles indicate calculated points, the connecting lines were drawn to help indicate trends.

D. SUGGESTED EXPERIMENTAL INVESTIGATIONS

Our studies on pumping of isomeric levels (Ref. 23) and the nuclear SF calculations discussed here indicate that experiments examining the interaction of the linear extinction coefficient μ, the competing phenomena characterized by Γ_3, and finite pumping times characterized by γ should be undertaken. We propose experiments performed in the optical or longer wavelength regime where SF has already been observed, be undertaken to check the theory developed here. Systems composed of CH_3F, HF, Na, C_s, or Tl could be used for this purpose since SF in them has already been observed. Introduction of varying concentrations of inert gases could be used, for example, to study the dependence of SF on μ in a gaseous medium. Variation in the length and intensity of pumping laser sources could be used to check the effect of the pumping rate γ, and the effect of competing transitions could be studied by controlling the inversion of different transitions through selective population of the lower levels (2 and 1 in Fig. 1), or through manipulation of relaxation rates through temperature or external fields.[8]

The second set of experiments we propose deal with nuclear transitions and the observations of modifications of the nuclear decay rates. These experiments can be done with the isomers identified in Ref 22. Pumping by thermal neutrons to produce inversion in a symmetric sample would be followed by observation of the total count rate from the isomeric level using a 4π detector to catch most of the radiation. Although non-cooperative emission would probably predominate, and only properly oriented and prepared small regions of the sample may produce SF pulses, these may be enough to be observed through decay curve modifications. We expect these experiments with arbitrary sample geometries would be much easier than single-whisker experiments usually described in the literature. Further, more detailed discussions of these two types of experiments will be presented elsewhere in future publications.

E. CONCLUSIONS

We have identified several features of nuclear transitions and radiation transfer through materials which have to be incorporated into an SF theory in order to determine the feasibility of nuclear SF. The Haake-Reibold model of SF was generalized to treat transport phenomena and used to study the effects of competing transitions, electronic

---

[8] Further discussions of the effects will be left to future publications.

attenuation of the photon beam, and finite pumping time on the development of SF pulses. It was determined that the electronic attenuation slows down the development of the SF pulse (increases τ_D) and lowers the emitted intensity but does not produce a hard threshold on SF as it does on ASE, as characterized by the Schawlow-Townes gain requirement. The competing transitions like (1) internal conversion, (2) branching transitions producing the emission of photons, and (3) γ emission with recoil (non-Mössbauer transitions) reduce the SF intensity but do not affect a strong shift in the pulse emission time until the rate of these processes approaches the SF delay time. All of these predictions, as well as the effect of the finite pumping time and geometry should be investigated further.

Finally, as a way of investigating the effects of electronic attenuation, competing transitions, and finite pumping time on SF, we propose that experiments at longer wavelength be performed using systems and conditions under which SF has been observed. Such experiments could be much more easily performed than nuclear experiments and would be valuable in verifying the theoretical results presented here.

II. SHORT WAVELENGTH SUPERFLUORESCENCE

If wavelengths associated with nuclear transitions are smaller than interatomic spacings, efficient radiation can only occur when conditions for Borrmann mode propagation are satisfied. Since superfluorescence is also necessary, the effect of wavelengths shorter than interatomic spacings on superfluorescence is also of interest. In particular, it is of some interest to determine the extent to which conditions for superfluorescence at short wavelengths may be in conflict with those for Borrmann mode propagation.

As observed in the introduction to Chapter I, in nuclear superfluorescence wavelengths associated with transitions of interest will, in fact, be smaller than the spacing of the contributing nuclei. The behavior of a similarly spaced classical periodic array of coherent sources suggests that for a potentially superfluorescent crystal, regarded as an array of identical nuclei, a first-order effect of such a short wavelength would be to limit collective radiation to certain directions. In fact, the relatively simple model of atomic super-fluorescence due to Bonifacio and Lugiato (Refs. 4 and 24) has sufficient scope to confirm the existence of such an effect.

The Bonifacio-Lugiato superfluorescence model for two-state atoms in a rectangular crystal lattice, as elucidated in Refs. 4 and 24, considers only the case in which the emitted radiation wavelength is larger than the atomic spacing. However, this limitation is not inherent in the model, despite its simplistic treatment of propagation and other possible geometrical effects.

Reference 25 treats the case of nuclear transitions, for which the wavelength is smaller than the atomic spacing, but the paper's discussion of superfluorescence is less informative than that of Refs. 4 and 24. This is partly because the Bonifacio-Lugiato model uses a representation for the collective excitation operator that relates it to the lattice structure, whereas Ref. 25 uses a representation that relates the operator to the phase of the emitted photons at the lattice sites.

In particular, when the wavelength of the emitted radiation is less than the atomic spacing, the B&L model implies that superfluorescence can only occur when the

wavelength and the crystal lattice structure are related in a certain way. In fact, the required relation is also sufficient for coupling of the emitted radiation to a Borrmann mode.

Reference 26 gives an analysis of superradiance that, like the B&L model, relates the collective excitation to the lattice structure and should therefore be capable of yielding the short wavelength superfluorescence conditions. Because its treatment includes more geometrical detail than the treatment of Refs. 4 and 24, for the long wavelength case Ref. 26 is, in fact, able to relate the spatial pattern of the radiation emitted by the collective atomic array to the characteristic shape of the active volume. The analysis of Refs. 4 and 24, however, is restricted to the case in which the active volume is a thin needle.

On the other hand, Ref. 26 shows that the needle shape provides the maximum gain, albeit in a single direction. Thus, to the extent that it is possible to implement, the needle is presumably the preferred shape for a superradiant structure. Therefore, it seems useful to consider the consequences of the B&L model for the short wavelength radiation that characterizes the nuclear case.

The interaction Hamiltonian originally introduced by B&L has the form

$$H_I = \frac{i\hbar}{\sqrt{V}} \sum_{j=1}^{N} \sum_{\mathbf{k}} g_{\mathbf{k}} \left\{ a_{\mathbf{k}}^{\dagger} r_j^{-} \exp\left[i (\omega_o - \omega_j) t - i\mathbf{k}\cdot\mathbf{x}_j \right] - \text{H.C.} \right\} , \qquad (27)$$

where $\mathbf{k}$ is the emitted photon wave vector for a particular mode, $\mathbf{x}_j$ is the position vector of the j^{th} lattice site, $a_{\mathbf{k}}$ is the corresponding photon creation operator, ω_o is a mean reference frequency, and r_j^{-} is the de-excitation operator for the atom at the j^{th} lattice site. B&L also define the reciprocal lattice vectors α, each component of which has the form $(2\pi/L)n$, $n = 0, 1, ..., N-1$, where L is the corresponding lattice dimension. They define the collective excitation and de-excitation operators $R^{\pm}(\alpha)$ as functions of α by

$$R^{\pm}(\alpha) = \sum_{j=1}^{N} r_j^{\pm} \exp(\pm i\, \alpha \cdot \mathbf{x}_j) , \qquad (28)$$

from which it can be shown that

$$r_j^{\pm} = \frac{1}{N} \sum_{\alpha} R^{\pm}(\alpha) \exp(\mp i\, \alpha \cdot \mathbf{x}_j) . \qquad (29)$$

On substituting eq. (29) into eq. (27) it follows that

$$H_I(t) = \frac{i\,h}{\sqrt{V}} \sum_{\alpha} \sum_{K} g_k \left[a_k^{\dagger} R^{-}(\alpha)\, f^*(k - \alpha, t) - H.C. \right] \quad . \tag{30}$$

where

$$f(\eta, t) = \frac{1}{N} \sum_{j=1}^{N} \exp(i\eta \cdot x_j) \exp\left[i(\omega_j - \omega_o)\, t \right] \quad . \tag{31}$$

The time-dependent factors in eq. (31) are separated out on the assumption that they can be replaced by an average over all atoms and that, because the frequencies ω_j associated with the individual atoms are uncorrelated, they can be removed from $f(\eta, t)$ and subsumed in the coupling constant g_k, which then becomes time dependent. This time dependence of g_k is a way of introducing inhomogeneous broadening.

At this point, B&L introduce the assumption that the atomic spacing, given by

$$d = L/N \ ,$$

is much smaller than the photon wavelength, which implies that the function $f(\eta)$ (wherein the time dependence is no longer indicated for the reason just noted) is large when η vanishes and is otherwise small. However, if this assumption is not made then $f(\eta)$ will be large whenever $\eta \cdot x_j = 2\pi\upsilon_j$, $\upsilon_j = 0, \pm 1, \ldots$ and otherwise small.

The interaction that results in photon emission when cooperative de-excitation of the atoms takes place can only occur when $f(k - \alpha)$ in eq. (30) is not negligible for some value of k and α, i.e., when

$$(k - \alpha) \cdot x_j = 2\pi\upsilon_j \quad , \tag{32a}$$

where υ_j is in the set: $0, \pm 1, \ldots$, which implies that

$$d/\lambda - n/N = \upsilon, \; n = 0, 1, \ldots, N - 1 \quad , \tag{32b}$$

where υ is in the set: $0, \pm 1, \ldots$. In eq. (32) it is tacitly assumed that the propagation direction is along a narrow, needle-shaped active volume, in which only a single plane wave photon mode is supported. More generally, λ should be interpreted as λ_j the photon wavelength divided by the component of the unit vector in the propagation direction along the lattice direction defined by the x_j.

It follows from eq. (32b) that the possible values of υ must be non-negative. Thus,

$$\lambda_j = L/(N\upsilon_j + n_j),\ 0<n_j<N,\ \upsilon_j \geq 0\ . \tag{33}$$

On setting $\upsilon_j = 0, 1, \ldots$ in succession it follows from eq. (33) that for $\upsilon_j = 0, \lambda_j > d$, for $\upsilon_j = 1, d > \lambda_j > d/2$, for $\upsilon_j = 2, d/2 > \lambda_j > d/3$, etc. That is, for any given photon wavelength one and only one value of υ exists that will satisfy the required condition.

Reference 25 gives as the condition for a Borrmann mode the relation

$$|\mathbf{k} - \alpha| = |\mathbf{k}| \tag{34}$$

for some reciprocal lattice vector α. To satisfy eq. (34) it is sufficient that $\mathbf{k} = \alpha'$ for some reciprocal lattice vector α',[8] a condition that eq. (33) implies. That is, the condition implied by the B&L model for superradiance in a crystal is sufficient for coupling to a Borrmann mode, the propagation direction of which will be determined by the ratio of the wavelength λ to the atomic spacing d in accordance with eq. (33).

---

8 Then, e.g., $\alpha = 2\alpha'$ will satisfy (34).

III. USE OF A HEAT SINK TO PROTECT THE LASING MATERIAL AFTER UPCONVERSION

A. INTRODUCTION

It has been recognized for a long time that heating during the pumping stage would pose a serious problem for a γ-ray laser (Ref. 27). Avoiding high temperatures is crucial, since the Mössbauer Effect will be needed to preserve coherence among the photons. This restricts the temperatures of operation to well below the Debye temperature. One recent proposal to get around this suggests looking for an isomer with a nearby state at slightly higher energy (Ref. 28). The isomer can be slowly pumped without heating problems, and the lasing then triggered by rapid "upconversion" to the nearby state. This would lead to a single-pulse laser.

We have shown previously that upconversion with 100 eV to 10 keV photons will lead to catastrophic heating via the photoelectric effect (Ref. 29). We have also presented preliminary calculations which indicate that the heat cannot effectively be conducted away (Ref. 30). In this paper we show that the heating problem gets progressively more severe with decreasing photon energy all the way down to the ionization threshhold. Furthermore, in this chapter and the next we confirm that conductive cooling of the lasing material does not appear to provide a solution. The essence of the problem is that heat sinks with sufficient heat capacity to store the heat from the photoelectric heating of the lasing material are so large they generate and trap enough photoelectrons themselves to heat up to temperatures where they are useless.

Before presenting the calculations in the next section, the physics underlying the results will be sketched. There are three dimensionless ratios that largely control heating effects. The first is the ratio of the energy required per atom to melt a sample or heat it to the Debye temperature compared to the energy of the nuclear excitation in the upconversion. Specific heats of melting are orders of magnitude smaller than the lowest known nuclear transition energy (73 eV). We will consider energies as low as the inonization threshold, but these energies are still large compared to the energies required for melting or heating to the Debye temperature.

The second and third ratios characterize the relative probability of upconversion of the nucleus versus photoionization of the atom. For ideal beams tuned to the nuclear resonance energy, the relevant ratio would be the photoelectric cross section divided by the nuclear resonant cross section. For ordinary nuclear transitions, involving keV energies or greater, very small leakage of the upconversion energy will destructively heat the sample consequently. For very low energy transitions, should any exist, nuclear resonance cross sections are very small, and the photoelectric cross sections comparable or even larger. More energy goes into photoelectric heating than into nuclear upconversion.

Finally, in the real world, photon beams have finite widths. These beams are very broad compared to the nuclear states. The ratio of the photoelectric excitation to nuclear excitation will always be higher that the ratio of photoelectric to resonant cross sections by approximately the ratio of beam width to resonance width. For current beams, this leads to enormous effective increase in the photoelectric cross section.

Addition of a heat sink to conduct away the energy fails because the heat sink itself is heated to high temperature by photoelectrons produced within either the heat sink or the lasing material. Basically, viewed as a function of the radius of the heat sink, by the time the heat sink is large enough to handle the heat and electrons from the lasing material and still remain at low temperature, it is so large that the direct photoelectric heating of the heat sink is fatal.

B. CALCULATIONS

We want to consider the temperature rise in a heat sink used for temperature control of the lasing material in a γ-ray laser. The essential properties of the heat sink are good thermal conductivity and low photoelectric cross section, with the latter being most important. For this reason, we have considered lithium as our heat sink material. For the lasing material we continue to base our model on the 14.4 keV Mössbauer transition in Fe^{57} (Ref. 29). Note the calculations use the solids with the lowest photoelectric cross section and the highest Debye temperature, which is the optimum combination.

In this section, we will compute the temperature of a Li heat sink itself, under various assumptions about the upconversion transition in the lasing material. There are four sources of heat. First, heat produced by the photoelectrons in the iron which is conducted to the heat sink. Second, if the photon energy is high enough, the photoelectrons produced in the Fe will not be trapped there. They will continue out into the Li, where they will continue to deposit energy. Assuming no change in dE/dx, the energy

deposition will be linear in the path length in the lithium. The energy deposition per atom, or the temperature increase, will vary as the reciprocal of the diameter of the heat sink. These first two contributions favor a large heat sink. The direct heating due to photoelectrons produced within the lithium itself increases quadratically with the diameter of the heat sink, and favors a small heat sink. Finally, as the residual ion from which the electron was removed returns to its gound state, energy from photons and Auger electrons is deposited. These contributions are assumed to have radiation lengths characteristic of 100 eV photons, and have a total energy deposition limited to the initial photon energy minus the photoelectron energy.

The baseline calculation assumed a 0.01μ Fe wire embedded in a Li heat sink. Borrmann reduction of the photoelectric effect by a factor of 100 was assumed for both materials. The probability of upconversion of the Fe^{57} was held constant at 1 percent. The basis for these choices is described in Ref. 29.

Assuming the number of lithium atoms is large compared to the iron atoms, the total energy deposited per atom of Li,Q, can be written

$$Q = P_{PE}\left[\left(\frac{dE}{dx}\right)_{Fe}\frac{a_{Fe}}{2}\left[\left(\frac{a_{Fe}}{a_{Li}}\right)^2\left(\frac{\rho_{Fe}}{\rho_{Li}}\right)\right]\right.$$
$$+\left(\frac{dE}{dx}\right)_{Li}\frac{a_{Fe}^2}{a_{Li}}\frac{\rho_{Fe}}{\rho_{Li}}\Big)$$
$$+\frac{\mu(Li)\,a_{Li}}{\mu(Fe)\,a_{Fe}}\left(\frac{dE}{dx}\right)_{Li}\frac{a_{Li}}{2}$$
$$\left.+\,(E_\gamma - E_e)\,(1-\exp(-a_{Li}/a_{RAD}))\right].$$

P_{PE} is the probability of producing a photoelectron per iron atom in the lasing sample. For a given size iron sample, this depends on the beamwidth, and the energy of the transition. $dE/dx)_y$ is the energy lost by the electron per unit length in material y (Ref. 31). Technically, the two values for Li should be different, since iron and lithium produce different energy photoelectrons. The smaller value was used in all cases in keeping with our neglect of the increase in dE/dx as the electron slows down. The radius or width of the material y is a_y, and the number density ρy the reciprocal mean free paths for the photoelectrons labeled μ(y), and the radiation length characterizing the low-energy photons and Auger electrons is a_{RAD} (Ref. 31).

In the above expression, the four terms correspond to the four physical sources discussed above. The optimum value of a can be found by differentiation. For incident photons with about 10 keV energy, the second and third terms are dominant. This leads to the approximate result

$$a_{Li} = a_{Fe} \sqrt[3]{\frac{\mu(Fe)}{\mu(Li)} \frac{\rho_{Fe}}{\rho_{Li}}}$$

$$= 0.32\,\mu \quad .$$

A numerical solution to the minimum heating leads to values of a_{Li}/a_{Fe} around 30, so we used a_{Li} = 0.30 μm in these calculations. The overall energy scale is set by the probability of the photoelectric effect occuring per iron atom. This depends on the size of the iron sample, the upconversion percentage, the relative sizes of upconversion and photoelectric cross sections, the Borrmann reduction of the photoelectric effect, and the photon beamwidth. We assume a 0.01 μm Fe sample, and Borrmann reductions of 100 in both Fe and Li. These choices are discussed in our earlier work (Ref. 29). The physical cross sections are known (Ref. 32). The essential remaining parameter is the beam spread, or more properly, the ratio of the beam spread to the width of the nuclear state. We have used 10^6 as our baseline value. By comparison, the width of the 14 keV state in Fe^{57} is seven orders of magnitude smaller than the smallest beam spread ever achieved in this energy region.

Using 10^6 as our value for the ratio of beam spread to intrinsic state width, we find approximately 0.25 eV/atom energy depositon in Li, corresponding to a temperature of around 800 K. This temperature is well above the Debye temperature of any material, and clearly does not represent a solution to the heating problem. Improved beam resolution does allow for a solution. For a beam spread of 10^5 times the intrinsic state width, the heating would be minimal, and the heat sink would work. (See more detailed calcualtion of this case in the next section.) However, the improvements in beam resolution must be accompanied by dramatic increases in intensity before this becomes feasible. Current beams have only a few tens of photons per typical nuclear state width.

As the energy decreases, the photoelectric cross sections increase, except at shell crossings. The rate of energy loss increases, and the width of the nuclear state decreases. These features all tend to make the heating get worse as the energy decreases. For the case under consideration, the peak resonance and photoelectric cross sections are plotted as a function of the resonance energy in Fig. 6. The peak resonance cross section is computed

assuming a nuclear structure matrix element equal to that of the 14 keV transition in Fe^{57}, and incorporating the energy cubed phase space factor in the excitation width and the wavelength squared factor in the cross section.

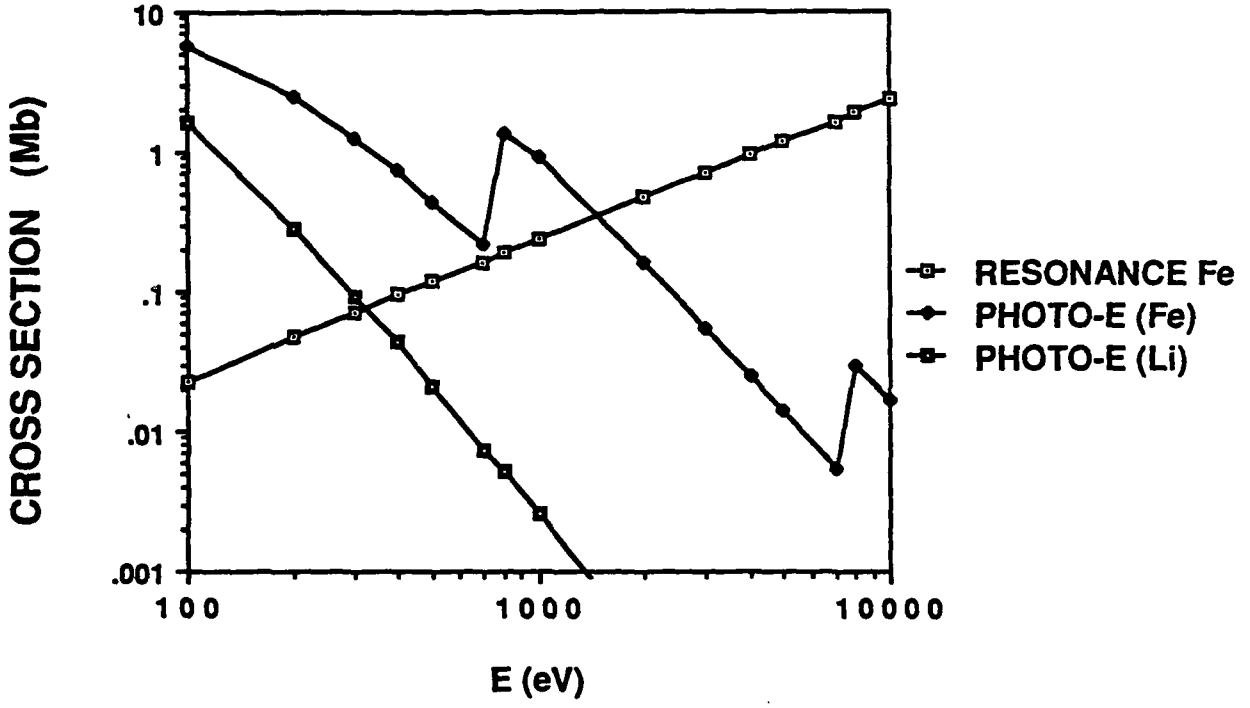

Figure 6. Resonance and Photoelectric Cross Sections

With the exception of the shell crossings, the heating problem gets progressively worse as the energy decreases. Even at the K-shell crossing, the situation is no better than at 10 keV. The next physical threshold at which this situation could change is the ionization threshold, at around 10 eV. Below that energy, it might be possible to upconvert a nuclear state with a laser if such a low-energy nuclear transition existed.

C. CONCLUSIONS

Upconversion of an isomer to a nearby excited state for the purposes of initiating γ-ray lasing has been investigated from the point of view of photoelectric heating of the lasing material. This has long been known to be a serious problem, because it is necessary to maintain temperatures low compared to the Debye temperature in order to exploit the Mössbauer Effect and achieve coherence.

In the 10 keV regime, nuclear resonance cross sections are large compared to photoelectric cross sections. Nevertheless, available beams are so wide compared to nuclear intrinsic state widths that the photoelectric heating would destroy a sample before 1 percent upconversion was possible. This is true even with substantial suppression of the photoelectric cross sections via the Borrmann Effect. To achieve upconversion without excess heating would require a beam with 10^{15} photons/burst with a 0.005 eV spread. As the energy decreases, the requirements on the spectral resolution become more severe, until the ionization threshold is crossed and the photoelectric effect vanishes.

Upconversion of nuclear states in the 10 eV to 10 keV energy regime will not be possible without improvements of several orders of magnitude in both beam intensity and beam resolution. This conclusion cannot be evaded by resort to a heat sink, because any heat sink large enough to remove sufficient heat from the lasing material would be so large that it traps too much heat itself.

IV. BLACKBODY NUCLEAR SPECTROSCOPY

A. INTRODUCTION

One can imagine two approaches to building a γ-ray laser. One could induce decay by manipulating the lifetime of a long-lived state, or one could pump nuclei up to a short-lived state. One difficulty with the second process is that power requirements, and attendant heating and sample destruction problems, make pumping of nuclear levels infeasible. This can be partly evaded by using an isomer, which can be pumped slowly, without excessive heating or power requirements, in order to store most of the energy to be released by the laser. Subsequently, lasing can be initiated by another pumping step, sometimes called upconversion, which is easier to accomplish.

When upconversion from an isomer is examined more closely, it becomes clear that, at least for transitions in the 10 eV to 10 keV region, heating of the sample due to the photoelectric effect is still a problem. We believe this is a solid result, demonstrated by both "back-of-the-envelope" and detailed analyses reported previously. Nevertheless, the result is controversial; we believe this because other workers have asserted that in the 50 keV region heating will not be a problem. We suspect that the heating problem at higher x-ray energies will depend strongly on Z, and may hinge on the feasibility of conductive cooling with low Z materials. These are worthwhile questions for further analysis.

Here, however, we look at the other end of the energy spectrum. Below about 10 eV the photoelectric cross section vanishes because the available energy is below the ionization potential. As a result, the heating will drop precipitously. This has motivated us to consider how one would find nuclear levels with short lifetimes located near isomers. By "near" in this context we mean below the ionization threshold, so we are talking about "optical nuclear transitions."

The existence of nuclear energy levels with short lifetimes lying near longer-lived isomeric levels has not yet been shown experimentally, due to the present limitations of nuclear spectroscopy, but theoretical models anticipate their existence. These short-lived states are essential to proposed two-stage pumping schemes for the development of γ-ray lasers, where the nucleus is "pumped" from the storage isomer to the nearby level from

which the lasing transition can take place. For this reason and for pure research purposes, various studies have been done on possible methods of locating such energy levels.

Previous studies on the feasibility of verifying the existence of these transfer levels have included work done by R.C. Haight and G.C. Baldwin (Ref. 33) of the Los Alamos National Laboratory (LANL), and E.C. Zimmermann (Ref. 34) of the Institute for Defense Analyses (IDA). The Baldwin and Haight study looked at the prospect of using broadband radiation to excite the transfer level. Short pulses of blackbody radiation produced by a laser-target interaction would be used to illuminate the isomer, and a small band of this spectrum would convert the isomer to the transition level. It was concluded by Haight and Baldwin that this method would prove to be too restrictive to be widely useful. In order for a sufficient amount of the isomer to be converted to the transfer level in 10^{-9} s (the length of typical laser pulses), the multipolarity of the transition could only be E1 or M1, the transition strengths would need to be close to the single particle value, and the transition energy would be limited to the range greater than 100 eV for the transition strengths to be large enough and less than 10 k_BT for the photon density to be high enough.

The method proposed by Zimmermann requires heating long-lived Mössbauer isotopes to high temperatures. This should thermally excite a sufficient amount of the isomer to the transfer level to noticeably increase the rate of decay to ground state. An estimate for the value of ΔE (the energy separation between the two levels) could be found by slowly increasing the temperature from 300 K and noting increase in the decay rate with temperature. This method is based on the assumption that rapid thermal equilibration of the two excited states holds, and if this assumption is incorrect, the increase in the decay rate at elevated temperatures might not be noticeable.

This study examines a potential method for locating transfer levels which uses a cavity (either a blackbody cavity or a coherent source cavity) filled with a dilute atomic vapor, containing the requisite isomeric energy levels. A vaporous substance is used so as to avoid unwanted solid-state material effects. The isomers will be illuminated with either the continuous photon spectrum associated with the radiation from a blackbody, or with the radiation produced by a coherent, tunable source (such as a microwave power source or a laser). Either of these methods of photoexcitation should produce an intense photon flux, and both methods would be relatively cheap and easy to use.

For ease of calculation, this study has chosen a doubled count rate as a benchmark value, i.e., a short-lived nearby energy level is assumed to have been successfully located when the induced decay rate is equal to the spontaneous decay rate.

This method, unlike that proposed by Haight and Baldwin, allows for a longer count time and therefore a more gradual heating of the isomer. This study assumes the isomers will be heated to between 1000 K and 5000 K. Unlike the method proposed by Zimmermann, the thermal equilibration is calculated rather than assumed. Another possible advantage to using this method is that the energy of the transfer state need not be known to be within any specific energy range, it can be searched for over a broad range of values. Transfer levels for more than one isomeric level can be searched for simultaneously, as long as the energies of the isomers associated with the various target nuclei are distinct.

For a blackbody cavity, the count rate is given by

$$\frac{dN}{dt} = \int_0^\infty cn_k \, \sigma(k) \, dk \quad ,$$

where cn_k is the photon flux in photons/cm^2·s·Δk, which for a blackbody is

$$cn_k = c\frac{k^2}{\pi^2}\frac{1}{e^x - 1} \quad , x = \frac{\bar{h}ck}{k_B T} = \frac{E}{k_B T}$$

and $\sigma(k)$ is the Breit-Wigner cross section for low-energy photon scattering

$$\sigma(k) = \frac{\lambda\lambda o}{2\pi} \frac{\Gamma_e \Gamma_i}{(E - E_o)^2 + (\Gamma_t/2)^2} \quad ,$$

where Γ_e, Γ_i, and Γ_t are the elastic, inelastic, and total widths; E and E_o are the energies of the particle and the resonance; and λ and λ_o are the wavelengths of the particle and the resonance. Therefore, the count rate is

$$\frac{dN}{dt} = \int_0^\infty \frac{k^2}{2\pi^3} \frac{c}{e^x - 1} \frac{\lambda\lambda_o \Gamma_e \Gamma_i}{(E - E_o)^2 + (\Gamma_t/2)^2} \, dk \quad .$$

We assume that the inelastic width is approximately equal to the total width ($\Gamma \equiv \Gamma_t$), and that the elastic width is

$$\Gamma_e \cong 2.1 \times 10^{-20} E_\gamma^3 \quad ,$$

where E_γ is the decay energy in eV. This assumes an M1 transition with a strength of 1 Weisskopf Unit, characteristic of the expected width of a strong single-particle magnetic dipole transition.

The count rate integral will have non-negligible contributions at k = 0 (E = 0) and at resonance (E = E_o). This motivates us to divide the total contribution into two pieces, i.e.,

$\frac{dN}{dt} = \frac{dN_{res}}{dt} + \frac{dN_{zero}}{dt}$. The motivation for this is that the low-frequency and on-resonance contributions are physically quite different, and the low-frequency modes might be eliminated or damped in a plasma. If possible, we would want to neglect them. This proves to be sensible in the region $4kT < E_0 \lesssim 20$ kT; for E_0 above 4 kT there is a minimum between the zero-energy and resonance "peaks." For E_0 above 20 kT, the exponential decrease of n_k begins to overwhelm the resonance contribution.

Assuming that $(E - E_0) >> \Gamma_t$, (i.e., far off resonance), the zero-energy peak contribution to the count rate is approximately

$$\frac{dN_{zero}}{dt} = \frac{\Gamma_t}{\hbar} (k_B T)^2 (2.1 \times 10^{-20}) \frac{\pi}{3} \quad .$$

This result is obtained by replacing the full expression for $\sigma(k)$ with the zero-energy coefficient of $1/k$, and evaluating the resulting integral analytically. This eliminates the resonance peak at $E = E_0$ from the calculation. Since the enhanced decay rate is inversely proportional to the mean lifetime of the excited state, in order to double the spontaneous decay rate we would need

$$1/\tau_{isomer} = 1/\tau^* (k_B T)^2 (2.2 \times 10^{-20}) \quad ,$$

where $1/\tau^*$ is the reciprocal of the excited state lifetime, which, according to the energy-time uncertainty principle, satisfies the relation $1/\tau \leq \Gamma/h$. Therefore, we have

$$\tau_{isomer} \geq \tau^* (6.1 \times 10^{21}) (1000/T)^2 \quad .$$

Thus, we would require an isomer with a mean lifetime some 20 orders of magnitude greater than the excited state lifetime. In general, the greatest increase in decay rate that could be expected would occur if the M1 transition connected nearby states where the lower state had a primary decay mode of multipolarity M (L + 1) and the upper state decay by multipolarity E (L) (see sketch below).

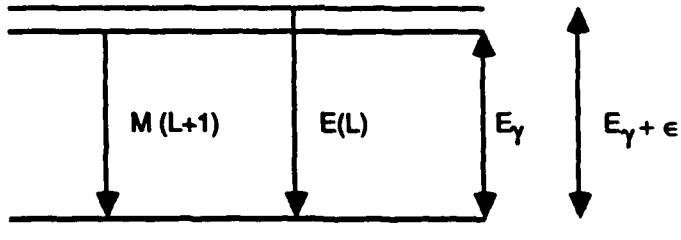

Again, using the Weisskopf estimates we find for the ratio of radiative widths

$$\frac{\Gamma_{E(L)}}{\Gamma_{M(L+1)}} \approx \frac{10^{19}}{E_\gamma^2}$$

if both transitions are of energy E_γ (in eV). In order to achieve the needed enhancement we require

$$\frac{\Gamma_{E(L)}}{\Gamma_{M(L+1)}} \geq 6.1 \times 10^{21} \left(\frac{1000}{T}\right)^2$$

which means that the transition energy of the isomer to the ground state, E_γ, must be

$$E_\gamma \leq \sqrt{\frac{1 \times 10^{19}}{6.1 \times 10^{21}} \left(\frac{T}{1000}\right)^2} \cong 0.1 \text{ eV for } T = 2500 \text{ K} \quad .$$

Grouped states would thus be required in the sense that the isomer and the higher-lying, rapidly-decaying state would both need to be very close to a third state to which they both could decay. This appears sufficiently implausible to us that we will not pursue it further.

The contribution of the decay rate integral from near-resonance (within m widths) is

$$\frac{dN_{res}}{dt} = \int_{E_o - m\Gamma}^{E_o + m\Gamma} cn_k \, \sigma(k) \, dk \quad .$$

Provided only that $k_B T$ is large compared to the total width, n_k can be factored from the expression. The count rate can then be approximated by the full integral

$$\frac{dN_{res}}{dt} = cn_k(k_o) \int_{-\infty}^{\infty} \sigma(k) \, dk = 4 \, (2.1 \times 10^{-20}) \frac{1}{\hbar} \frac{E_o^3}{e^{E_o/k_B T} - 1} \quad .$$

Figure 7 shows the lifetime (reciprocal of the count rate) as a function of the energy for values of the temperature ranging from 1000 K to 5000 K. The increase in lifetime at

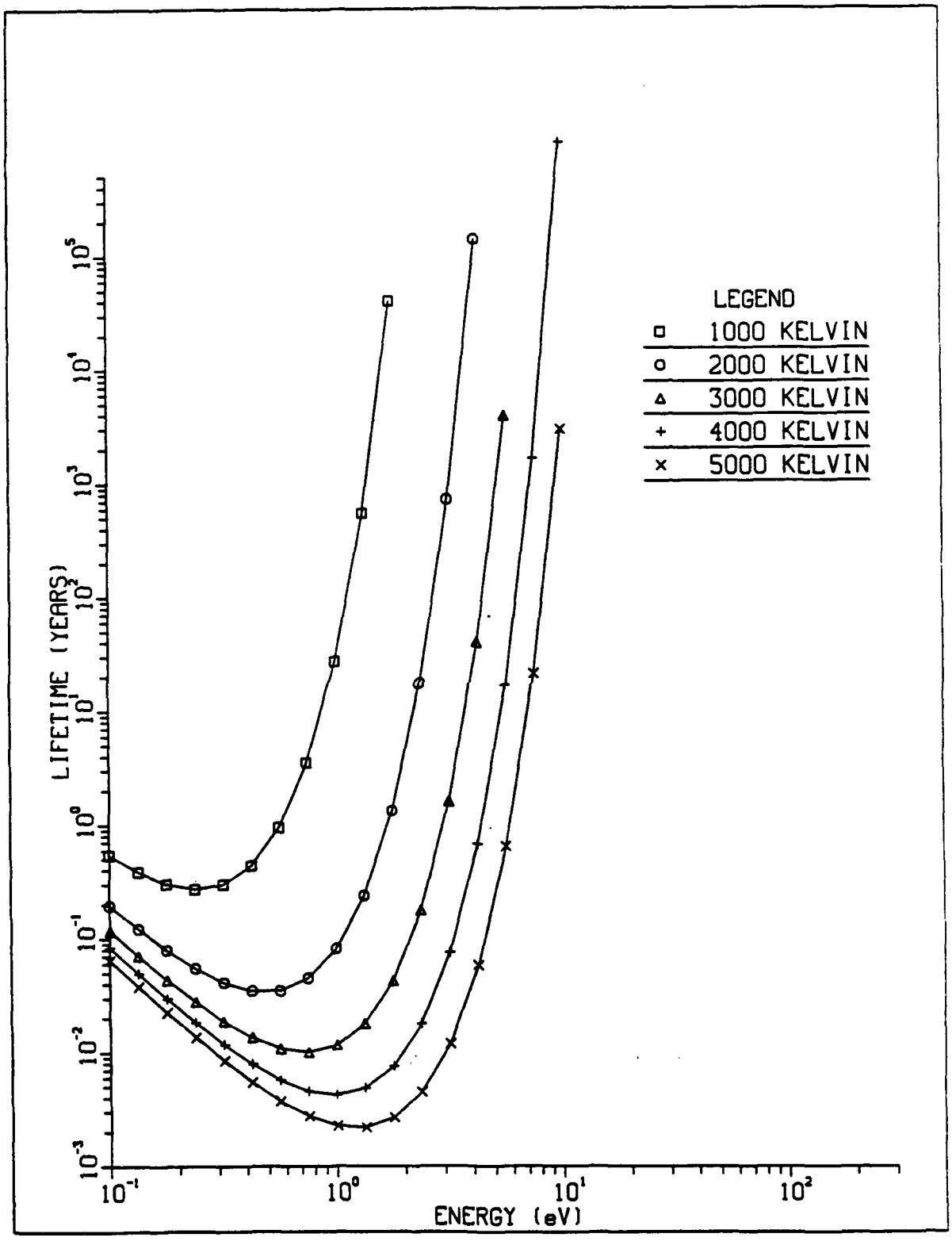

Figure 7. Lifetime vs. Energy for Various Temperatures

lower energies is due to the decrease in the Breit-Wigner cross section which goes to zero as the energy of the transition goes to zero. The increase at higher energies is due to the decreasing photon flux, which is a characteristic of the blackbody curve at high energies. For a blackbody source at 5000 K, an excited state lifetime of 1 year corresponds to an energy of approximately 6 eV. Figure 8 shows the lifetime as a function of the energyfor a blackbody at 5000 K and a blackbody at 50,000 K. This curve supports the Baldwin-Haight conclusion that the use of short pulses of blackbody radiation would not be useful in searching for the desired short-lived energy levels. A lifetime of 10^{-9} s would be well off the bottom of the curve shown, requiring an unreasonably high blackbody temperature. From this we conclude that photoexcitation using a blackbody source would be a useful method for searching for low-excitation transitions, based on an isomer, for energies from 0.1 to 10 eV.

The results of these blackbody calculations can be summarized as follows:

1. The contribution to the excitation is dominated by the photon's near-resonance.
2. A nuclear state approximately 0.1 eV to 10 eV above an isomer could be detected in a blackbody cavity if it had a fairly strong M1 transition connecting it to the isomer. This depends in detail on the strength of the transition and the lifetime of the isomer.
3. These results are consistent with those of Baldwin and Haight in the sense that even at 50,000 K, there is scant probability of a count after 1 ns.

For photoexcitation using a coherent power source (e.g., a microwave power source), we assume that the photon flux follows a Gaussian distribution such that

$$n_k = C_1 \int_{-\infty}^{\infty} e^{-[(k-k_o)/W_k]^2} \, dk \quad ,$$

where C_1 is a normalization constant and W_k is the width of the peak. Integrating over all possible wave numbers, we find that the total photon flux is

$$n_k = C_1 \sqrt{\pi} \; W_k \quad .$$

The energy flux rate is the product of the photon flux and the energy per photon:

$$\text{energy flux rate} = C_1 \sqrt{\pi} \; W_k \, \bar{h} \, c k_o \quad .$$

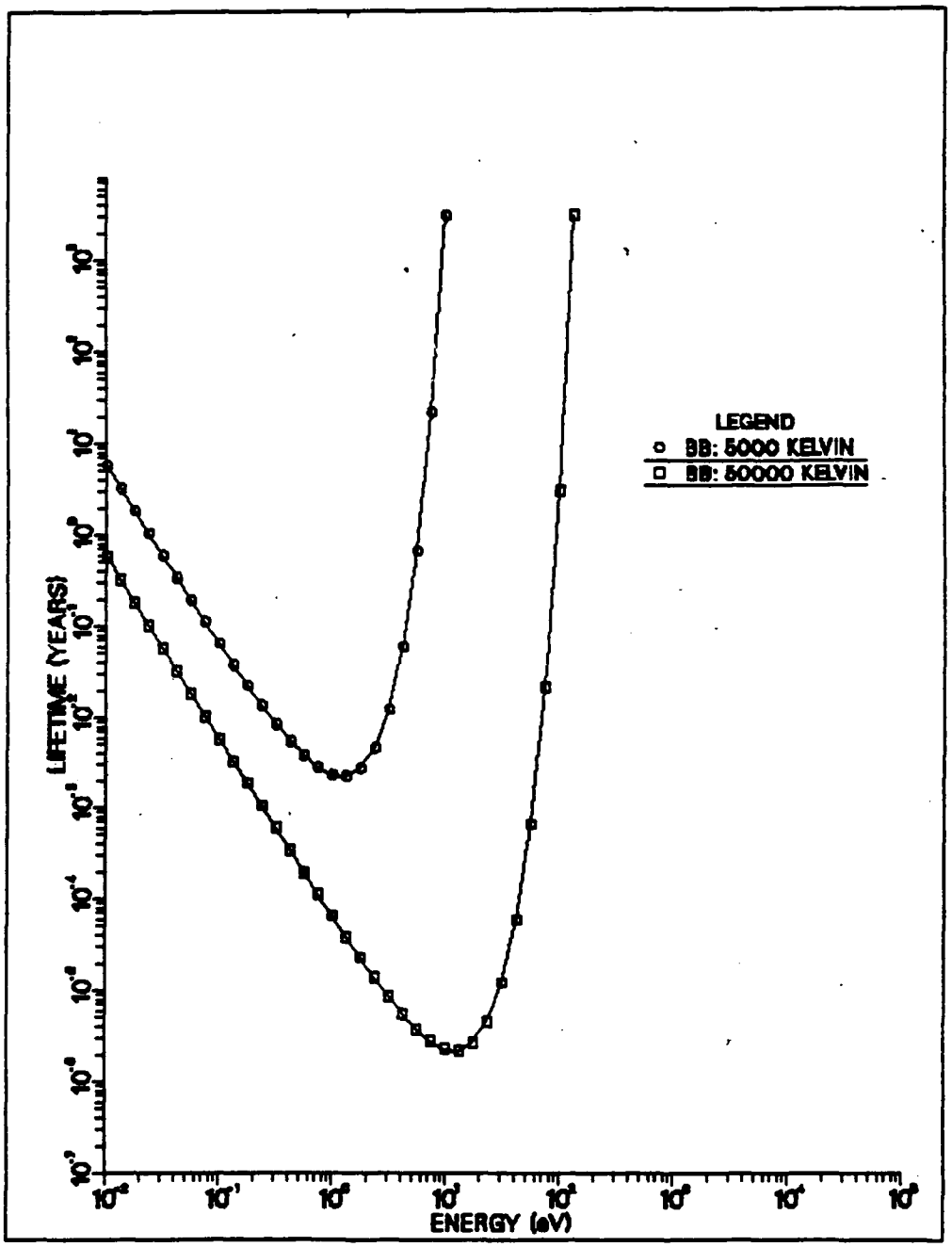

Figure 8. Lifetime vs. Energy for Temperatures of 5000 a:.. 50,000 K

Equating this with the power per cross-sectional area of a microwave cavity, C_1 is found to be

$$C_1 = \left(\frac{P}{A}\right)\left(\frac{1\,eV}{1.60 \times 10^{-19}\,J}\right)\left(\frac{1}{\sqrt{\pi}\ W_k \hbar\, ck_o}\right) .$$

where P is the power of the source in watts, and A is the cross-sectional area of the source cavity. For a 1-kW power source with a cross-sectional area of 100 cm^2, C_1 is approximately $1.78 \times 10^{27}/k_o^2$. One of the factors of k_o comes from the assumption that the width of the peak is a function of k_o (we used $W_k = k_o/1000$) and the other factor of k_o comes from the energy per photon, $E = hck_o$. Therefore, the total induced decay rate corresponding to the use of a coherent power source is

$$\frac{dN}{dt} = (5.24 \times 10^3)\, \pi^{3/2}\, c^2\, h^2 / E_o \quad .$$

The possibility of using other types of coherent sources, such as lasers, should also be considered. Figure 9 shows the lifetime as a function of energy for various types of sources. Included are a 1-kW coherent power source, characteristic of a commercially available microwave, and various types of continuous wave lasers, along with the ranges of energies over which they are tunable.

We find that below about 1 eV a tunable, relatively high energy resolution (i.e., coherent) source would be more effective than using blackbody radiation. At very low energies, microwave sources would suffice. Near 1 eV, IR lasers would be needed. For this search not to be hopelessly tedious, it would be necessary that lasers be available which were tunable over a few percent of their centroid energy, at least. At present tunable lasers are "tunable" over a few natural line widths. This situation is expected to improve, perhaps in the next five years.

B. SUMMARY

Upconversion schemes for a γ-ray laser would be greatly aided by near-degeneracy of nuclear levels connected by an M1 transition of appreciable strength. We refer to such a transition as an optical nuclear transition. We have investigated mechanisms for locating such states. At present, the best technique would be to heat a sample of the isomer in a blackbody cavity and look for enhanced decays as a result of photoexcitation of the nearby state. This would be feasible in the energy region from 0.1 eV to 10.0 eV.

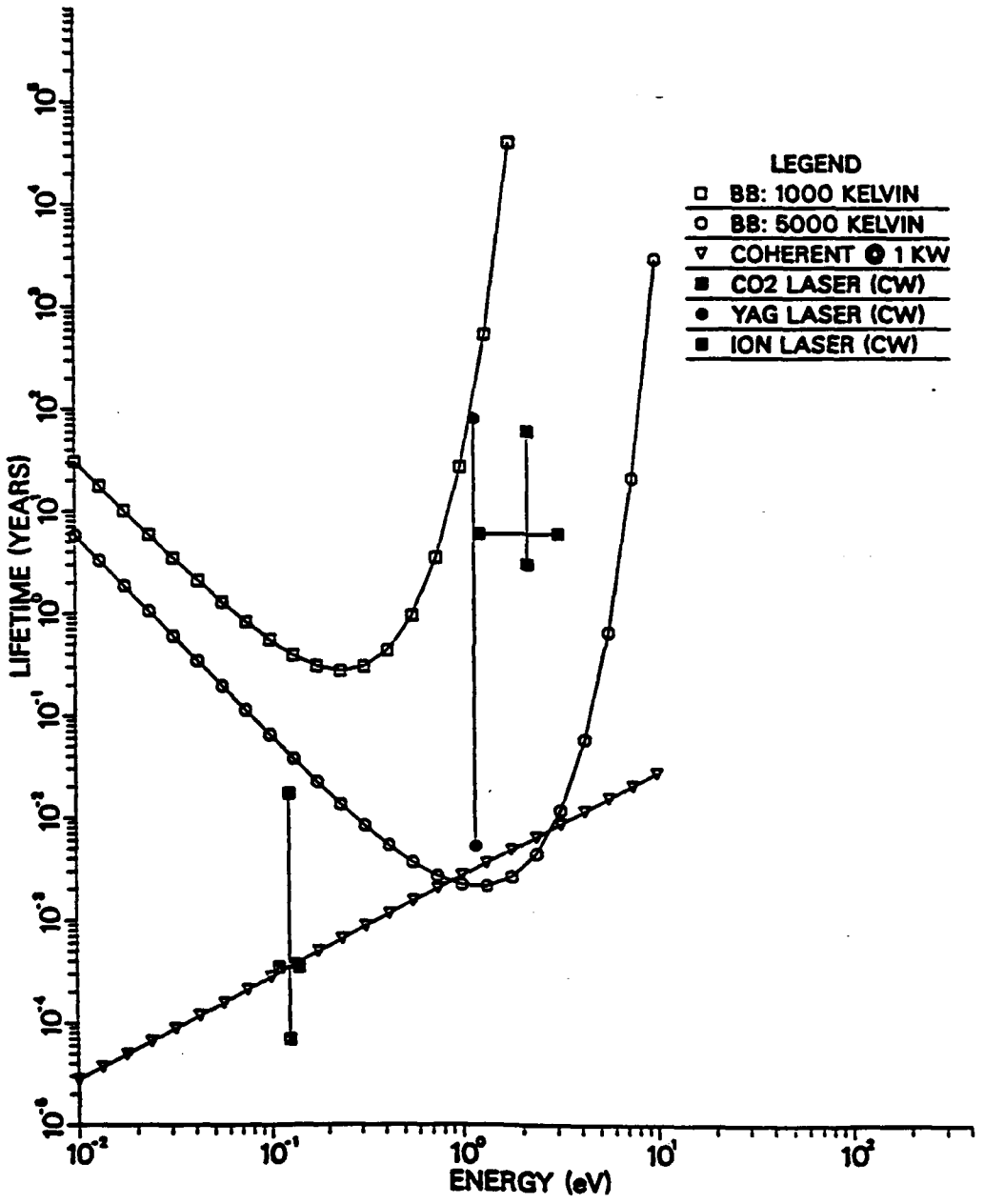

Figure 9. Lifetime vs. Energy for Various Sources

For energies below about 0.1 eV, the cross section is too small for this approach to be feasible. The transition could be driven with commercially available coherent sources, if the energy was right. Coherent sources tunable over a wide range are expected in the fairly near future, at which time the search for optical nuclear transitions could proceed down to very low energy.

The efforts that would be required using coherent sources at present seem unwarranted. Driving the transitions with blackbody radiation, however, should be a fairly cheap, easy experiment which might produce some interesting nuclear spectroscopy, in addition to advancing the feasibility of the γ-ray laser.

V. ENERGY DISSIPATION DURING PUMPING OF γ-RAY LASER

A. INTRODUCTION

Upconversion of an isomeric nuclear level to a short-lived nearby level suitable for stimulated emission is currently the most popular concept for producing inversion in a nuclear system (Ref. 3). The pumping mechanism can be either accomplished through a direct interaction of electromagnetic radiation with the nucleus (Ref. 35) or through an intermediate step involving first laser excitation of electrons followed by energy transfer between atomic electrons and the nucleus (Ref. 36). For both mechanisms, large electronic absorption of the laser beam could produce material modification resulting at least in a reduction of the Mössbauer and Borrmann effects and possibly in destruction of the crystalline structure of the sample. Sparrow (Ref. 37) has estimated the heating effects as a function of pumping beam intensity, width, and energy using thermodynamic arguments. He also calculated the effect of a heat sink in reducing the temperature rise (Ref. 38).

The main purpose of this chapter is to extend the previous calculations of D. Sparrow (Refs. 30, 37, 38) to more realistic geometries, including different material combinations and, most importantly, to calculate dynamic or transient effects and study the approach to steady state. The second purpose is to use a general approach, applicable by a change of one input parameter, to rectangular, cylindrical and spherical geometries, to the analysis of heat conduction problems specialized to the cylindrical case.

This approach is valid for general, time-varying, extended heat sources. This capability will be useful to investigate the heating problem and the effectiveness of proposed solutions.

To carry out this program we address the general problem of heat generation in specific regions of a system and its transfer to other areas of the system through the process of diffusion. The computer program used to perform the calculations is based on a finite element technique described in Appendix D. The code is written assuming axial symmetry but otherwise permits rather general conditions. The heat generation and thermal properties of the media can vary with time and space in an arbitrary way.

Consider an arbitrary geometry with the medium of interest composed of two regions. One region (I, the active volume) is composed of a good Mössbauer isotope that absorbs the radiation preferentially in a nuclear transition with some radiation absorbed by the atoms leading to production of heat in the sample. Another region (II) acts as a heat sink for the active region because of its high thermal conductivity, low absorption in the wavelength of the pumping radiation, and high specific heat. How effective can such a heat sink be in preventing the temperature rise in the active volume from melting the crystal? This question has been addressed systematically by Dr. David A. Sparrow who calculated heat generated in the active region for a hypothetical isotope having the best Mössbauer properties known (Fe^{57}), together with an assumed isomeric storage level within eV to keV of the Mössbauer upper state. Such an isomer is not known to exist and represents an extreme optimistic case. According to other calculations (Sparrow, Ref. 38), which assumed an infinite conductivity of the sink medium (II), the heat generated would still destroy the crystal. It was decided that more realistic cases should be treated to examine the phenomena. In the present study, we performed calculations using real thermal properties of the media and realistic space variations of the heat generation in the media (I & II) to determine under what conditions a passive heat sink can protect the active region from being destroyed during the pumping process.

B. CALCULATIONS/RESULTS

1. Specific Geometry

The calculations were performed for a cylinder of one material (Fe^{57}) encased in a sleeve of another material (Li). The geometry is shown in Fig. 10. In (a) the cylinder of diameter D_1 is the active region and the sleeve of outer diameter D_2 is the heat sink. In (b) a cut containing the axis of the cylinder (shaded) is shown with the four test points at which the temperature as a function of time is calculated are indicated. In (c) two assumed heat-generation profiles which are functions of the radius x are shown.

2. Types of Calculations

A set of calculations were performed with an initial step function temperature profile and no additional heat input. Generally, the temperature was assumed to be 100 K initially in medium I and 0 °C in medium II. Both temperature profiles as a function of radial direction, and temperature changes at the four points shown in Fig. 10(b) are graphed in Figs. 11 and 12.

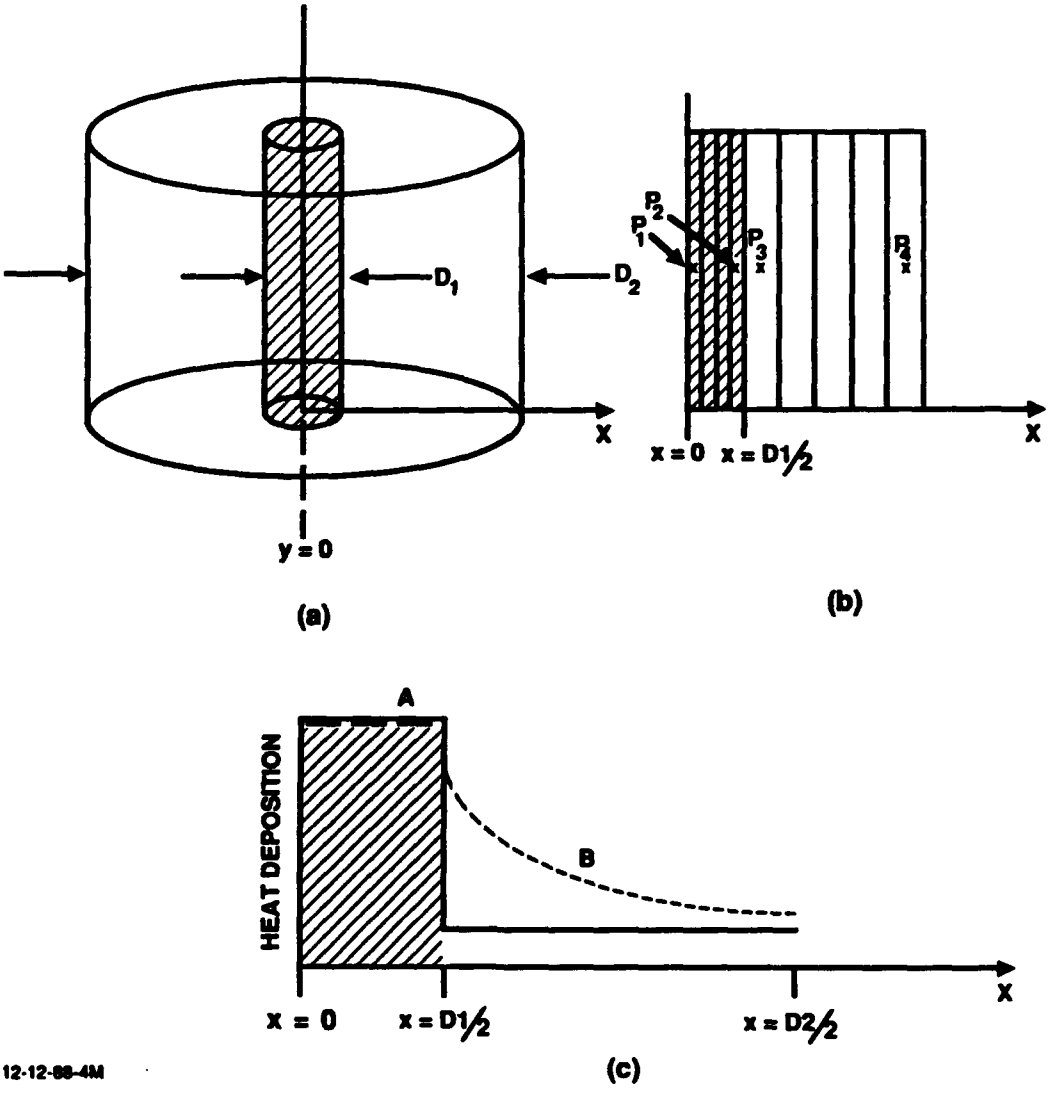

Figure 10. System Definition. (a) Geometry used in the calculations, (b) Position in the system of special points for which temperature as a function of time is plotted in subsequent figures, (c) Spatial distribution of heat sources.

A set of calculations were performed with initial temperature 0 °C through the medium and a heat input (due to radiation ionization) assumed in each medium. Two different radial functions of the heat input were assumed as shown graphically in Fig. 10(c):

(a) 1.03×10^9 Cal/cm^3/s Region I

1.88×10^7 Cal/cm^3/s Region II

(b) 1.03×10^9 Cal/cm^3/s Region I

$\frac{1.29 \times 10^7}{X}$ Cal/cm^3/s Region II.

3. Calculated Specific Results

Our first study dealt with the dynamics of the approach to equilibration. For the system shown in Fig. 10 with $D_1 = 0.2$ μ and $D_2 = 2.0$ μ and either all iron or iron and lithium combination, Figs. 11(a,b,c,d) show that the system (inside case), $r < D_1/2$ temperature decreases to about 10 percent of its initial temperature in just over 1 ns. Thus, heat removal by passive diffusion effectively occurs on the time scale of 1 ns for this combination of geometry and thermodynamic properties. Any attempts at active heat removal, such as flowing coolants past the whisker combination or thermoelectric cooling would have to do much better than this in order to be useful.

When we introduce a distributed heat source into the problem there is an initial fast rise in temperature followed by a steady state situation during the course of the heating (pumping). The nonlinear region lasts for about 1 to 5 ns, depending on the exact conditions. The approach to equilibrium is exhibited clearly in Fig. 12(k), where the temperature difference in time at a particular point is plotted as a function of time.

Our results are summarized in Fig. 13, which compares the steady state part of the heating curves for (a) an iron whisker $D_1 = 0.1$ μ and no sink ($D_2 = 0$) and two heating curves calculated for an iron whisker with a lithium sink with a constant heat source in each region (b) and a radial varying heat source in region II (c). The final temperatures after a 1 μs pulse are 513 °C for (a), 76.0 °C for (b), and 64.2 °C for (c).

All the calculations were done assuming a source beamwidth to linewidth ratio of $\Delta E/\Gamma = 10^4$, which is a very optimistic assumption. Perhaps a more realistic assumption would be $\Delta E/\Gamma = 10^6$, which would increase the temperature rise by two orders of magnitude.

C. CONCLUSIONS

A heat conduction program written for cylindrical geometry (axial symmetry) and capable of dealing with arbitrary material combinations and heat source locations was used to examine the heating problem resulting from photon pumping of a γ-ray laser.

Our calculations showed that for a system on the order of microns in diameter, passive heat transfer from the active core to the reservoir occurred on the order of nanoseconds. Any active technique for cooling the active core region of the γ-ray laser would have to be faster to be useful.

It was also determined that after a few nanoseconds the system approached a steady heat flow situation during constant heat input. Where comparisons could be made our results compare well with the steady-state idealized geometry calculations of Sparrow (Ref. 37 and Chapter IV of this report).

Figure 11. (a) Temperatures at points 1, 2, 3, 4 (positions of points shown in Fig. 10) after an initial condition of 100 °C in region I composed of iron (D_1 = 0.2 μ) and 0 °C in region II composed of lithium (D_2 = 2.0 μ). There are no heat sources in I or II. The temperature profiles at several times for this case are shown in (b) (when the thickness of region II is doubled the results do not change substantially).
(c) The same situation as in (a), except region II is composed of iron.
(d) Temperature profiles for (c).

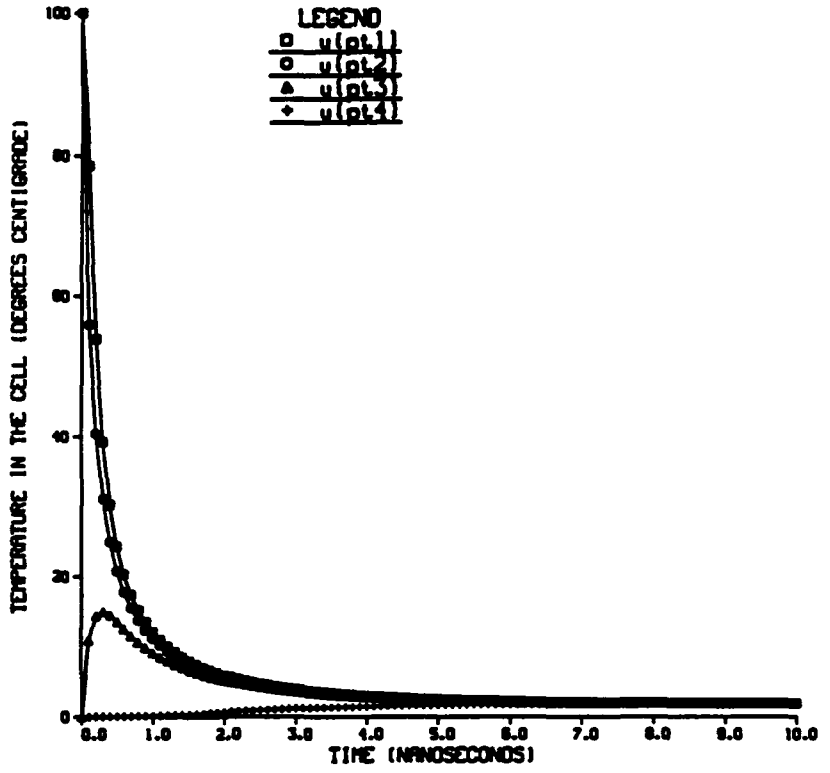

(a)

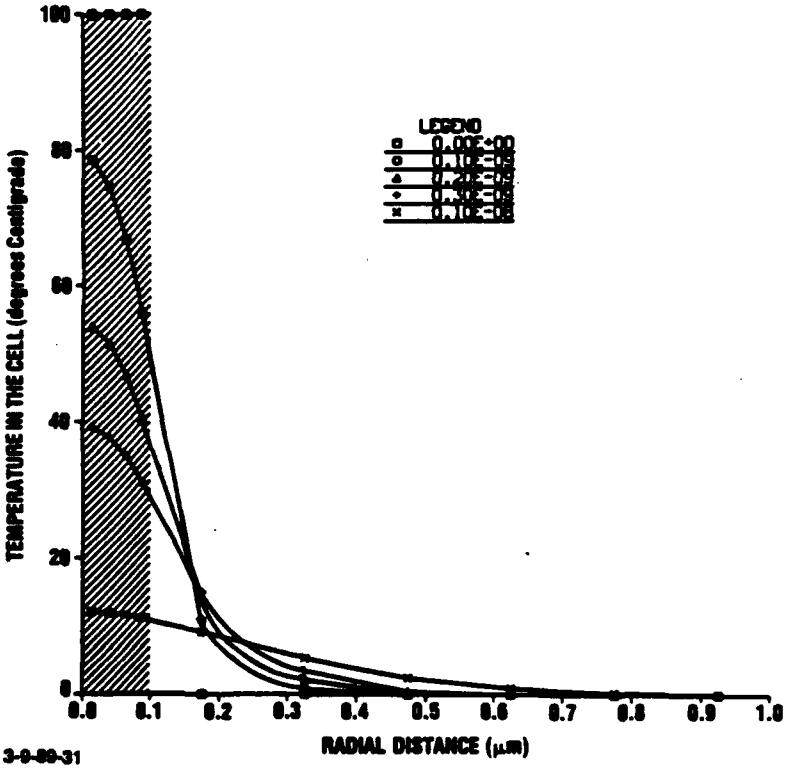

(b)

Figure 11, continued

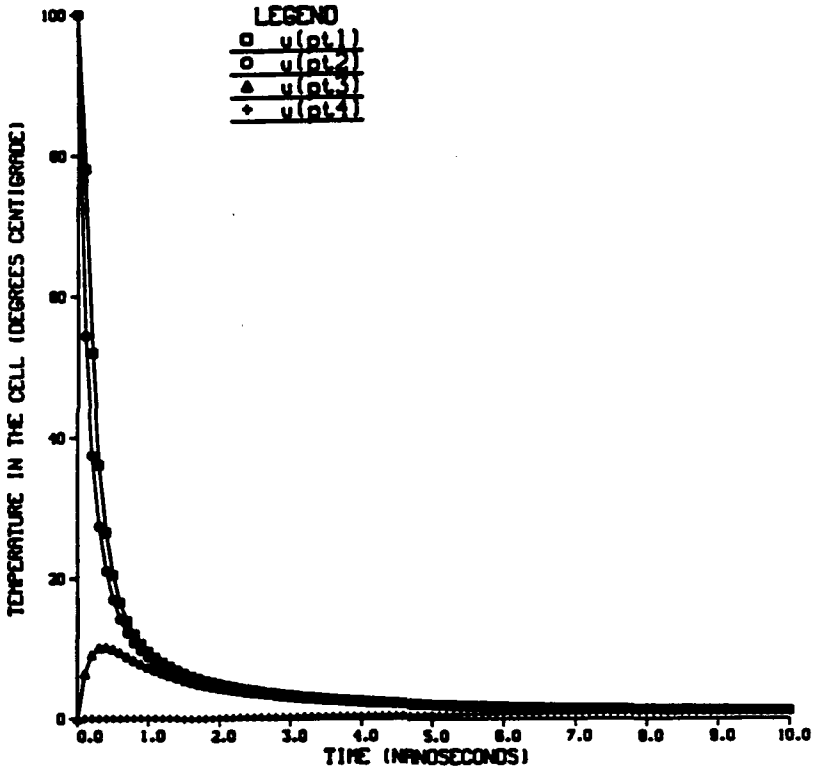

(c)

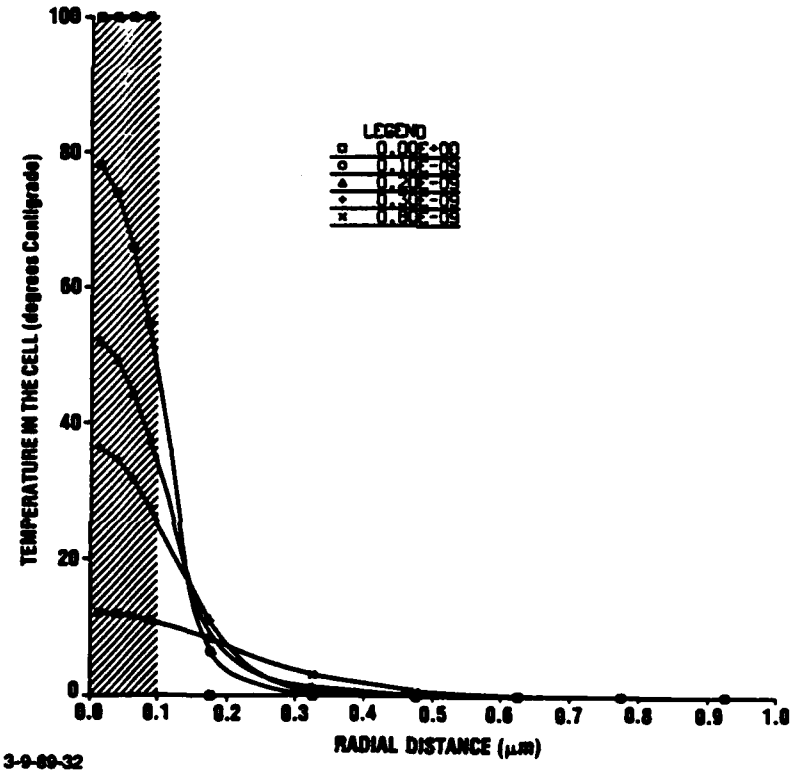

(d)

3-9-89-32

Figure 11, continued

Figure 12. (a) Temperature changes at points 1, 2, 3, 4 assuming initial T = 0 °C in both regions and a heat input of 1.03×10^9 Cal/cm^3/s in region I (iron), and 1.88×10^7 Cal/cm^3/s in region II (lithium) are presented.
(b) Temperature profiles for selected times of case (a) are shown.
(c) Same as in (a) except the heat input in region II is a function of radius,

$$\frac{1.29 \times 10^3 \text{ Cal/cm}^3\text{/s}}{x \text{ (in cm)}}$$

(d) Temperature profiles for selected times of case (b).
(e) Same as (c) except the conductivity in region II is increased by a factor of five (hypothetical material indicated as Li*) without changing the other properties.
(f) Temperature profile for selected times of case (e).
(g) Same as (c) except the specific heat in region II increased by a factor of five (hypothetical material indicated as Li**) without changes in the other properties.
(h) Temperature profiles for selected times of case (g).
(i) Same as (c) except heat input in region II is increased by an order of magnitude because region II starts at x = 0.01 instead of 0.1 and

$$\frac{1.29 \times 10^3 \text{ Cal/cm}^3\text{/s}}{x \text{ (in cm)}}$$

(j) Temperature profiles for case (h) at selected times.
(k) Change in temperature at points (1) as a function of time $[\Delta t = T(t + \Delta t) - T(t)]$ for cases 12(a) and 12(b), showing the approach to steady state.

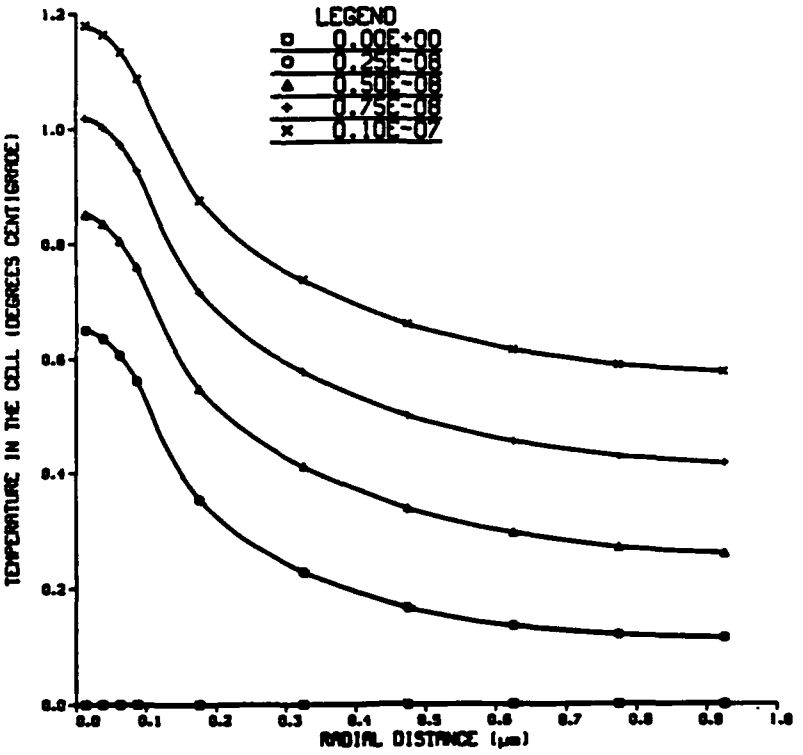

(a)

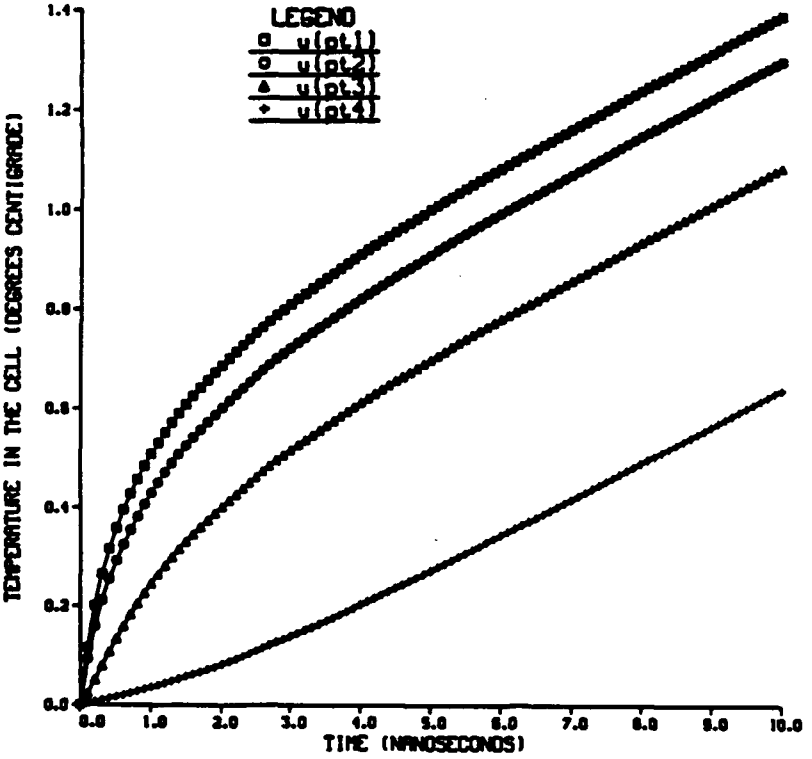

(b)

Figure 12, continued

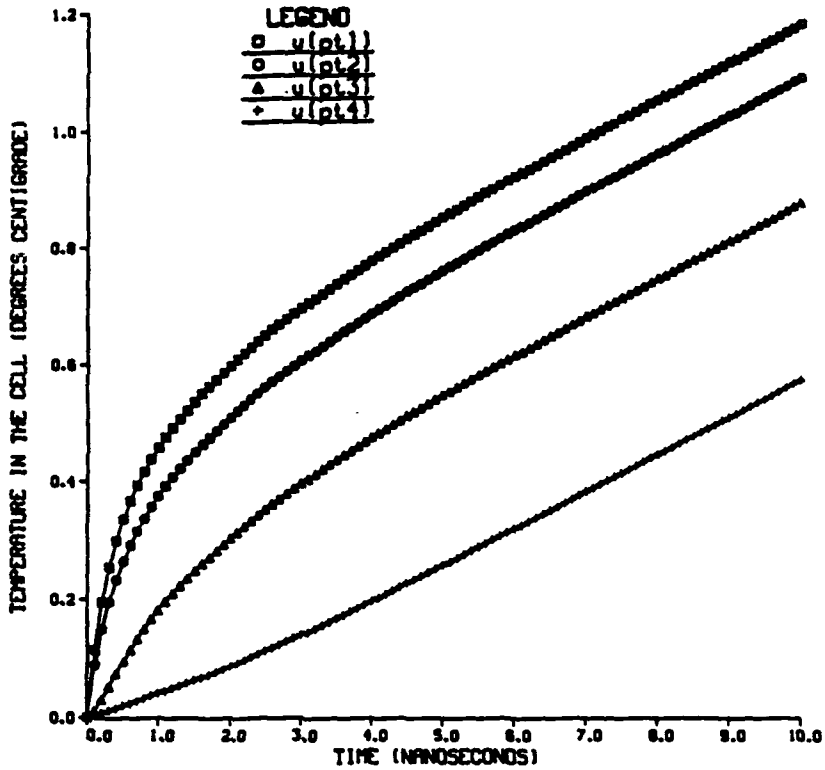

(c)

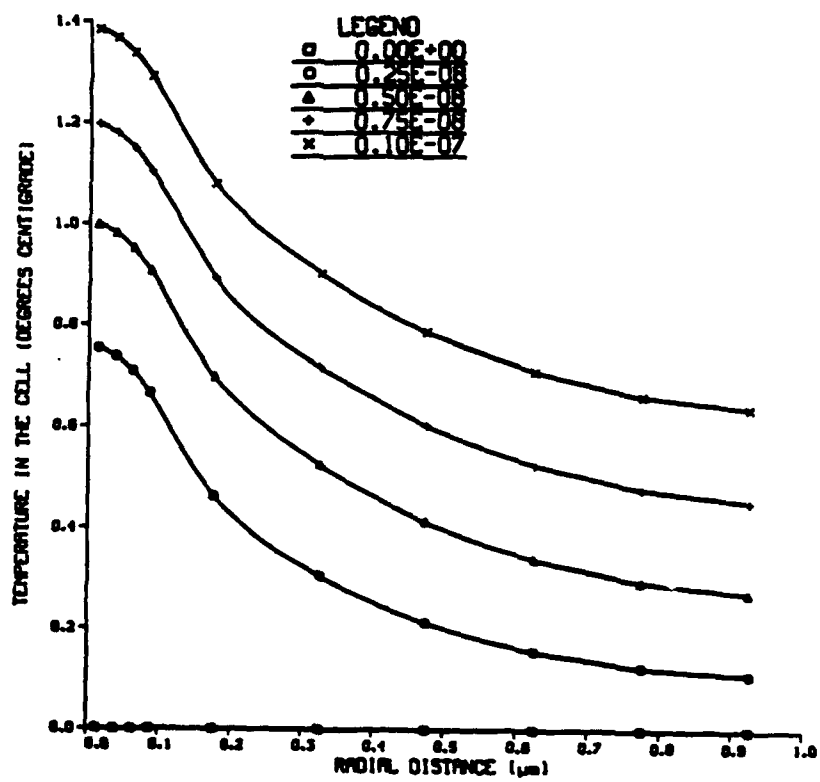

(d)

Figure 12, continued

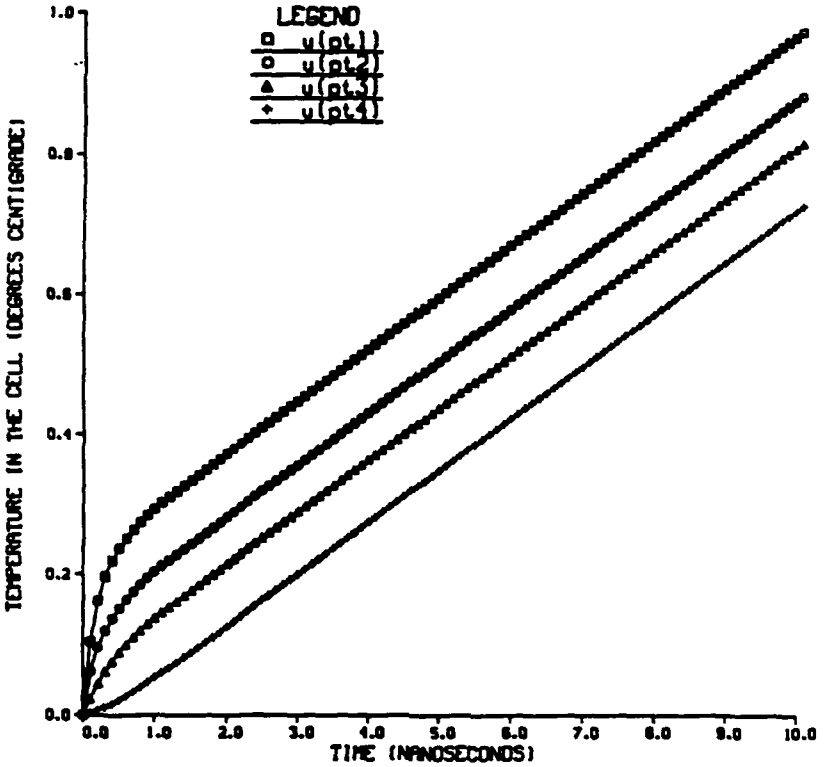

(e)

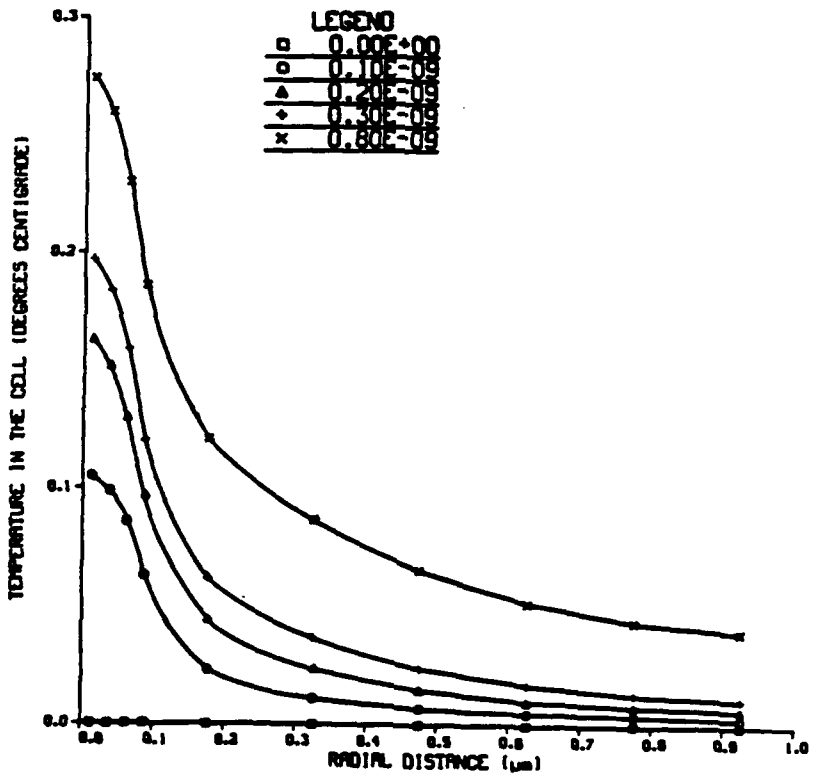

(f)

Figure 12, continued

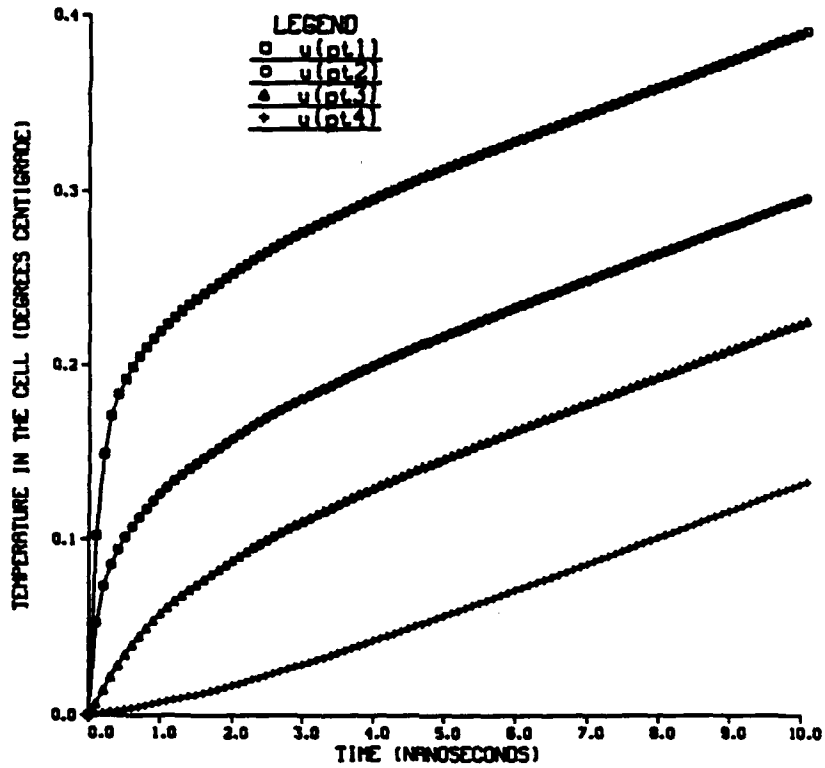

(g)

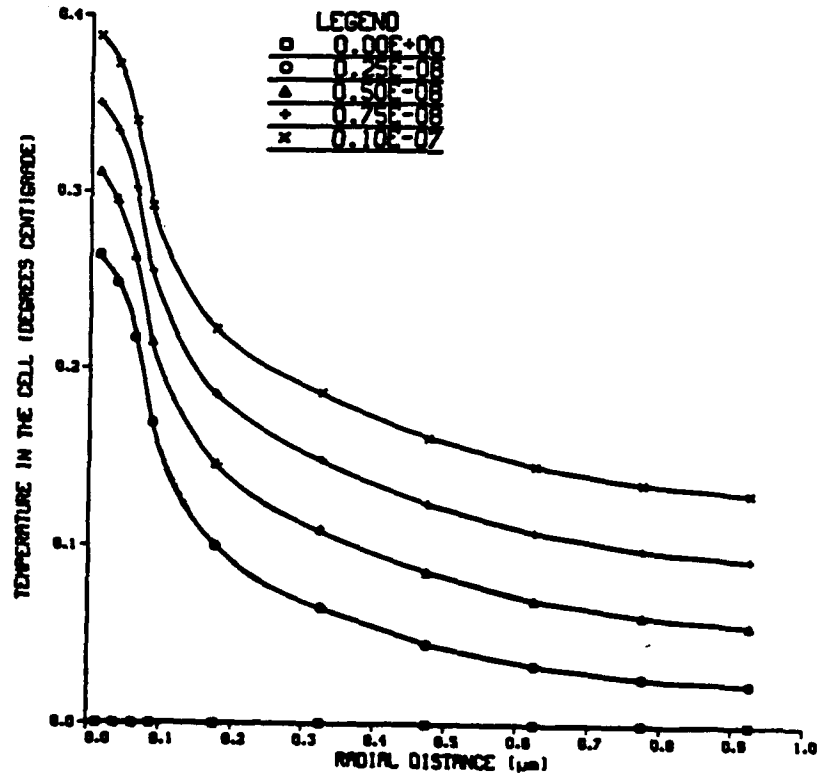

(h)

Figure 12, continued

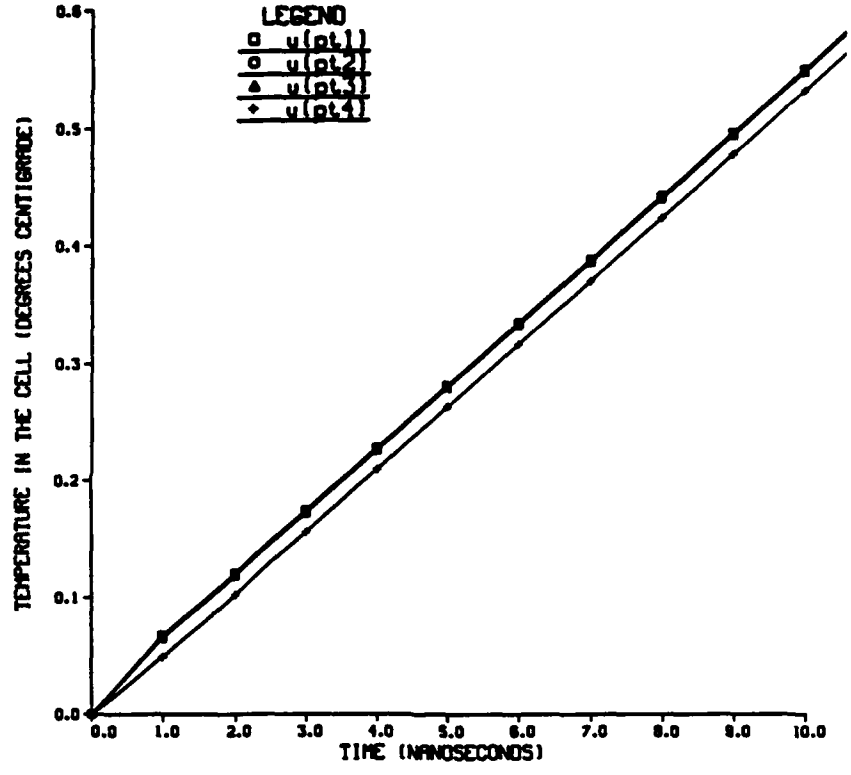

(i)

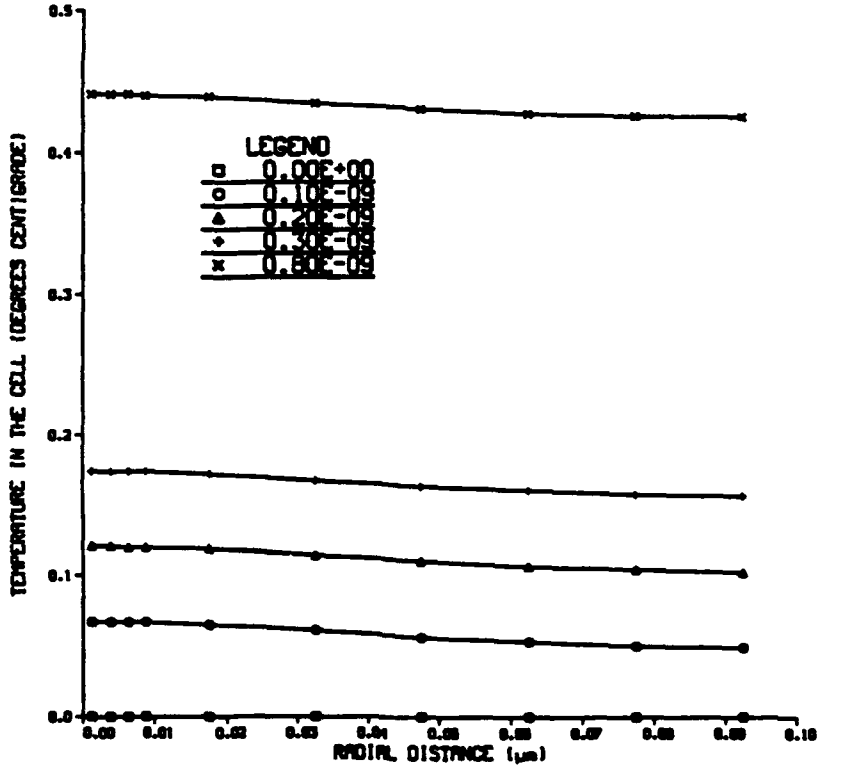

(i)

Figure 12, continued

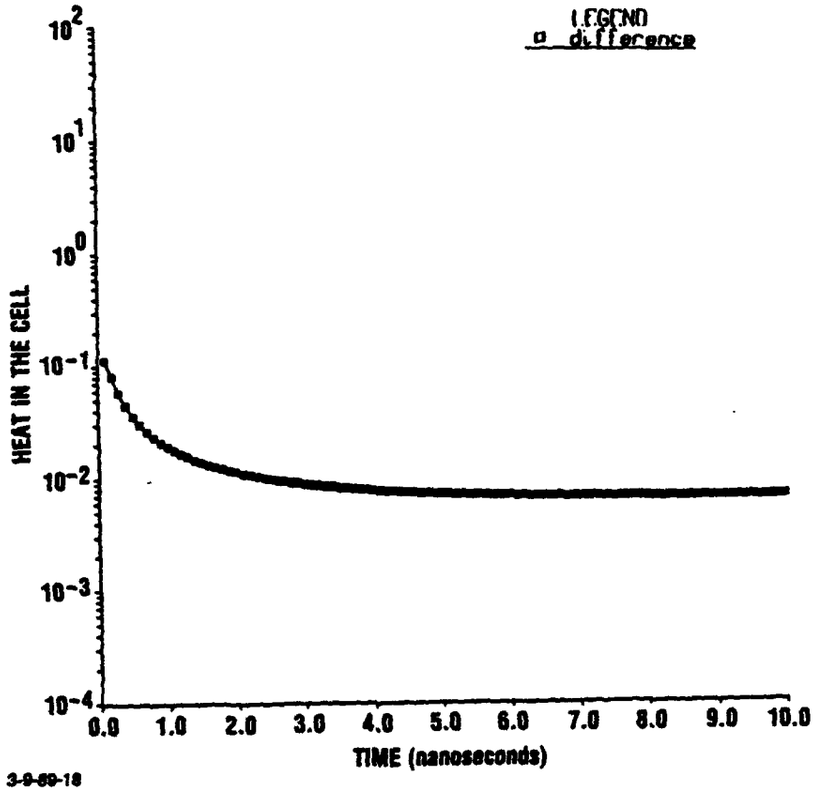

(k)

Figure 12, continued

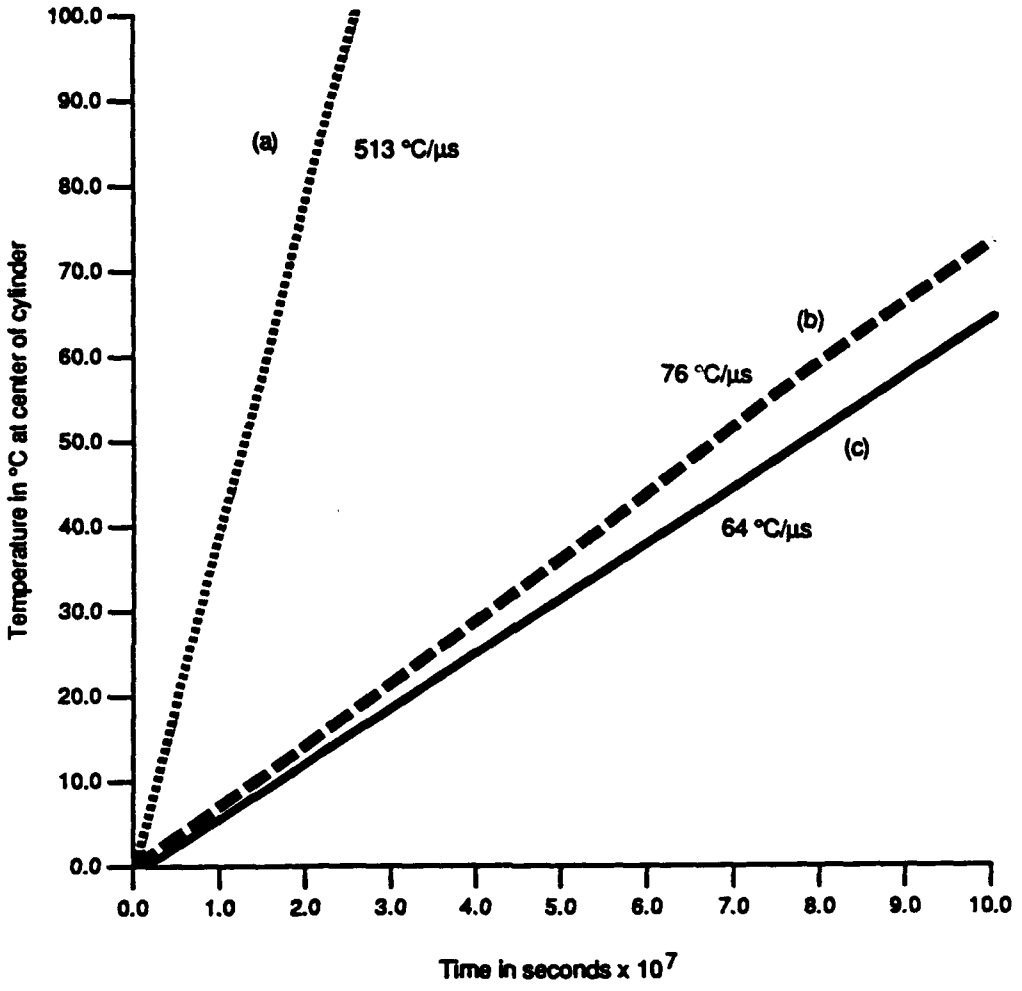

Figure 13. (Summary figure) Temperature change in central iron cylinder (pt. 1) under different conditions, assuming the initial temperature is T = 0 °C for both regions and D_1 = 0.2 μ, D_2 = 2.0 μ. The solid curve shows the temperature when the heat inputs are:

1.03×10^9 **Cal/cm^3/s in region I, and**

1.88×10^7 **Cal/cm^3/s in region II**

The dashed curve gives the temperatures when the heat input is a function of radius in region II, i.e., 1.29×10^3/Cal/cm^3/s. The dotted curve gives the temperature at point 1 when region II does not exist.

VI. RESPONSE OF NUCLEI TO FIELD FLUCTUATIONS

A. INTRODUCTION

One of the early concepts introduced for developing a γ-ray laser (Ref. 38) was based on the idea of direct emission from isomeric nuclear levels. Such levels, because of their long lifetime, permitted long pumping times and were considered to be good storage levels. Unfortunately, because of the narrow natural linewidths associated with the long lifetimes, and the relatively large environmental effects, causing inhomogeneous broadening, resonance conditions for transitions involving such levels are difficult to achieve. Several approaches to alleviate the problem have been put forth. One of the approaches proposes to reduce the line broadening by external fields (Refs. 39 and 40). It has been argued, however, that in order to narrow the inhomogeneously broadened line by any technique, a time on the order of the lifetime of the nuclear state would have to be expended (Ref. 27). The basis of the argument was the time energy uncertainty principle (Refs. 41 and 42), $\Delta E \Delta t > \bar{h}$, with the interpretation that $\Delta E = \Gamma$, the natural linewidth of the transition, and $\Delta t = \tau$ the lifetime. It was stated that in order to remove inhomogeneous broadening by any means the technique used would have to be applied for at least as long a time as τ.

We have argued that this was not so (Ref. 1, Ch. 4) and that in fact the length of time the line narrowing technique would have to be applied depended on the strength of the interaction causing the inhomogeneous broadening. The appropriate condition, in fact, is that the time for narrowing would have to be shorter than h/H_{eff} (Ref. 43, p. 911) where H_{eff} is the average perturbation causing the broadening. The time energy uncertainty with $\Delta E = \Gamma$ and $\Delta\tau = \tau$ (as interpreted by the author of Ref. 27) had nothing to do with the phenomena in question. The time required to remove the field depends on the strength of the field and not on the ultimate linewidth, because the effect of the external fields is to cancel out the inhomogeneous field by shifting the resonance lines and does not affect the inherent resolution of the nuclear energy system.

In this paper we calculate the time required to remove or set up a hyperfine pattern which for different strengths at different lattice points in the sample produces

inhomogeneous broadening. The calculation is based on the Blume theory of time-dependent hyperfine interaction and was originally applied to relaxation phenomena (Ref. 43).

B. THEORETICAL BACKGROUND[9]

The probability of emission of a photon with energy $E = \hbar\omega$ and wave vector $\vec{k}$ by a nucleus making a transition from state e to g is given by

$$P_{eg}(\vec{k},\omega) = \frac{|\langle g| V^{(+)} |e\rangle|^2}{(\hbar\omega + E_g - E_e)^2 + (\Gamma/2)^2} \quad , \tag{35}$$

where $V^{(+)}$ is the interaction Hamiltonian between the nucleus and the electromagnetic field for the emission of the photon, $|e\rangle$ and $|g\rangle$ are the excited and ground states for the nucleus with unperturbed energies E_e and E_g, respectively, as shown in Fig. 14(a) and Γ is the total linewidth at half maximum. For the rest of this paper we assume units with $\hbar = 1$.

The Hamiltonian for the matter system including all the nuclear, atomic, and solid-state terms is given by H, so that

$$H\,|e\rangle = E_e\,|e\rangle$$

$$H\,|g\rangle = E_g\,|g\rangle \quad .$$

To obtain the experimentally observed lineshape $I(\omega)$ we have to average over all the possible initial states $|e\rangle$ and sum over all the final states $|g\rangle$. In order to take into account the dynamic phenomena due to time-dependent Hamiltonians, we transform to the time domain to get

$$I(\omega) = \int_0^\infty dt' \int_0^\infty dt''\; e^{i\omega(t'-t'') - \Gamma/2(t'+t'')} \langle V^{(-)}(t'')\, V^{(+)}(t') \rangle \quad , \tag{36}$$

where

$$V^{\pm}(t) = \exp\left[i \int_0^t H(t')\, dt' \right] V^{(\pm)} \exp\left[-i \int_0^t H(t')\, dt' \right] . \tag{37}$$

---

9 This discussion follows the analysis of M. Blume presented in Ref. 43.

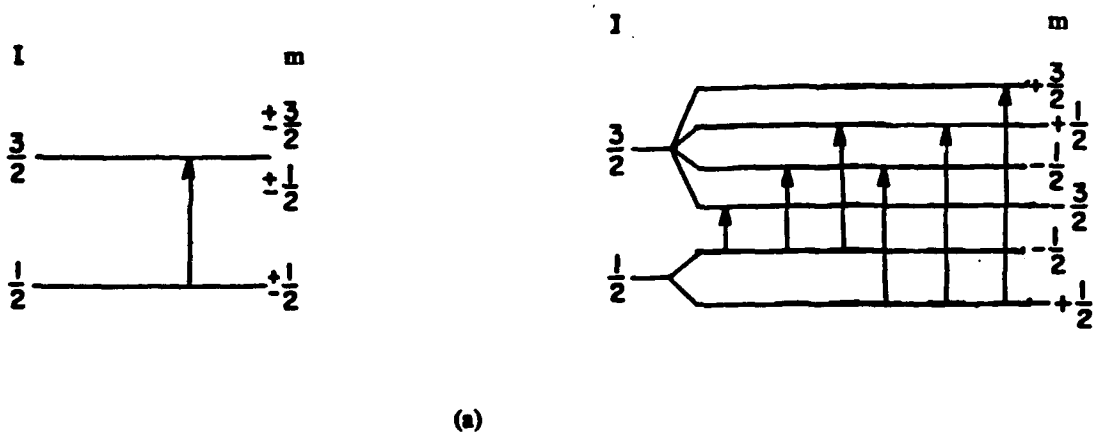

(a)

(b)

Figure 14(a). Energy levels of an Fe^{57} nucleus without a magnetic field present (left) and with a magnetic field present, causing a Zeeman splitting in the levels (right); (b) Absorption spectra of Fe^{57} corresponding to the level splitting shown in (a).

In case the Hamiltonian is not explicitly time-dependent, eq. (37) reduces to

$$V^{\pm}(t) = e^{iHt}\ V^{(\pm)}\ e^{-iHt} \quad , \tag{38}$$

and if in the experiment only photons emitted between times τ and $\tau + \Delta\tau$ are recorded, the two integrals in the lineshape eq. (36) should be taken between τ and $\tau + \Delta\tau$ instead of 0 and ∞.

In the case of a standard Mössbauer experiment with the nuclei unpolarized and when no measurement of the initial state is made

$$< V^{(-)}(t'')\, V^{+}(t') > = < V^{(-)}\, V^{(+)}(t' - t'') > \quad ,$$

and eq. (36) can be written as

$$I(\omega) = \frac{2}{\Gamma}\ \mathrm{Re} \int_0^{\infty} d\tau\ e^{-i\omega\tau - \frac{\Gamma}{2}\tau} < V^{(-)}\, V^{(+)}(\tau) > \tag{39}$$

Let us consider a nucleus in a time-dependent magnetic field H(t) = h f(t), where h is the maximum value of the magnetic field and f(t) a function of time that varies between 0 and 1. The Hamiltonian is given by

$$H(t) = H_0 + g\mu I_z\, h\, f(t) \quad , \tag{40}$$

with g the gyromagnetic ratio, μ the magnetic moment of the nucleus, and I_z the spin component in the z direction which is also the field direction. H_0 is the unperturbed nuclear Hamiltonian so that, $H_0 |I_1 m_1> = E_1 |I_1 m_1>$ and $H_0 |I_0 m_0> = E_0 |I_0 m_0>$ with I_1, m_1 and $I_0 m_0$ representing the excited state spin and z-component (magnetic quantum number) of the nuclear excited and ground states, respectively.

Consider the special case of Fe^{57} with $I_1 = 3/2$ and $I_0 = 1/2$. The energy levels are shown in Fig. 14(a) for the zero field case on the left and for the nucleus in a finite field H on the right. Figure 14(b) shows the corresponding Mössbauer spectra taken in the scattering geometry (total scattering cross section measured).

Suppose the magnetic field varies with time. Blume has shown that in this case the correlation function can be represented as

$$< V^{(-)} V^{(+)}(t) > = e^{i(E_o - E_1)t} \frac{1}{2I_1+1} \sum_{m_o m_1} \left| < I_o m_o \right| V^{(+)} \left| I_1 m_1 > \right|^2$$

$$\times \; e^{i(g_o m_o - g_1 m_1)\, \mu h \int_o^t f(t')\, dt'} \; , \qquad (41)$$

with the matrix elements of $V^{(\pm)}$ proportional to the Clebsh-Gordon coefficients.

C. RESULTS

Let us consider, for simplicity, only the outer lines of the split spectrum and the transition $(I_1 m_1) = (3/2, 3/2)$ to $(I_o m_o) = (1/2, 1/2)$ as shown by the solid vertical line in Fig. 15.

Equation (41) then reduces to

$$< V^{(-)} V^{(+)}(t) > = e^{-i\omega_{10} t}\; Q(3/2, 1/2, 1/2, 1/2)\, e^{-i\delta \int_o^t f(t')\, dt'} \; , \qquad (42)$$

with

$$\delta = (g_1 m_1 - g_o m_o)\, \mu h \text{ and } \omega_{10} = E_1 - E_o \; .$$

and Q is the time independent transition matrix element.

If we further assume that the field varies exponentially with t with time constant γ and shift the energy reference by ω_{10}, then

$$f(t) = e^{-\gamma t} \; ,$$

$$\int_o^t e^{-\gamma t'}\, dt' = \frac{1}{\gamma} \left(1 - e^{-\gamma t}\right)$$

and the part of the spectrum representing the $(I_1 m_1) = (3/2, 3/2) \rightarrow (I_o m_o) = (1/2, 1/2)$ transition, leaving out the factor Q, is given by

$$I(\omega) = \frac{2}{\Gamma} \text{ Re} \int_o^\infty d\tau \; \exp\left[-i\, \omega\tau - (\Gamma/2)\tau \;\; \frac{i\delta}{\gamma} \left(1 - e^{-\gamma\tau}\right) \right] \qquad (43)$$

This can be integrated numerically to obtain the lineshape for arbitrary values of the parameters. For two limiting cases the solutions can be expressed in closed form.

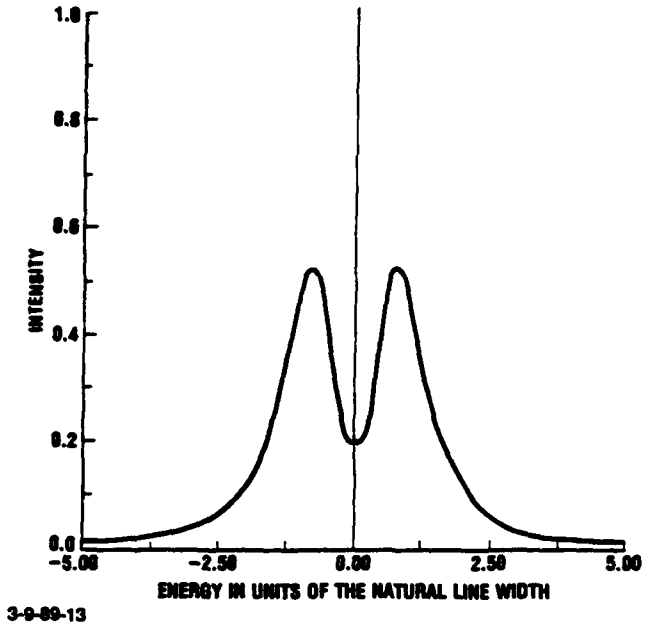

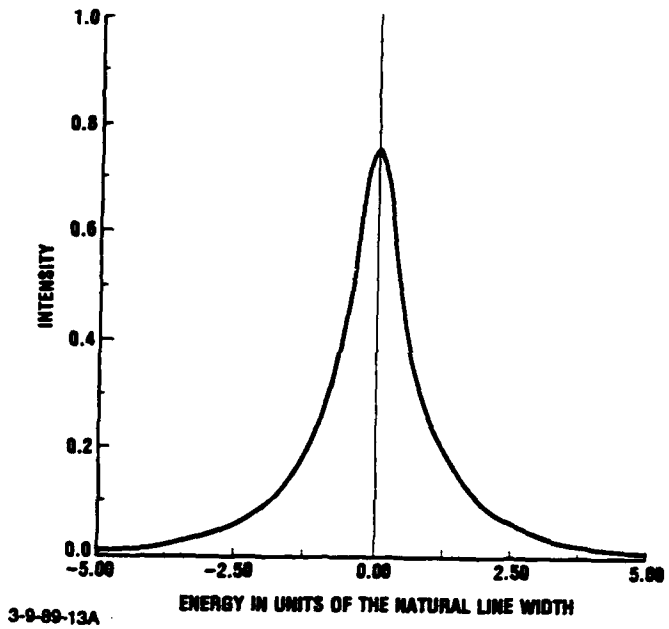

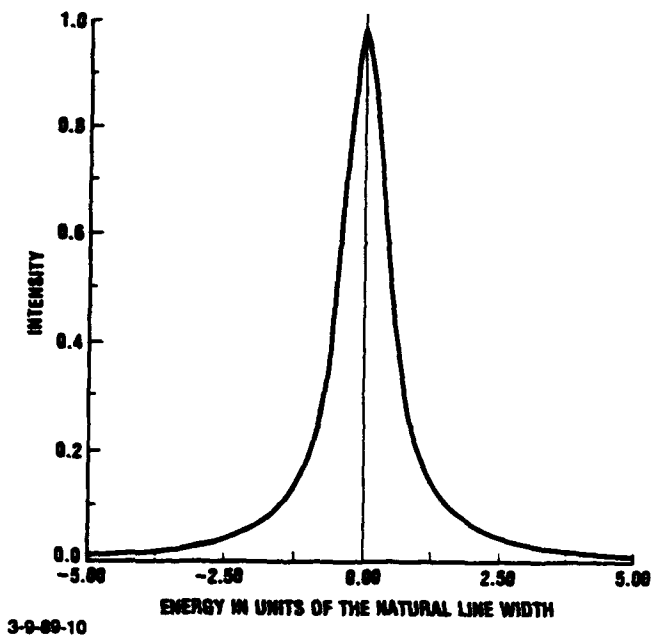

Figure 15. Absorption cross section of Fe^{57} showing only the outer lines, as indicated in Fig. 14(b) when $\Gamma = 1.0$ and $\delta = 1.0$ and $\gamma = 0.1$ in (a) and $\gamma = 10^2$ in (b) and $\gamma = 5 \times 10^2$ in (c)

Case (a) when $\Gamma \approx \delta$ and $\gamma >> \Gamma$ we get

$$I(\omega) = \frac{1}{\Gamma}\,\mathrm{Re}\left[\frac{1}{\Gamma - i\omega} + \frac{i\,\delta}{\left(\frac{\Gamma}{2} - i\omega\right)\left(\frac{\Gamma}{2} + \gamma - i\omega\right)} - \frac{\delta^2}{\left(\frac{\Gamma}{2} - i\omega\right)\left(\frac{\Gamma}{2} + \gamma - i\omega\right)\left(\frac{\Gamma}{2} + 2\gamma - i\omega\right)}\right]$$

$$I(\omega) = \frac{1}{2\left(\frac{\Gamma^2}{4} + \omega^2\right)} - \frac{\delta\,(\gamma + \Gamma)\,\omega}{\Gamma\left(\frac{\Gamma^2}{4} + \omega\right)\left[\left(\frac{\Gamma}{2} + \gamma\right)^2 + \omega^2\right]} + \frac{\delta^2\left[3\omega^2\left(\frac{1}{2}\,\Gamma + \gamma\right) - \frac{\Gamma^3}{8}\right]}{\Gamma\left(\frac{\Gamma^2}{4} + \omega^2\right)\left[\left(\frac{\Gamma}{2} + \gamma\right)^2 + \omega^2\right]\left[\left(\frac{\Gamma}{2} + 2\gamma\right)^2 + \omega^2\right]}\,. \tag{44}$$

Case (b) when $\Gamma >> \gamma$ and $\Gamma \approx \delta$ we get

$$I(\omega) = \frac{2}{\Gamma}\,\mathrm{Re}\int_0^\infty e^{-i\omega\tau - \left(\frac{\Gamma}{2}\right)\tau - i\,\delta\,\left(\tau - \frac{1}{2}\,\gamma\tau^2\right)}$$

$$I(\omega) = \frac{2}{\Gamma}\,\mathrm{Re}\,\frac{\frac{\Gamma}{2} - i\,(\omega + \delta)}{(\omega + \delta)^2 + \frac{\Gamma^2}{4}} \sum_{m=0}^{\infty} \frac{(-1)^m\,(2m)!}{m!\,(2z)^{2m}} \tag{45}$$

where

$$z = \frac{(1 - i)}{2\sqrt{\gamma\,\delta}}\left[i\,\frac{\Gamma}{2} - (\omega + \delta)\right]$$

The first term in the series is 1 so that in the limit $\Gamma >> \gamma$ the line shape approaches a Lorentzian centered at $\Delta\omega$ and with a full width at half maximum of Γ.

Figure 15(a) shows a split spectrum for values of $\gamma < \Gamma$, and $\delta = \Gamma$ ($\gamma = 10^{-1}$, $\Gamma = 1$, $\delta = 1$). Figure 15(b) shows a collapsed spectrum for $\gamma = \Gamma = \delta$ and Fig. 15(c)

shows an enhanced collapse with a narrower line spectrum for $\gamma = 5\Gamma$ and $\delta = \Gamma$. Figure 16(a) shows a completely split spectrum with $\gamma/\Gamma = 10^{-4}$ and $\delta/\Gamma = 10$, while Fig. 16(b) shows a completely narrowed single line with $\gamma/\Gamma = 10^3$ and $\delta/\Gamma = 100$.

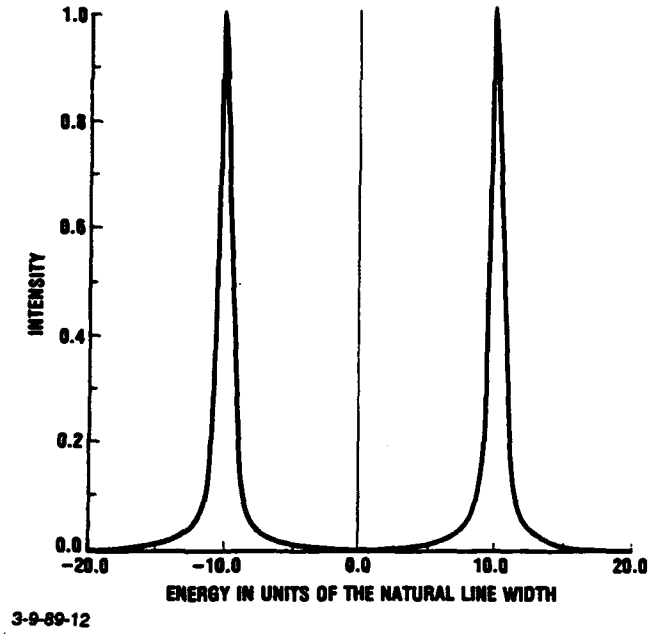

(a)

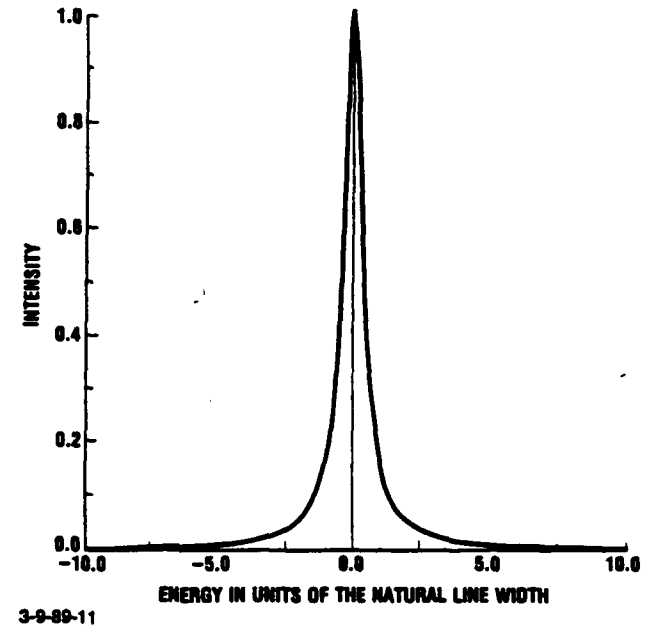

(b)

Figure 16. Absorption cross section of Fe^{57} showing only the outer lines as indicated in Fig. 15(b) for the case when $\gamma = 10^2$, $\Gamma = 1.0$, $\delta = 10$ in (a), and $\gamma = 10^5$, $\Gamma = 1$, $\delta = 100$ in (b).

These results show that the nuclear resonant lineshape will show a full split spectrum as in Fig. 16(a) if the change of field is slow ($\gamma << \Gamma$) compared to the decay time of the nucleus. In this situation most nuclei will be exposed to the field during their lifetime and while they decay. If the field decay is fast ($\gamma >> \Gamma$) the spectrum will show a collapsed lineshape similar to the one shown in Fig. 14(b) on the left. This implies that it does not require time on the order of a lifetime of the nuclear state to effectively remove the inhomogeneous broadening.

D. CONCLUSIONS

Special cases for low and high relaxation $\gamma << \Gamma$ and $\gamma >> \Gamma$, respectively, with $\Gamma \approx \delta$, indicate that the natural lifetime of the nuclear state Γ sets the lower limit on the width of the spectra obtained for these cases but does not for fast relaxation prevent a good definition of the spectrum. Thus in a very short time during which the hyperfine interaction changes value the nuclear resonance spectrum follows this change quickly. In a time much less than the natural lifetime the spectrum changes from being representative of one hyperfine interaction to being representative of another. The nuclear system quickly responds to the change of fields in its environment. Thus, if inhomogeneous broadening is represented by a sum of spectra representative of different fields at different nuclear sites, if these fields can be changed in a time Δt much shorter than the natural lifetime, the resulting spectra taken over a lifetime of the nuclear state will represent the final hyperfine interaction spectrum.

This result is important to the γ-ray laser feasibility study because it shows that inhomogeneous broadening can be reduced quickly by applying sufficiently strong and appropriate external fields. Inhomogeneous broadening of several orders of magnitude higher than the natural lifetime of the isomer can be removed by fields in a time shorter than the natural lifetime of the isomer. Such a fast mechanism could be used to trigger the lasing or superfluorescent emission by providing a strong resonance overlap of narrow resonance lines quickly.

VII. REFERENCES

1. "IDA Gamma-ray Laser Annual Summary Report (1985): Investigation of the Feasibility of Developing a Laser Using Nuclear Transitions," IDA Paper P-2021 (Rev.), Edited by Bohdan Balko, Leslie Cohen, and Francis X. Hartmann, June 1986.

2. B. Balko, L. Cohen, and D.A. Sparrow, "IDA Gamma-ray Laser Annual Summary Report (1986): Investigation of the Feasibility of Developing a Laser Using Nuclear Transitions," IDA Paper P-2004, December 1988.

3. *Proceedings of the IST/IDA Gamma-ray Laser Workshop*, Edited by Bohdan Balko, Leslie Cohen, and Francis X. Hartmann, IDA Memorandum Report M-162, January 1986.

4. R. Bonifacio and L.A. Lugiato, *Phys. Rev. A*, 11 (5), 1507-1521, May 1975.

5. M. Feld, "Superradiance and Laser-Controlled Gamma Emission," *Proceedings of The IST/IDA Gamma-ray Laser Workshop*, Edited by Bohdan Balko, Leslie Cohen, and Francis X. Hartmann, IDA Memorandum Report M-162, January 1986.

6. N. Skribononitz, I.P. Herman, J.C. MacGillivray, and M.S. Feld, *Phys. Rev. Lett.*, 30 (8), 308, 1973.

7. Q.H.F. Vrehen and H.M. Gibbs in *Dissipative Systems in Quantum Optics*, ed. R. Bonifacio, Springer-Verlag, N.Y., 1982.

8. M. Gross and S. Haroche, *Phys. Rep.* 93 (5), 301-396, 1982.

9. M.F.H. Schuurmans, Q.H.F. Vrehen, and D. Polder, in *Adv. At. Mol. Phys.*, 17, 167, 1981.

10. G.T. Trammel in *Chemical Effects of Nuclear Transformations*, International Atomic Energy Agency, 1961.

11. G.C. Baldwin and M.S. Feld, *J. Appl. Phys.*, 59, 3665, 1986.

12. H.J. Lipkin, *Phys. Rev. Lett.*, 58 (12), 1176-1179, 23 March 1987.

13. Personal communication, J. Eberly, University of Rochester.

14. Agda Artna-Cohen in "IDA Gamma-ray Laser Annual Summary Report (1985): Investigation of the Feasibility of Developing a Laser Using Nuclear Transitions," Edited by Bohdan Balko, Leslie Cohen, and Francis X. Hartmann, IDA Paper P-2021, June 1986.

15. M.S. Feld and J.C. MacGillivray, "Coherent Nonlinear Optics, Recent Advances" in *Topics in Current Physics*, Vol. 21, Edited by M.S. Feld and V.S. Letokhov, Springer-Verlag, Berlin Heidelberg, 1980.

16. J. Mostowski and B. Sobolewska, *Phys. Rev. A*, 30 (3), 1392, 1984.

17. S. Prasad and R.J. Glauber, *Phys. Rev. A*, 31 (3), 1583, 1985.

18. F. Haake and R. Reibold, *Phys. Rev.*, 29, 3208, 1984.

19. M.F.H. Schuurmans and D. Polder, *Phys. Lett.*, 72A (415), 306, 1979.

20. J. Okada, K. Ikeda, and M. Matsuoka, *Opt. Commun.* 27 (3), 321, 1978.

21. G.T. Trammell and J.P. Hannon, *Opt. Commun.* 15 (3), 325, 1975.

22. J.C. MacGillivray and M.S. Feld, *Phys. Rev. A*, 14 (3), 1169, 1976.

23. B. Balko, *J. Quant. Spectros. Radiat. Transfer, Special Issue on γ-Ray Lasers*, 40 (6), 637-795, 1988.

24. R. Bonifacio and L.A. Lugiato, "Cooperative Radiation Processes in Two-Level Systems: Superfluorescence II," *Phys. Rev. A*, 12 (2), 587-598, 1975.

25. J.H. Terhune and G.C. Baldwin, "Quantum Theory of Nuclear Superradiance in Crystals," unpublished preprint.

26. N.E. Rehler and J.H. Eberly, "Superradiance," *Phys. Rev. A*, 3, (6), 1735-1751, 1971.

27. G.C. Baldwin, J.C. Solem, and V.I. Gol'danskii, *Rev. Mod. Phys.*, 53, Part 1, 687, 1981.

28. C. Collins, F.W. Lee, D.M. Shemwell, and B.D. DePaola, *J. Appl. Phys.*, 53 (7), 4645, 1982.

29. B. Balko, L. Cohen, D. Sparrow, and J. Nicoll, "IDA Gamma-ray Laser Summary Report (1987): Investigation of the Feasibility of Developing a Laser Using Nuclear Transitions," IDA Paper P-2083, December 1988.

30. D.A. Sparrow, *Bull. Am. Phys. Soc.*, 33, 1017, 1988.

31. M.J. Berger and S.M. Seltzer, "Stopping Powers and Ranges of Electrons and Positions," National Bureau of Standards, NBSIR 83-2550-A, 1983.

32. C.G. Wohl, et al., *Rev. Mod. Phys.*, 56, No. 2, Part II, S57, 1984.

33. R.C. Haight and G.C. Baldwin, "Assessment of a Method Proposed for Finding Transfer Levels for Isomeric Deexcitation," in *Optical Science and Engineering Series 6, Advances in Laser Science--I*, American Institute of Physics Conference Proceedings No. 146, Edited by William S. Stwalley and Marshall Lapp, 1986.

34. E.C. Zimmermann, "Proposed Screening Experiment for Candidate Nuclei for a Three-Level, Two-Pump, Gamma-ray Laser," in *IDA Gamma-ray Laser Annual Summary Report (1985): Investigation of the Feasibility of Developing a Laser Using Nuclear Transitions*, IDA Paper P-2021 (Rev.), Edited by Bohdan Balko, Leslie Cohen, and Francis X. Hartmann, June 1986.

35. C.B. Collins, "Coherent and Incoherent Upconversion Techniques for the Pumping of a Gamma-Ray Laser," in *Proceedings of the IST/IDA Gamma-ray Laser Workshop*, IDA Memorandum Report M-162, Edited by Bohdan Balko, Leslie Cohen, and Francis X. Hartmann, January 1986.

36. J.C. Solem and G. Rinker, "Nuclear Interlevel Transfer Driven by Electronic Transitions," in *Proceedings of the IST/IDA Gamma-ray Laser Workshop*, IDA Memorandum Report M-162, Edited by Bohdan Balko, Leslie Cohen, and Francis X. Hartmann, January 1986.

37. D.A. Sparrow et al., Chapter IV of *IDA Gamma-ray Laser Annual Summary Report (1986): Investigation Into the Feasibility of Developing a Laser Using Nuclear Transitions*, IDA Paper P-2004, December 1988.

38. V. Vali and W. Vali, *Proc. IEEE*, 51, 1822, 1963.

39. A.V. Andreev, Y.A. Il'inskii, and R.V. Khokklov, *Sov. Phys. JETP*, 40, 816, 1975.

40. Y.A. Il'inskii and R.V. Khokklov, *Sov. Phys. JETP*, 38, 809, 1974.

41. L. Mandlestam and I.G. Tamm, *J. Phys.*, 9, (4), 249, 1945.

42. V. Fock and N. Krylov, *J. Phys.*, 9, (2), 112, 1947.

43. M. Blume in *Hyperfine Structure and Nuclear Radiations*, Edited by Mathias and Shirley, North Holland, Amsterdam (1968).

44. D. Polder, M.F.H. Schurmans and Q.H.F. Vrehen, *Phys. Rev. A*, **19**, 3, pp. 1192-1203, 1979.

APPENDIX A

DERIVATION OF THE HAAKE-REIBOLD EQUATIONS

APPENDIX A
DERIVATION OF THE HAAKE-REIBOLD EQUATIONS

The purpose of this appendix is to justify the system of eqs. (1-3) in Chapter I for the excited population number operators N_j, the polarization operators $R_{ij}^{\pm}$, and the electric field operators $E_{ij}^{\pm}$. These equations are given in Ref. A-1 without derivation.

Reference A-2 derives similar equations for a two-level atomic system, but does not indicate how to generalize the theory to multi-level systems. This appendix will attempt to fill in the steps needed to extend the derivation of Ref. A-2 to the present case of interest.

For this purpose it will be necessary to use generalized commutation relations given by Ref. A-3 for operators S_{kj}* that effect a transition from state j to state k in a multi-level system. The commutation relations are

$$\left[S_{jk}, S_{mn}\right] = S_{jn}\delta_{km} - S_{mk}\delta_{nj} \ . \qquad \text{(A-1)}$$

Reference A-3 neither derives nor gives a reference for (A-1), which does, in fact, reduce to the familiar two-level commutation relations (cf., Ref. A-4, which derives them)

$$\left[R^{+}, R^{-}\right] = R_3, \left[R_3, R^{\pm}\right] = \pm R^{\pm} \qquad \text{(A-2)}$$

for the polarization $R^{\pm}$ and inversion R_3. The identification between the operators labeled S in (A-1) and the operators labeled R in (A-2) required for this reduction is

$$S_{10} = R^{+}, S_{01} = R^{-}, S_{11} - S_{00} = R_3 \ . \qquad \text{(A-3)}$$

---

* To avoid confusion with the electric field the letter S is used here to designate the transition operators instead of E, which Ref. A-3 uses for that purpose.

The identification eq. (A-3) for the two-level case suggests the appropriate corresponding identification for the operators pertinent to the multi-level case leading to the eqs. (1-3) in Chapter I. Thus, generalizing eq. (A-3), it will be assumed that

$$S_{ii} = N_i \, , i = 0, 1, 2, 3 \quad ,$$

$$S_{ij} = R_{ij}^{+} \, , S_{ji} = R_{ij}^{-} \, , i = 2, 3, \; j = 1, 2, \quad i > j \quad . \tag{A-4}$$

Following Ref. A-2, the Hamiltonian for the non-interacting atoms is given by a sum, over all atoms in the system, of terms

$$H_A = \bar{h} \left[\omega_{31}\left(N_3 - N_1\right) + \omega_{32}\left(N_3 - N_2\right) + \omega_{21}\left(N_2 - N_1\right) + \omega_{43}\left(N_4 - N_3\right) + \omega_{10}\left(N_1 - N_0\right) \right] . \tag{A-5}$$

The interaction Hamiltonian is given by a sum, over all atoms in the system, of terms

$$H_{AF} = i\bar{h} \left[g_1 E_{31} \left(R_{31}^{-} - R_{31}^{+} \right) + g_2 E_{32} \left(R_{32}^{-} - R_{32}^{+} \right) \right] \quad . \tag{A-6}$$

The Heisenberg equation of motion for any operator 0 of interest in terms of the Hamiltonian H will have the form

$$d0/dt = (i/\bar{h}) \; [H, 0] \quad . \tag{A-7}$$

However, the eqs. (1-3) of Chapter I cannot be derived entirely from a relation of the form eq. (A-7); the loss and source terms are *ad hoc* additions to equations that are obtainable from a Hamiltonian.

The Hamiltonian to be used to obtain the Heisenberg equations before the addition of the *ad hoc* terms consists of the standard free photon field contribution plus the sum over all atoms of the single atom expressions given by eq. (A-5) and eq. (A-6). On substituting

the N_i and the $R_{ij}^{\pm}$ into the resulting equation of the form eq. (A-7) and then using eqs. (A-1, A-3, A-4), the following equations are obtained:

$$dN_1/dt = g_1 E_{31}\left(R_{31}^{+} + R_{32}^{-}\right),$$

$$dN_2/dt = g_2 E_{32}\left(R_{31}^{+} + R_{32}^{-}\right),$$

$$dN_3/dt = -\left[g_1 E_{31}\left(R_{31}^{+} + R_{31}^{-}\right) + g_2 E_{32}\left(R_{32}^{+} + R_{32}^{-}\right)\right],$$

$$dR_{21}^{\pm}/dt = i\left(\pm\omega_{31} \mp \omega_{32} \pm 2\omega_{22} + -\omega_{10}\right) R_{21}^{\pm} + g_1 E_{31} R_{32}^{\mp} + g_2 E_{32} R_{31}^{\pm},$$

$$dR_{31}^{\pm}/dt = i\left(\pm\omega_{32} \pm 2\omega_{31} \mp \omega_{21}\right) R_{31}^{\pm} + g_1\left(N_3 - N_1\right) E_{31} - g_2 E_{32} R_{21}^{\mp},$$

$$dR_{32}^{\pm}/dt = i\left(\pm\omega_{31} \pm 2\omega_{32} \mp \omega_{21}\right) R_{32}^{\pm} + g_2\left(N_3 - N_2\right) E_{32} - g_1 E_{31} R_{21}^{\mp}. \qquad \text{(A-8)}$$

Equations (A-8) are at the stage of corresponding equations for the two-level atomic system in Ref. A-2 which Ref. A-2 then modifies by separating the electric field and polarization operators into their positive and negative frequency parts, neglecting rapidly oscillating terms in the process. Applying the same process to (A-8) results in the eqs. (1-2) of Chapter I minus the source and loss terms. Equation (1a) is not included because the right hand side consists only of a source and a loss term.

Equations (3a, 3b) in Chapter I can be derived from Maxwell's equations with a polarization source exactly as in Ref. A-2 by assuming that the radiation due to a particular transition depends only on the polarization associated with that transition. The results appear to differ somewhat in form from the corresponding results given in Ref. A-2. However, it can be seen by inspection that the differences are due to the use of a retarded time coordinate and neglect of spectral broadening in Chapter I as in Ref. 1.

Actually, two discrepancies between the equations derived in the manner summarized in this appendix and eqs. (1-3) will exist as eq. (A-8) now stands. These are the presence of the coupling constant g_i in all six equations and the presence of a term involving the ω_i in each of the last three equations. The first discrepancy can be accounted for as due to a normalization of the electric field and the second as due to irrelevant phase factors in the polarization operators.

REFERENCES

A-1. F. Haake and R. Reibold, "Interplay of Superfluorescence and Incoherent Processes in Multilevel Systems," *Phys. Rev. A*, 29, 3208-3217, 1984.

A-2. F. Haake et al., "Delay-Time Statistics of Superfluorescence Pulses," *Phys. Rev. A*, 23, 1322-1333, 1981.

A-3. R. Gilmore et al., "Classical Quantum Correspondence for Multilevel Systems," (12) 1019-1031, 1975.

A-4. L. Allen and J.H. Eberly, *Optical Resonance and Two-Level Atoms*, Ch. 2, Wiley-Interscience, New York, 1975.

APPENDIX B

COMPUTER CODE FOR TRIPLE INTEGRAL CALCULATION

COMPUTER CODE FOR TRIPLE INTEGRAL CALCULATION

B1. BACKGROUND

In this appendix we describe the algorithm used to compute the superfluorsecent pulse from the closed form (triple integral) expression derived in Chapter I. The physics of the problem is modeled by the set of differential equations with stochastic source terms given in chapter I, section 2.

The algorithm makes use of the following expressions derived in chapter I:

Equation (1):

$$I(t) = \frac{g^2\gamma}{N} e^{-\Gamma t} \int_0^t \int_0^1 I_0^2 \left[2\sqrt{k(t,t')\ x'}\right] e^{-\mu x' + (\Gamma-\gamma)\,t'}\, dx'\, dt'$$

Equation (2):

$$k(t,t') = 2\int_{t'}^{t} N_3(t'')\, dt'' + N_0\left[\frac{e^{-\gamma t'} - e^{-\gamma t}}{\gamma}\right] - N_0\,(t - t')$$

Equation (2'):

$$k(t,t') = k_0(t) - k_0(t')$$

$$\text{i.e.,}\quad \hat{k}_0(t) = \frac{2\gamma N_0}{\Gamma - \gamma}\left(\frac{e^{-\Gamma t}}{\Gamma} - \frac{e^{-\gamma t}}{\gamma}\right) - N_0\left(\frac{e^{-\gamma t}}{\gamma} + t\right)$$

$$\text{and}\quad k_0(t) = 2\int_0^t N_3(t'')\, dt'' - N_0\left(\frac{e^{-\gamma t}}{\gamma} + t\right)$$

Equation (3):

$$N_3 = \frac{\gamma N_0}{\Gamma - \gamma}\left(e^{-\gamma t} - e^{-\Gamma t}\right) - \beta \int_0^t e^{\Gamma(t-t')} I_1(t')\, dt'$$

$$= N_A - N_B$$

$$\beta = \frac{1}{g} + \mu \bar{I}$$

Equation (4) - (Linear approximation):

$$\hat{N}_3 = \frac{\gamma N_0}{\Gamma - \gamma}\left(e^{-\gamma t} - e^{-\Gamma t}\right)$$

Equation (5) - (Linear approximation):

$$\hat{k}(t, t') = \frac{2\gamma N_0}{\Gamma - \gamma}\left[\frac{e^{-\gamma t} - e^{-\gamma t}}{\gamma} - \frac{e^{-\Gamma t'} - e^{-\Gamma t}}{\Gamma}\right] + N_0\left(\frac{e^{-\gamma t'} - e^{-\gamma t}}{\gamma}\right) - N_0(t - t')$$

B2. STEP BY STEP DESCRIPTION OF ALGORITHM

Fig. B1 shows the step by step iteration process used in the algorithm. Initially the linear approximation, function I(t), is used to calculate two starting pointsby iteration; then from these a two point, linear, extrapolation procedure is set up and used to project an initial point for the next set of iterations. The steps are indicated and numbered on the left, while the equations from which the equations in the codes are derviced are indicated on the right in paranthesis.

Step 1 Calculate $\hat{I}(t)$ on the range $t = 0$ to $t = t_n$ from (1) and (5)

$$\hat{I}(t) = \frac{g^2\gamma}{N} e^{-\Gamma t} \int_0^t \int_0^1 I_0^2\, 2\sqrt{\hat{k}(t,t')\, x'}\; e^{-\mu x' + (\Gamma - \gamma) t'}\, dx'\, dt' \qquad (1)$$

$$\hat{k}(t,t') = \frac{2\gamma N_0}{\Gamma - \gamma}\left(\frac{e^{-\gamma t'} - e^{-\gamma t}}{\gamma} - \frac{e^{-\Gamma t'} - e^{-\Gamma t}}{\Gamma}\right) \qquad (5)$$

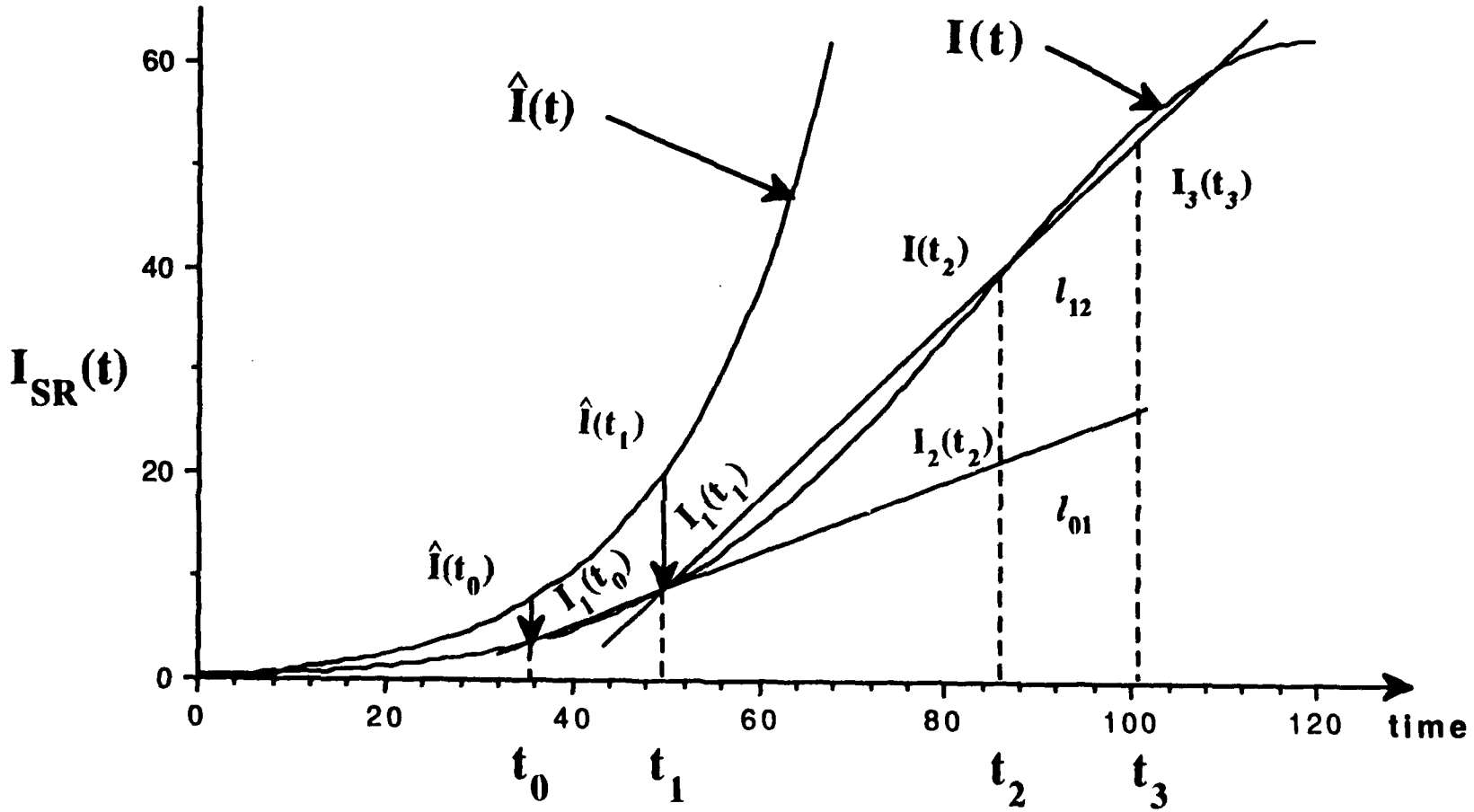

Figure B1. Schematic showing numerical procedure for calculating SF pulse. $\hat{I}(t)$ gives the linear solution and I(t) the final solution, including the non-linear terms.

$$+ N_0 \left(\frac{e^{-\gamma t'} - e^{-\gamma t}}{\gamma} \right) - N_0 (t - t')$$

Step 2 Use $\hat{I}(t)$ to calculate $I_1(t)$ and $I_1(t_1)$ from equations (2), (3) and (1) (with I(t) substituted for $\hat{I}(t)$):

$$N_3(t_0) = \frac{\gamma N_0}{\Gamma - \gamma} \left(e^{-\gamma t} - e^{-\Gamma t} \right) - \beta \int_0^t e^{-\Gamma (t - t')} \hat{I}(t')\, dt' \qquad (3)$$

where $\beta = \frac{1}{g} + \mu \bar{I}$

$$k(t,t') = 2 \int_{t'}^{t} N_3(t'')\, dt'' + N_0 \left[\frac{e^{-\gamma t'} - e^{-\gamma t}}{\gamma} \right] - N_0 (t - t') \qquad (2)$$

$$I_1(t_0) = \frac{g^2 \gamma}{N} e^{-\Gamma t} \int_0^t \int_0^1 I_0^2 \left[2\sqrt{k(t,t')\, x'} \right] e^{-\mu x' + (\Gamma - \gamma) t'}\, dx'\, dt'$$

Step 3 Use points $I_1(t_0)$ and $I_1(t_1)$ to calculate slope S_{01} of line l_{01}, and then use S_{01} and $\Delta t = t_2 - t_1$ to calculate $I_2(t_2)$ which is initial estimate for $I(t_2)$.

Step 4 Use eqs (1), (2) and (3) to calculate first iteration estimate for $I(t_2)$ in the following way: use $I(t_2)$ for I(t) in eq. 3 and then the resulting N_3 in eq. 2 to get first iteration result for I(t).

Second iteration - use I(t) in step 3 and 4 to calculate the new I(t). Then, with these two point replacing $I_1(t_0)$ and $I_1(t_1)$, repeat step 2 and continue this process until convergence is satisfactory.

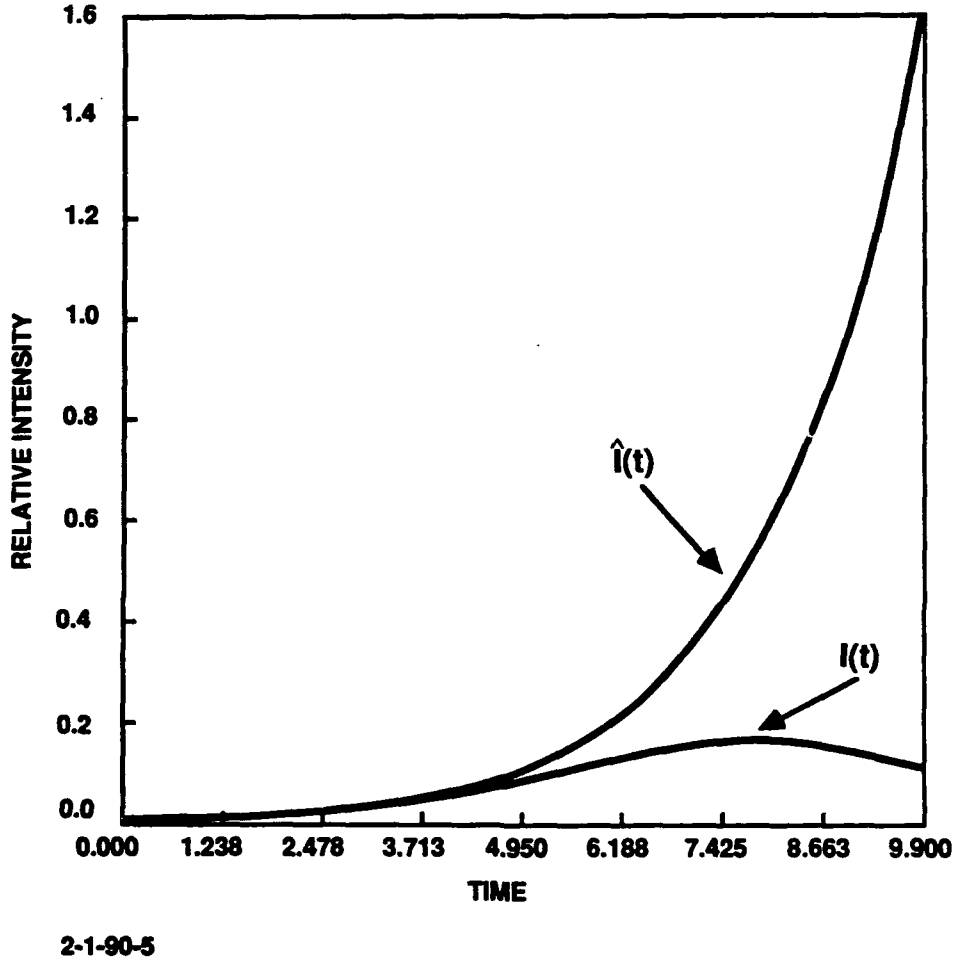

Figure B2. Sample output for N = 10^3 and $\gamma = 50$, $\Gamma = 10^{-3}$ and $\Delta t = T = t_{i+1} - t_i = 0.1$, showing the linear solution $\hat{I}(t)$ and the final result I(t). Time is in units of τ_{SF}.

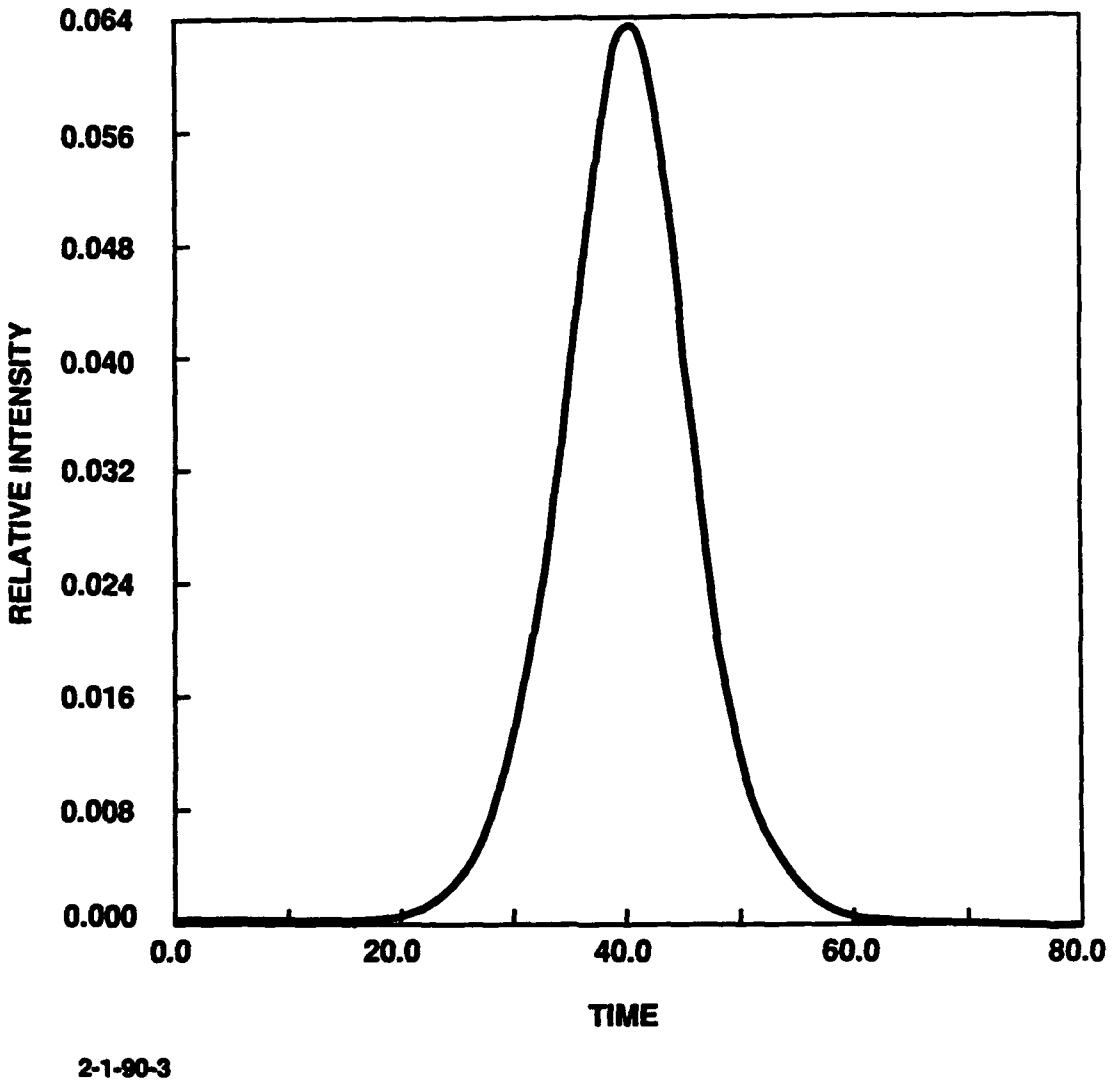

Figure B3. Another sample run with N = 10^{10} showing the final result after an average of three iterations per time point.

DESCRIPTION/DATA AND VARIABLE NAMES

Following is a description of the data written to the various unit numbers in the FORTRAN program. In the command procedure these unit numbers are assigned to ASCII files which can be edited or printed.

Unit	Description of the Data
12	T, iteration #1 to 3; N_3, result of eq. 1 w/o the dt' integral; , result of eq. 1
14	1st 30 entries in the k(t,t') array
15	T; eq. 1 before integral; integral in eq. 1, eq. 1, counter
17	T, eq. 1 before double integral, N_A; N_B; N_3, result of eq. 1 w/o the dt integral, slope between this poin t and previous point, slope value

Variable Names

Text	Computer Code	
g	G	
γ	GAMSML	(input)
N	N	(input)
Γ	GAMLRG	(input)
μ	MU	(input)
N_o	NO	(input)
$2*\sqrt{k(\tau,t')x'}$	Besl	
$\Gamma-\gamma$	GLMGS	
$\gamma-\Gamma$	GSMGL	
$\bar{l}$	LBAR	

$\frac{g^2\gamma}{N}$	GSTGSDN	
dx increment	DELTAX	(input)
	TCHANGE	
location in $\int_0^t$	T	
minimum t in $\int_0^t$ (usually 0)	TMIN	
the t in $\int_0^t$	TMAX	
increment in $\int_0^t$	TINCR	

The subroutine name and equation number in the text are correlated in the following way: Subroutine Eq. 1 is equation number 1.

LISTING OF PROGRAM

```
      PROGRAM BESAPRJ2
C     Written by Karen K. Garcia
C     April 21, 1989
C     This program uses a Bessel function
C     from the IMSL routines
      PARAMETER (NSIZE=1000,KSIZE=1000)
      DIMENSION IPK1(300)
      REAL X(NSIZE), EQ16ARR(NSIZE), NO, MU, G, LBAR,
     *     N, N3, KTTP(KSIZE,KSIZE), NA, NB, NAPART1
      COMMON /BLOCK1/ NO, MU, GAMLRG, GAMSML, KTTP
      COMMON /BLOCK2/ YINPT, G, N3, Y(NSIZE), Y2(NSIZE), NA, NB
      COMMON /BLOCK3/ NAPART1, BTA, SLOPEVAL(NSIZE), TCHANGE
      COMMON /BLOCK4/ EQ20T1
      G = 1.0
      WRITE(6,*)'Enter min, max and incr of time'
      READ(5,*)TMIN,TMAX,TINCR,tmax2
      WRITE(6,*)' 1st TMAX= ',TMAX
      WRITE(6,*)' 1st TMAX2= ',TMAX2
C
      WRITE(6,*)'Enter delta x value'
      READ(5,*)DELTAX
C
C     Read in the values for the input data
      WRITE(6,*)'Type value for No'
      READ(5,*)NO
      WRITE(6,*)'Type the value for MU'
      READ(5,*)MU
      WRITE(6,*)'Type the value for large gamma'
      READ(5,*)GAMLRG
      WRITE(6,*)'Type the value for N'
      READ(5,*)N
C
C     Check the initial value for lbar
      lbar = 0.1
      ICNT = 1
C
      WRITE(6,*)'Type the value for small gamma'
      READ(5,*)GAMSML
      WRITE(6,*)'Type value for the start of the slope'
      READ(5,*)TCHANGE
C
      GLMGS = GAMLRG - GAMSML
      GSMGL = GAMSML - GAMLRG
      GSTGSDN = (G**2 * GAMSML) / N
      NAPART1 = (GAMSML * NO) / (GAMLRG - GAMSML)
      BTA = (1.0 / G) + (2.0 * 0.5*MU * LBAR)
      EQ20T1 = (2.0 * GAMSML * NO) / GLMGS
C
C
      YMIN = 9.0e20
      YMAX = -9.0E20
      I = 1
      NCALL = 1
      OPEN(UNIT=15,DISPOSE='KEEP',STATUS='NEW')
      WRITE(15,15)
15    FORMAT(2x,'T',4X,'EQ16 TERM 1',2X,
     *     ' INTEG',2X,'EQ16&20',3X,'ICNT')
C     Check to see if tmin = tmax
```

```
      IF(TMAX-TMIN.LT.TINCR)GOTO 25
      ITER = 0
      T = TMIN
      DO WHILE(T.LE.TMAX)
        CALL EQ1(TSUM,TINCR,NCALL,T,ITER,
     *           ICNT,GLMGS,DELTAX)
C
C       Save the X values
        X(I) = T
C
C       Compute the equation labelled 16
        EQ16T1 = GSTGSDN * EXP(-GAMLRG * T)
        EQ16ARR(I) = EQ16T1
        Y(I) =  EQ16T1 * TSUM
        YMIN = MIN1(YMIN,Y(I))
        YMAX = MAX1(YMAX,Y(I))
        WRITE(15,20)X(I),EQ16T1,TSUM,Y(I),I
 20      FORMAT(1X,F6.2,2X,E8.2,3X,E10.4,3X,E10.4,3X,I4)
        I = I + 1

C       Check against the array size
        IF(I.GT.NSIZE)THEN
        WRITE(6,*)'INCREASE ARRAY DIMENSION. (NSIZE)'
        CALL EXIT
        END IF
        T = T + TINCR
      END DO
 25   CONTINUE
      CLOSE(UNIT=15,DISPOSE='KEEP')
      OPEN(UNIT=14,DISPOSE='KEEP',STATUS='NEW')
C     write out the KTTP array
       write(14,*) 'columns 1 - 10'
       write(14,27)
 27    format(1x,10x,'0',10x,'1',10x,'2',10x,'3',10x,'etc.')
      DO II = 1,30
        WRITE(14,26)ii,(KTTP(II,JJ),JJ=1,10)
      END DO
       write(14,*)' '
       write(14,*) 'columns 11 - 20'
       write(14,*)' '
      DO II = 1,30
        WRITE(14,26)ii,(KTTP(II,JJ),JJ=11,20)
      END DO
       write(14,*)' '
       write(14,*) 'columns 21 - 30'
       write(14,*)' '
      DO II = 1,30
        WRITE(14,26)ii,(KTTP(II,JJ),JJ=21,30)
      END DO
      CLOSE(UNIT=14,DISPOSE='KEEP')
 26   FORMAT(i4,10(1X,E10.4))
C*************************************************************************
C     END OF FIRST EQUATIONS SET, START OF SECOND EQUATIONS SET
C*************************************************************************
C
      I = I - 1
      LASTI = I
      NCALL = 2
```

```
C
C       Write the headers for the second equation set
        OPEN(UNIT=12,DISPOSE='KEEP',STATUS='NEW')
        OPEN(UNIT=17,DISPOSE='KEEP',STATUS='NEW')
        WRITE(12,30)
 30     FORMAT(5X,'T',5X,'J',8X,'N3',15X,'IHAT(T)',
     *      12X,'IPRIME(t)')
        WRITE(17,199)
 199        FORMAT(4X,'T',2X,'EQ1 TERM 1',4X,'NA',7X,'NB',
     *      7X,'N3',6X,'Ihat(t)',4X,'Slope value',4X,
     *      'I(t) Nth',5X,'SLOPE')
C       Compute the second set of equations
        ICNT = 0
C
C       6/6/89 KKG Copy the Ihat array to the new I array
C       This will be used for the iterations
        DO IFILL = 1,LASTI
         Y2(IFILL) = Y(IFILL)
        END DO
C
        DO J = 1, LASTI
C        Restore the x value from the above computation
         T = X(J)
C
C        Iterate over the re-substitution of the I(t) term.
         DO K = 1,3
C
C        Equation 1 parameters
C          TSUM - output
C          TINCR, NCALL, T - input
           CALL EQ1(TSUM,TINCR,NCALL,T,K,
     *          ICNT,GLMGS,DELTAX)
C
         YINPT = EQ16ARR(j) * TSUM
         Y2(J) = YINPT
         WRITE(12,35)T,K,N3,Y(J),YINPT
 35      FORMAT(1X,f6.2,1X,I4,3(1X,E20.13))
         END DO
         IF(j.GT.1)THEN
C
C        Compute the slope
         SLOP = (Y2(j) - Y2(j-1))
     *          / (X(j) - X(j-1))
         WRITE(12,*)'SLOPE BETWEEN ',j-1,
     *          ' AND ',j,' IS ',SLOP
                write(12,*)'the values are y2(j,j-1),x(j,j-1)',y2(j),
     *          y2(j-1),x(j),x(j-1)
         END IF
         IF(T.GE.TCHANGE)THEN
           SLOPEVAL(J+1) = Y2(J) + (SLOP * TINCR)
           Y2(J+1) = Y2(J) + (SLOP * TINCR)

         END IF
C        write data to unit 17

        IF(J.EQ.1)THEN
         WRITE(17,200)T,EQ16ARR(J),NA,NB,N3,Y(j),
     *          SLOPEVAL(J+1),Y2(J)
```

```
        ELSE
         WRITE(17,200)T,EQ16ARR(J),NA,NB,N3,Y(j),
     *          SLOPEVAL(J+1),Y2(J),SLOP
        END IF
 200      FORMAT(1X,F6.2,5(2X,E8.2),4(3X,E10.4))
        END DO
        CLOSE(UNIT=12,DISPOSE='KEEP')
        CLOSE(UNIT=17,DISPOSE='KEEP')
CKG     END DO
      END
C*********************************************************************
C     ALL SUBROUTINES BELOW HERE
C*********************************************************************
C*********************************************************************
C       EQUATION 1
C*********************************************************************
C
      SUBROUTINE EQ1(TSUM,TINCR,NCALL,T,ITER,
     *    ICNT,GLMGS,DELTAX)
C
C       Equation 1 parameters
C       TSUM - output
C       TINCR, NCALL, T - input
C
        PARAMETER (NSIZE=1000,KSIZE=1000)
        REAL NO, MU, N, N3, KTTP(KSIZE,KSIZE),NA,NB,G,NAPART1,
     *      TEMPEQ16T2, EQ16T2
        DOUBLE PRECISION EQ16T3, EQ16T3N2, DEQ20, DXPRIME
        COMMON /BLOCK1/ NO, MU, GAMLRG, GAMSML, KTTP
        COMMON /BLOCK2/ YINPT, G, N3, Y(NSIZE), Y2(NSIZE),
     *      NA,NB
        COMMON /BLOCK3/ NAPART1, BTA, SLOPEVAL(NSIZE), TCHANGE
        COMMON /BLOCK4/ EQ20T1
C
C       VARIABLE DEFINITION
C         NCALL - Number of the equation set that
C         this subroutine is called for.
C         i.e. 1 - for first curve
C           2 - for second curve
C
        TTSUM = 0.0
        TSUM = 0.0
        TNEWSUM = 0.0
C       Check
        IF(T.LT.Tincr)GOTO 20
        TPRIME = 0.0
        TLAST = T - TINCR
        j0flg = 0
        DO WHILE(TPRIME.LE.TLAST)
C
         IF(NCALL.EQ.1)THEN
         IBSLFLG = 0
         CALL EQ5(EQ20,TPRIME,T,TINCR,GLMGS,tppt)
         IF(EQ20.LT.0.0)THEN
         WRITE(6,*)'J0 USED 1st eq. EQ20= ',EQ20,' tprime= ',tprime
          IBSLFLG = 1
         END IF
         ELSE IF (NCALL.EQ.2)THEN
```

```
          IBSLFLG = 0
        CALL EQ2(TINCR,EQ20,TPRIME,T,ITER,IBSLFLG)
         END IF
C
         XPRIME = 0.0
         TXSUM = 0.0
         IXCNT = 1
         XLAST = 1.0 - XPRIME
         EQ16T3P2 = (GLMGS * TPRIME)
         DO WHILE(XPRIME.LE.1.0)
C
C        Compute the equation labelled 16 integration portion
C
          XPPT = XPRIME + DELTAX
          IF(IBSLFLG.EQ.0)THEN
        DEQ20 = EQ20
        DXPRIME = XPRIME
           EQ16T2 = DBSI0(2.0D0 * DSQRT(DEQ20 * DXPRIME))
         ELSE IF(IBSLFLG.EQ.1)THEN
           IF(J0FLG.EQ.0)THEN
             WRITE(6,*)'J0 BESSEL FUNCTION USED'
             WRITE(6,*)'XPRIME,TPRIME',XPRIME,TPRIME
             J0FLG = 1
           END IF
C        7/3/89 Put Irv Kay's J0 bessel function in here
           BESL = (2.0 * SQRT(EQ20 * XPRIME))
C
C        POWER SERIES
           IF(BESL.LT.10.0)THEN
          DO NBES = 1,18
           F1TOP = (-((BESL/2.0)**2)**NBES)
C          Compute N factorial
           rFACT = 1.0
           DO L = NBES,1,-1
             rFACT = rFACT * float(L)
           END DO
           F1BOT = rFACT ** 2
           EQ16T2 = (F1TOP / F1BOT) + 1.0
          END DO
C
C        ASYMPTOTIC
        ELSE IF (BESL.GE.10.0)THEN
          PI = 3.141592654
          F2TRM1 =  SQRT(2.0 / (PI * BESL))
          F2TRM2 = COS(BESL - (PI / 4.0))
          EQ16T2 = F2TRM1 * F2TRM2
        END IF
          END IF
            EQ16T2 = EQ16T2 ** 2
         EQ16T3N2 = 0.0D0
         EQ16T3 = 0.0D0
         EQ16T3P1 = -2.0 * 0.5*MU * XPRIME
         EQ16T3 = EXP(EQ16T3P1 + EQ16T3P2)
         EQ16T3N2 = EXP(EQ16T3P1 + GLMGS * TPPT)
         EQ16T3 = (EQ16T3 + EQ16T3N2) / 2.0D0
         IF(EQ16T3.LT.1.0E-10)THEN
           EQ16T3 = 1.0E-10
         END IF
```

```
          EQ16 = EQ16T2 * EQ16T3
          IF(IXCNT.EQ.1)THEN
           TXSUM = EQ16 * DELTAX
           PREVTX = TXSUM
           IXCNT = IXCNT + 1
           TXSUM = 0.0
          ELSE
          TXSUM = TXSUM + ((EQ16*DELTAX) + PREVTX)/2.0
          PREVTX = EQ16 * DELTAX
          END IF
          XPRIME = XPRIME + DELTAX
         END DO
           IBSLFLG = 0
         IF(Icnt.EQ.1)THEN
          TTSUM = TXSUM * TINCR
          PREVTT = TTSUM
          ICNT = ICNT + 1
          TTSUM = 0.0
         ELSE
          TTSUM = TTSUM + ((TXSUM*TINCR) + PREVTT)/2.0
          PREVTT = TXSUM * TINCR
         END IF
         TPRIME = TPRIME + TINCR
          END DO
          TSUM = TTSUM
 20     CONTINUE
C
       RETURN
       END
C
C*********************************************************************
C       EQUATION 2
C*********************************************************************
       SUBROUTINE EQ2(TINCR,EQ20,TPRIME,T,ITER,IBSLFLG)
        PARAMETER (NSIZE=1000,KSIZE=1000)
        REAL NO, MU, N, N3, N3SUMSAV, N3SUMPREV, N3SUMCUM,
     *      KTTP(KSIZE,KSIZE), K0T, K0TPR, NA, NB,K0TT2,
     *      K0TTPT2, NAPART1
        COMMON /BLOCK1/ NO, MU, GAMLRG, GAMSML, kttp
        COMMON /BLOCK2/ YINPT, G, N3, Y(NSIZE), Y2(NSIZE),
     *      NA,NB
        COMMON /BLOCK3/ NAPART1, BTA, SLOPEVAL(NSIZE), TCHANGE
C       Compute equation 2
        XN3 = 0.0
        xn3sum = 0.0
        IF(T.LT.TINCR)GOTO 20
        TVAL = 0.0
        K0TT2 = EXP(-GAMSML * T)/GAMSML
        DO WHILE(TVAL.LE.T)
         IF((TVAL-TINCR).LT.TINCR)THEN
           N3 = 0.0
           XN3 = 0.0
         ELSE
         TDPRIME = TVAL - TINCR
         CALL  EQ3(TINCR,TDPRIME,ITER)
           XN3 = N3
         END IF
         TDPRIME = TVAL
```

```
      CALL EQ3(TINCR,TDPRIME,ITER)
      XN3 = (XN3 + N3) /2.0 * TINCR
      xn3sum = xn3sum + xn3
      TVAL = TVAL + TINCR
      END DO
 20   CONTINUE
      xn3 = xn3sum
      K0T = 2.0 * XN3 - NO * (K0TT2 + T)
C
      XN3 = 0.0
      xn3sum =0.0
      IF(TPRIME.LT.TINCR)GOTO 25
      TVAL = 0.0
      K0TTPT2 = EXP(-GAMSML * Tprime)/GAMSML
      DO WHILE(TVAL.LE.TPRIME)
       IF((TVAL-TINCR).LT.TINCR)THEN
         N3 = 0.0
         XN3 = 0.0
       ELSE
         TDPRIME = TVAL - TINCR
         CALL EQ3(TINCR,TDPRIME,ITER)
         XN3 = N3
       END IF
       TDPRIME = TVAL
       CALL EQ3(TINCR,TDPRIME,ITER)
       XN3 = (XN3 + N3) /2.0 * TINCR
       xn3sum = xn3sum + xn3
       TVAL = TVAL + TINCR
      END DO
 25   CONTINUE
      xn3 = xn3sum
      K0TPR = 2.0 * XN3 - NO * (K0TTPT2 + Tprime)
      EQ20 = K0T - K0TPR

C     5/30/89 KKG Add code to set flag to use J0 bessel
c     function if eq20 less than 0.0
      IF(EQ20.LT.0.0)THEN
        IBSLFLG = 1
        EQ20 = ABS(EQ20)
      END IF
     RETURN
     END
C
C*********************************************************************
C      EQUATION 3
C*********************************************************************
     SUBROUTINE EQ3(TINCR,TDPRIME,ITER)
      PARAMETER(NSIZE=1000,KSIZE=1000)
      REAL NO, MU, N,  NBSUM, N3, NA, NB,
     *     NAPART1, KTTP(KSIZE,KSIZE), NAPART2, IOFT,
     *     N3SUMCUM, NBSUMSAV, NBSUMPREV, NB1, NB2
      COMMON /BLOCK1/ NO, MU, GAMLRG, GAMSML, kttp
      COMMON /BLOCK2/ YINPT, G, N3, Y(NSIZE), Y2(NSIZE),
     *     NA, NB
      COMMON /BLOCK3/ NAPART1, BTA, SLOPEVAL(NSIZE), TCHANGE
      NA = 0.0
      NB = 0.0
C     Compute equation 3
```

```
      NAPART2 = EXP(-GAMSML * TDPRIME)-EXP(-GAMLRG * TDPRIME)
      NA = NAPART1 * NAPART2
      NBSUM = 0.0
      IF(TDPRIME.LT.TINCR)GOTO 20
      ICNT = 1
      TVAL = 0.0
      DO WHILE(TVAL.LE.TDPRIME)
       NB1 = EXP(GAMLRG * (TDPRIME - Tval)) * Y2(ICNT)
       nbsum = nbsum + (nb1*tincr)
       ICNT = ICNT + 1
       TVAL = TVAL + TINCR
      END DO
      NB = BTA * NBSUM
20    CONTINUE
      N3 = NA - NB
     RETURN
     END
C
C*********************************************************************
C       EQUATION 5
C*********************************************************************
C
      SUBROUTINE EQ5(EQ20,TPRIME,T,TINCR,GLMGS,tppt)
       PARAMETER (KSIZE=1000)
       REAL NO, MU, GAMLRG, GAMSML, N, kttp(KSIZE,KSIZE)
       COMMON /BLOCK1/ NO, MU, GAMLRG, GAMSML, kttp
       COMMON /BLOCK4/ EQ20T1
C
C      Compute the equation labelled 20 or equation 5
C
       TPPT = TPRIME + TINCR
      EQ20T2 = EXP(-GAMSML * TPRIME)
      EQ20T2P2 = EXP(-GAMSML * T)
      EQ20T2 = (EQ20T2 - EQ20T2P2) / GAMSML
      EQ20T2N2 = (EXP(-GAMSML * TPPT) -
     *    EQ20T2P2) / GAMSML
      EQ20T3 = (TPRIME - T)
      EQ20T3N2 = (TPPT - T)
      EQ20T4 = NO * EQ20T2
      EQ20T4N2 = NO * EQ20T2N2
      EQ20T5 = NO * (T - TPRIME)
      EQ20T5N2 = NO * (T - TPPT)
      EQ20p = EQ20T1 * (EQ20T2 + EQ20T3) + EQ20T4 - EQ20T5
      EQ20N2 = EQ20T1 * (EQ20T2N2 + EQ20T3N2) +
     *    EQ20T4N2 - EQ20T5N2
      EQ20 = (EQ20p + EQ20N2) / 2.0
      IF(((int(t*(1.0/tincr))).GT.KSIZE).OR.
     *    (int(tprime*(1.0/tincr)).gt.ksize))THEN
       WRITE(6,*)'INCREASE SIZE OF KSIZE VARIABLE'
       CALL EXIT
      END IF
     kttp(int(t*(1.0/tincr)),int(tprime*(1.0/tincr))) = eq20
      RETURN
      END
```

APPENDIX C

A STUDY OF THE DIFFERENCE IN PULSE LINESHAPE FROM SF AND ASE

APPENDIX C

A STUDY OF THE DIFFERENCE IN PULSE LINESHAPE FROM SF AND ASE

Amplified spontaneous emission (ASE) and superfluorescence (SF) can be distinguished theoretically (Ref. C-1) and experimentally (Ref. C-2). In this section we discuss the differences between ASE and SF pulse shapes calculated in the semiclassical approximation. From the work of Trammell and Hannon (Ref. C-3) we obtain the pulse intensity for an initially Lorenzian pulse after passage through an amplifying medium of length *l*.

$$I_p(t) = e^{-\Gamma t} I_o^2 \left(\sqrt{K_o l \Gamma t \left(2e^{-\Gamma t} - 1 \right)} \right) e^{-\mu l} \quad ,$$

with

$$K_0 = \frac{2\pi\lambda^2 \, fg\Delta n^* \, (t)}{(\alpha + 1)\,(a + 1)} \quad ,$$

where

- λ is the wavelength on resonance
- f is the recoilless fraction
- g is the coupling constant (= 1 for present)
- Δn^* is the inversion density at t = 0
- α is the internal conversion coefficient
- a is the inhomogeneous broadening parameter.

From the work of Bonifacio and Lugiato (Ref. C-4) we obtain the pulse intensity for an SF emission which is given by

$$I_s(t) = \frac{1}{2} \frac{N'}{\tau_R} e^{-t/T_2^*} \operatorname{sech}^2 \left[\frac{1}{\tau_R} (t - t_D) \right] \quad ,$$

where

$\tau_D = 1/2\, \tau_R\, ln\, N$

N is the total number of cooperative nuclei

$$N' = \frac{f\,N}{(1+\alpha)\,(1+a)}$$

$\tau_R = k\,(g^2\,\rho) = 8\pi\,\tau_o/(\rho\lambda^2 l)$

τ_o is the natural lifetime

ρ = N/V is the density of radiators in the cooperation volume.

In making the comparison between $I_s(t)$ and $I_p(t)$ we assume the nominal values of:

$\tau_o = 1$ s,

$\rho = 10^{22}\ cm^{-3}$

$\lambda = 10^{-8}$ cm

$l = 1$ cm

$f = 10^{-1}$

$\alpha = 10$

$a = 0$

$V = 3 \times 10^{-8}\ cm^3$

$T_2^* \rightarrow \infty$.

Figure C-1 shows the variations of the ASE pulse $I_p(t)$ as a function of the inversion Δn^* for values of Δn^* from 10^{22} cm^{-3} to 10^{17} cm^{-3} and $\mu = 0$. Figure C-2 shows the variation in the pulse for $\mu = 0, 1, 10, 10^2$ and $\Delta n^* = 10^{22}$. Figure C-3 shows the SF pulses $I_{SF}(t)$ as a function of N = nV and Fig. C-4 shows the SF pulses as a function of μ. To perform this calculation both τ_R and τ_D were modified by the factor θ/μ as described in the text to take into account the reduction in the effective cooperative volume for large values of μ.

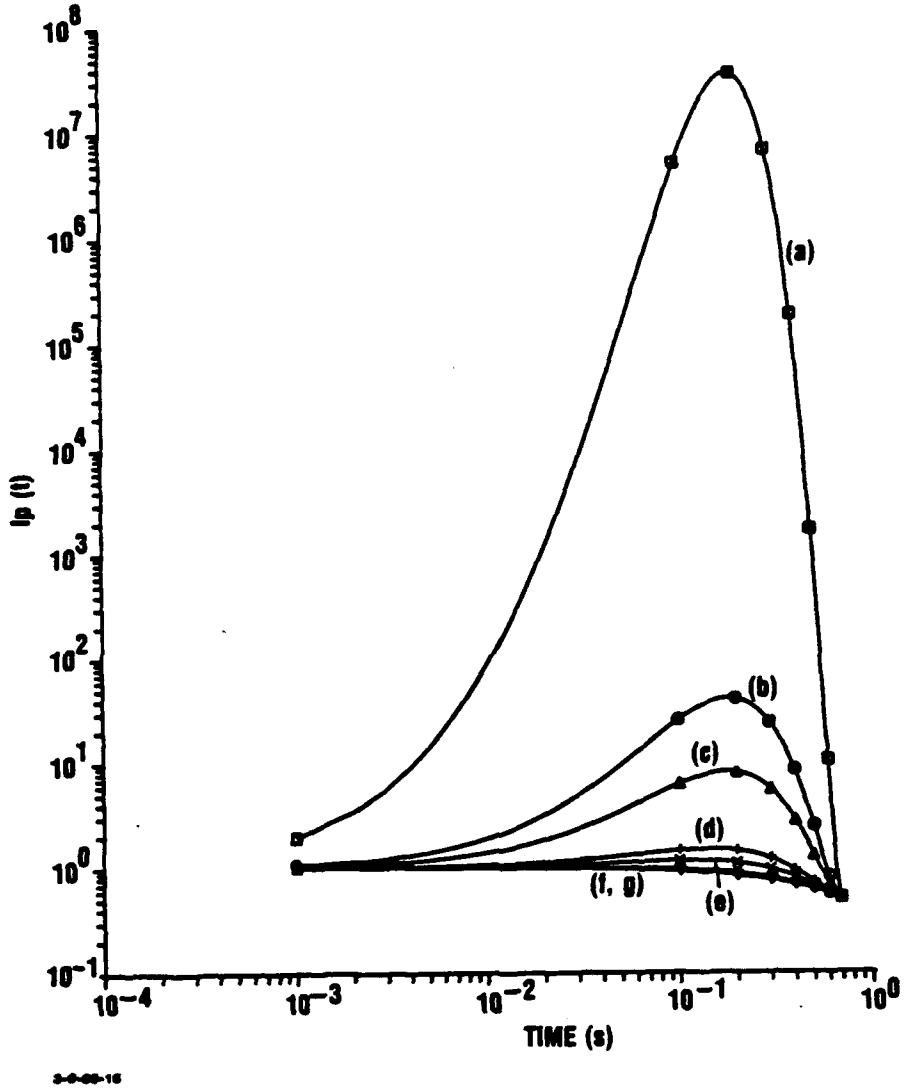

Figure C-1. The ASE pulse as a function of time for different initial inversion densities in cm^{-3}, (a) = 10^{22}, (b) = 10^{21}, (c) 5×10^{20}, (d) 10^{20}, (e) 5×10^{19}, (f) 10^{19}, (g) 10^{18}, and $\mu = 0$ and $\Gamma = 1\ s^{-1}$ for all cases.

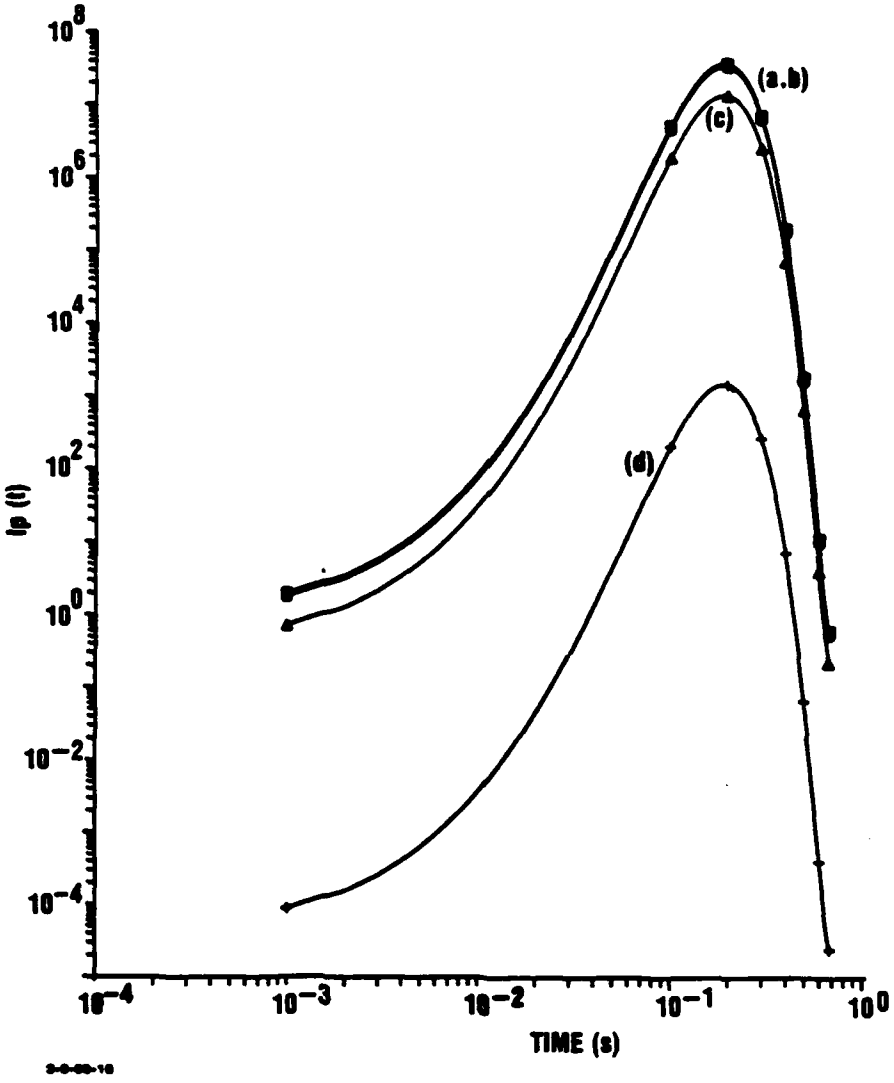

Figure C-2. The ASE pulse as a function of time for different values of μ (a) $\mu = 0$, (b) $\mu = 0.1$ cm^{-1}, (c) $\mu = 1$ cm^{-1}, (d) $\mu = 10$ cm^{-1}, and the initial inversion $\Delta n^* = 10^{22}$ cm^{-3} and $\Gamma = 1$ s.

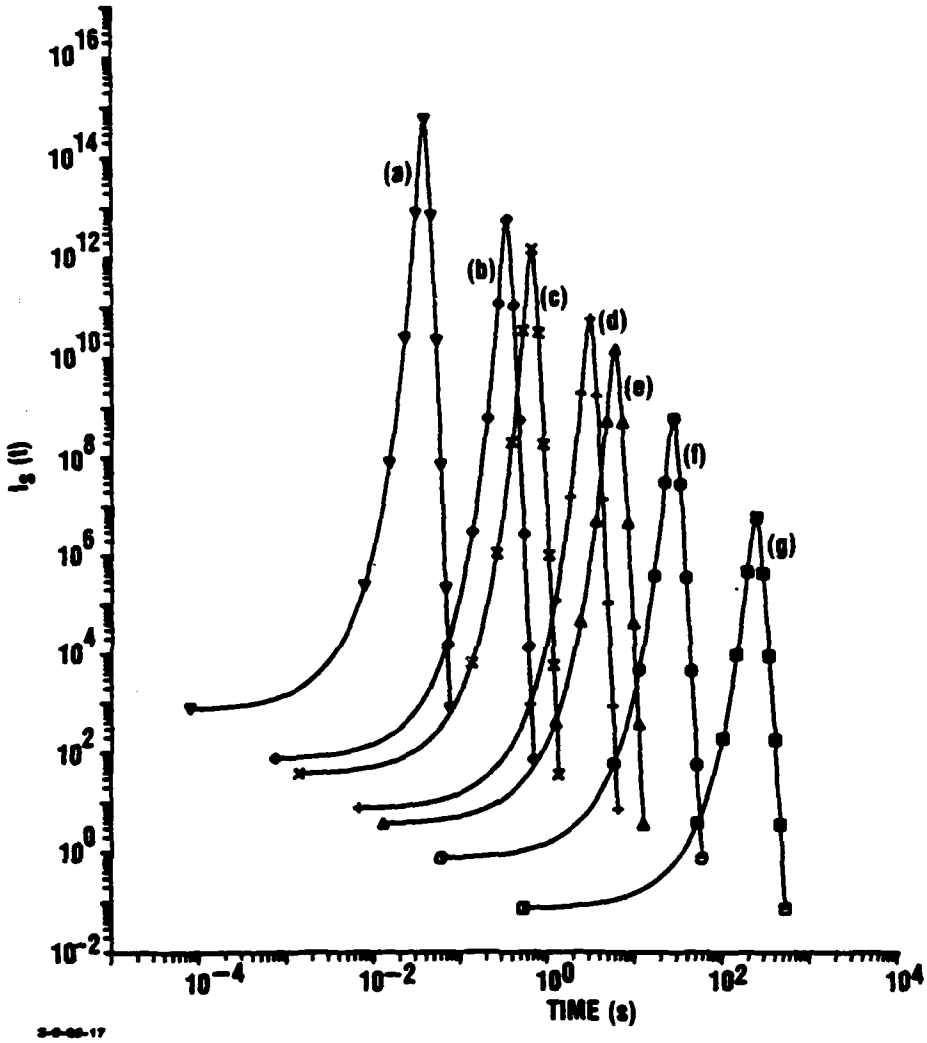

Figure C-3. The SF pulse as a function of time for different values of the initial inversion Δn^* in cm^{-3}, (a) = 10^{22}, (b) = 10^{21}, (c) 5×10^{20}, (d) 10^{20}, (e) 5×10^{19}, (f) 10^{19}, (g) 10^{18}, and for all cases $\Gamma = 1\ s^{-1}$, and $\mu = 0$.

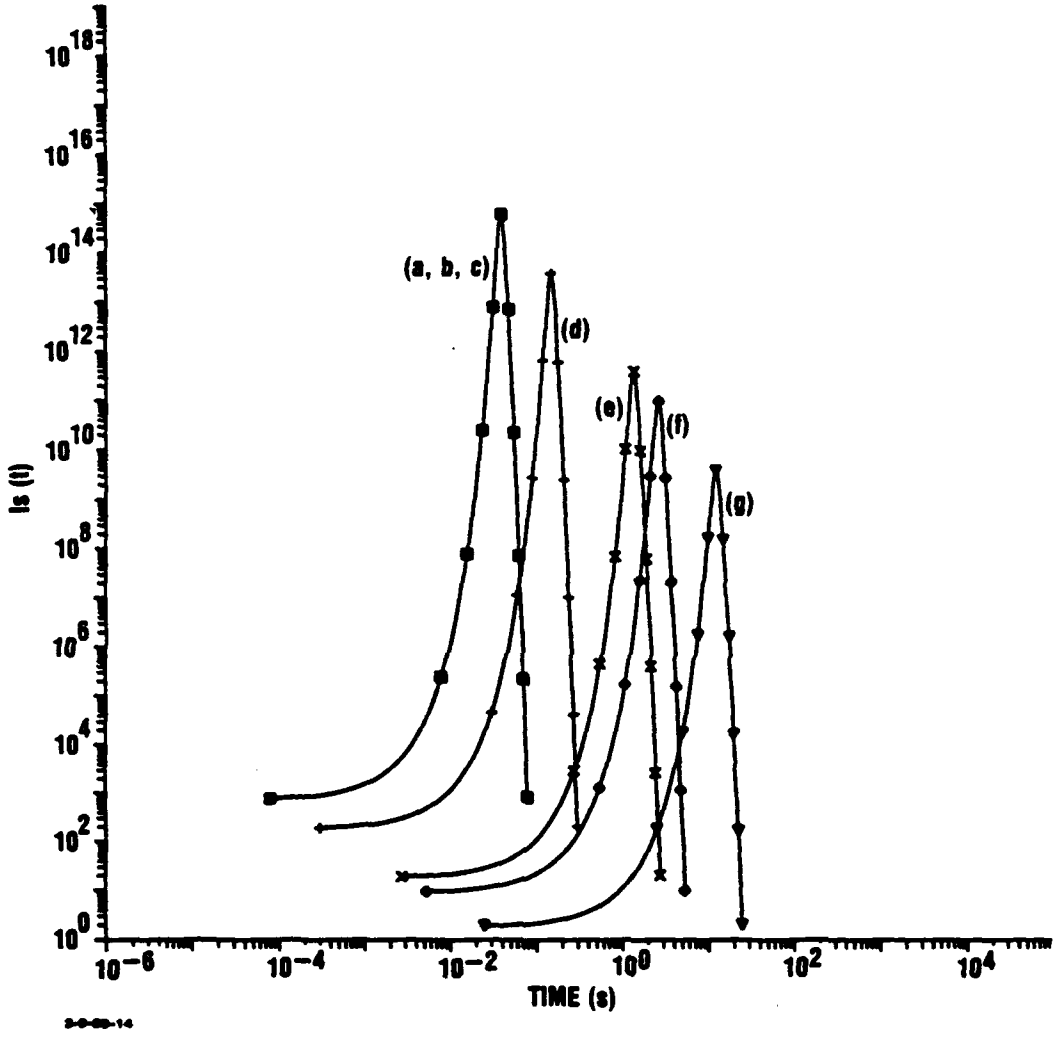

Figure C-4. The SF pulse as a function of time for different values of the *attenuation coefficient* μ *in* cm^{-1}, (a) = 0, (b) = 0.1, (c) 1.0, (d) 10, (e) 10^2, (f) 2×10^2, (g) 10^3, and for all cases $\Gamma = 1\ s^{-1}$ and $\Delta n^* = 10^{22}\ cm^{-3}$.

REFERENCES, APPENDIX C

C-1. M.F.H. Schuurmans and D. Polder, *Phys. Lett.*, *72A*, (415), 306, 1979.

C-2. J. Okada, K. Ikeda, and M. Matsuoka, *Opt. Commun. 27*, (3), 321, 1978.

C-3. G.T. Trammell and J.P. Hannon, *Opt. Commun. 15*, (3), 325, 1975.

C-4. R. Bonifacio and L.A. Lugiato, *Phys. Rev. A.*, *11*, (5), 1507-1521, May 1975.

APPENDIX D

METHOD OF ANALYSIS OF THERMAL TRANSFER

APPENDIX D

METHOD OF ANALYSIS OF THERMAL TRANSFER

D1. THE FINITE ELEMENT SIMULATION TECHNIQUE

The finite element simulation technique (FEST) has been described in Refs. D-1, D-2, and D-3 and has been used to treat several different types of problems. We will therefore only sketch the general procedure here.

FEST applies the laws of conduction of heat and mass action to a system composed of any number and variety of materials in the following way. The system is divided into a number of convenient cells, each with a definite density ρ, thermal conductivity K, specific heat c_p, and diffusivity κ. The temperature in each cell is specified initially and then a time interval is chosen over which conduction is to take place.

Heat conduction during the time interval Δt takes place from one cell to another according to Fourier's law of heat transfer. For cells (i) and (i – 1) this is given by

$$\Delta Q(i-1, i) = \frac{A(i, i-1)}{\Delta X(i, i-1)} K(i, i-1)(T_i - T_{i-1}) \Delta t \qquad \text{(D-1)}$$

where A(i, i – 1) is the area across which the transfer takes place, K(i, i – 1) the effective thermal conductivity between cells, which can be calculated from the thermal conductivities of the two cells, $\Delta X(i, i-1)$ the separation of the cell center, $T_i - T_i - 1$ the temperature difference, and $\Delta Q(i, i-1)$ is the heat transferred between cells i and i – 1 during the time interval Δt.

The temperature change in the ith cell after this transfer of heat between the ith cell and the two neighboring cells (i – 1) and (i + 1) is

$$\Delta T_i = [\Delta Q(i-1, i) - \Delta Q(i, i+1)](c_p \rho_i V_i) \quad , \qquad \text{(D-2)}$$

where V_i is the volume of cell i. The conductance is expressed as $cnd_i = K_i A_i/\Delta X_i$. When the medium changes at the interface between i and i + 1, we use instead the expression

$$2\, cnd_i\, cnd_{i+1} / (cnd_i + cnd_{i+1}) \quad .$$

This type of program allows for relatively easy solutions to complicated multi-layered boundary problems (Refs. D-4, D-5). Another medium can be added without an appreciable increase in complexity of the program, whereas in the usual numerical methods of solving the partial differential equation of heat conduction this is not the case.

In addition to the passive heat transfer due to thermal diffusion, one can take account of heat sources in the cell (*i*) in a natural way by including in addition to $\Delta Q(i-1, i)$ the term $\Delta Q(i) = H(i, t)\, \Delta t$ which gives the heat change due to a reaction occurring in the cell.

D2. STABILITY AND RESOLUTION

In any computational scheme a certain time interval Δt must elapse during which heat flows uninterruptedly between cells. If the Δt chosen is too large, then the equilibrium point will be passed and oscillations in the computed temperatures will lead to meaningless results. This is discussed in detail by Carslow and Jaeger (Ref. D-4) and Davids and Berger (Refs. D-2 and D-3). The well known condition which insures against such a blow-up is

$$XMOD = \kappa \Delta t/\Delta x^2 < 1/4 \qquad \text{(D-3)}$$

where Δx is the effective linear dimension of the cell in question and κ the effective thermal diffusivity between the cells. The above restriction on XMOD insures that during the time interval, Δt, energy conservation is preserved and not more than the available heat in a cell is allowed to flow out.

One of the means of reducing XMOD below the required value is to increase the cell size. This, however, tends to give us less spatial resolution than may be desirable for a particular problem. Furthermore, it is necessary to determine the number of cell divisions that should be made to obtain the desired resolution and accuracy. The general rule of thumb is that if S is the dimension of the material, a cell size of S/6 gives a "reasonable" solution. Each case must be handled separately and we have found that sometimes one or two cell divisions give sufficiently good results.

D3. TWO-DIMENSIONAL HEAT CONDUCTION--AXIAL SYMMETRY

In the heat conduction program with axial symmetry, each cell property which is involved in heat transfer in general is a function of two indices, I and J, corresponding to the radial and axial directions. A representative cell is shown in Fig. D-1. The geometrical cell properties are:

XR(I,J)	=	radial dimension
ZH(I,J)	=	vertical dimension
XS(I,J)	=	surface area in the radial direction
ZS(I,J)	=	surface area in the vertical direction.

Each cell is also characterized by a thermal conductivity K(I,J), specific heat C(I,J), and density D(I,J). At each moment in time the cell is characterized by a temperature U(I,J), and the laws of heat conduction are used to calculate the change in this temperature over the time interval T1.

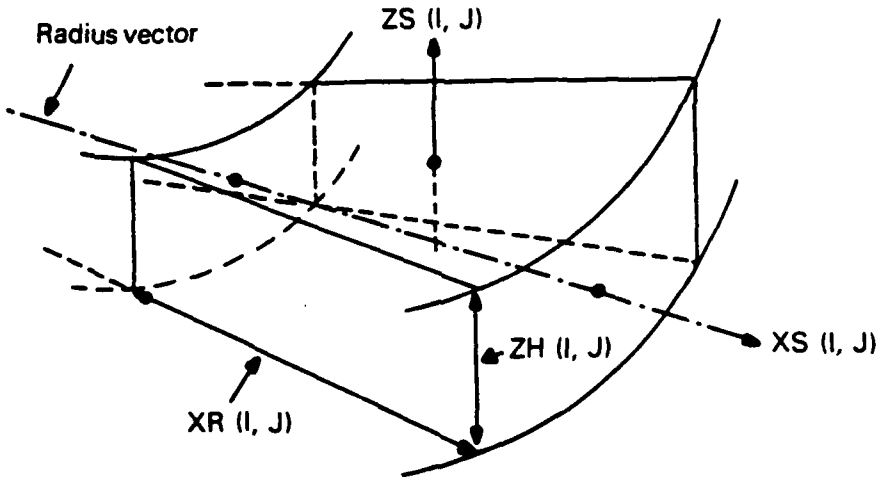

Figure D-1. Geometrical Properties of Representative Cell (I,J).

The various heat and temperature changes are shown in Fig. D-2. In the schematic drawing ZQ(I,J) is the heat transferred from cell (I,J) to cell (I,J + 1) and ZQ(I,J – 1) is the heat transferred from cell (I,J – 1) to cell (I,J). The quantities XQ(I,J) and XQ(I – 1,J) give the heat lost and gained in the radial direction. The heat transfer quantities and the resultant temperature changes are calculated by using the law of heat transfer and mass action as stated above.

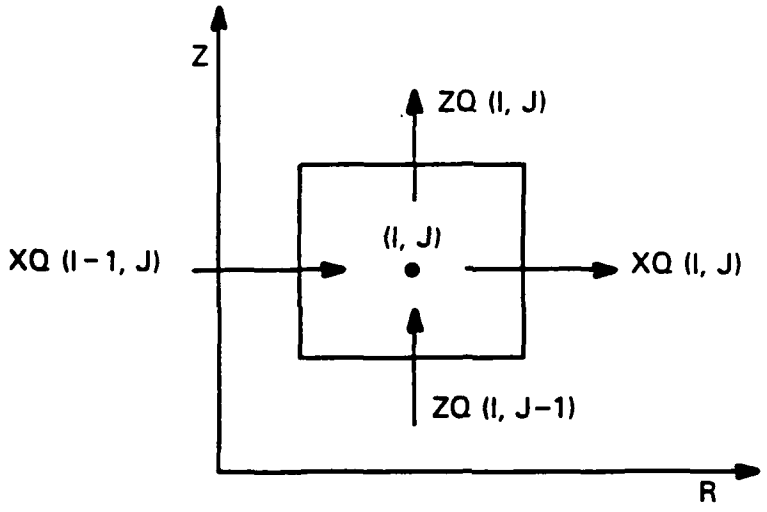

Figure D-2. Flow of Heat (ZQ, XQ) Associated With Cell (I,J).

REFERENCES, APPENDIX D

D-1. R.L. Berger and B. Balko, "Its Measurement and Control in Science and Industry," in *Temperature*, 4 (3), 2169, Edited by H.H. Plumb, ISA, Pittsburgh, 1972.

D-2. N. Davids and R.L. Berger, *Commun. ACM 7*, 547, 1964.

D-3. N. Davids and R.L. Berger, *Curr. Mod. Biol.*, 3, 169, 1969.

D-4. H.S. Carslow and J.C. Jaeger, *Conduction of Heat in Solids*, 2nd Edition, Oxford University Press, London, 1959.